Indoor Localization based on Multipath Fingerprinting

Evgeny Kupershtein

Indoor Localization based on Multipath Fingerprinting

Research Thesis

In Partial Fulfillment of the Requirements for the Degree of Master of Science in Electrical Engineering

Evgeny Kupershtein

Submitted to the Senate of the Technion - Israel Institute of Technology

Iyar, 5773 Haifa April 2013

The Research Thesis Was Done Under The Supervision of Professor Israel Cohen and Dr Mati Wax in the Faculty of Electrical Engineering.

The Generous Financial Help Of Alvarion and the Israel Science Foundation (Grant no. 1130/11) Is Gratefully Acknowledged.

I would like to express my sincere gratitude and appreciation to my advisors, Dr Mati Wax and Professor Israel Cohen, for their valuable guidance and constant encouragement throughout all stages of this research.

Dedicated to my parents.

Contents

List of Figures

List of Papers

1. E. Kupershtein, M. Wax, and I. Cohen, "Single-site emitter localization via multipath fingerprinting," *IEEE Transactions on Signal Processing*, vol. 61, no. 1, pp. 10–21, Jan. 2013.

2. E. Kupershtein, M. Wax, and I. Cohen, "Multipath fingerprinting via signal subspace in the frequency domain," *In preparation.*

Abstract

In recent years there has been a growing interest in position location in indoor venues. As more applications requiring indoor localization are emerging in the market, the demand for accurate and reliable localization increases. Unfortunately, the accuracy of available techniques is limited, and a dense and expensive deployment is required. The problem of accurate indoor localization is challenging due to severe multipath conditions existing in indoor environments. As a result, the classical position location techniques based on the line-of-sight (LOS) condition are not valid in such scenarios.

This research presents a novel method enabling single-site localization of wireless emitters in a rich multipath environment. The localization is based on a novel fingerprinting technique exploiting the spatial-temporal characteristics of the multipath signals received by the base station antenna array. The fingerprint is based on a lower dimensional signal subspace of the spatial-temporal covariance matrix, capturing the dominant multipath signals. The subspace approach does not require estimation of the directions-of-arrival and differential-delays of the multipath reflections, which is both difficult and computationally intensive problem in rich multipath environments. The proposed method exploits fingerprint matching based on the powerful similarity-profile criterion with effective complexity reduction techniques limiting the matching complexity and providing storage saving.

The proposed fingerprinting technique is investigated in the time and frequency domains showing a similar level of accuracy. Both approaches are applicable to most modern communication techniques and do not require new hardware on the user device.

Necessary and sufficient conditions that guarantee unique localization are presented. The performance is validated with both simulated and real data, demonstrating localization accuracy of about 1m in typical indoor environments.

List of Symbols

$\boldsymbol{A}$	Matrix including all the direction-of-arrival and differential-delay information of multipath reflections
$\hat{\boldsymbol{C}}$	Sample-covariance of an antenna array channel impulse response
$\mathcal{C}$	Set of all complex numbers
D	Sample interval
$\mathcal{D}_i$	Training samples (learning set) of the class ω_i
$\boldsymbol{F}$	Similarity-matirx
$\boldsymbol{G}$	Cholesky factor
$\boldsymbol{I}$	Identity matrix
J	Number of signal pilot subcarriers
K	Number of locations/classes in the database
L	Number of "snapshots" used for sample-covariance estimation at each database point during the off-line phase
M	Number of "snapshots" used for sample-covariance estimation during the on-line phase
N	Number of samples ("taps") in each "snapshots"; number of Fourier coefficients
$\boldsymbol{P}_A$	Projection operator onto the space spanned by the columns of the matrix $\boldsymbol{A}$
$\boldsymbol{P}_i$	Projection operator onto the signal subspace corresponding to the i-th location in the database
$P(\omega_i\|\mathbf{x})$	A posteriori probability (posterior)
$P(\omega_i)$	A priori probability (prior) of the class ω_i
$\boldsymbol{R}$	Expected value of $\hat{\boldsymbol{R}}_i$
$\hat{\boldsymbol{R}}$	Sample-covariance matrix computed in the on-line phase
$\hat{\boldsymbol{R}}_i$	Sample-covariance matrix computed in the off-line phase and corresponding to the i-th location in the database
$\widetilde{\boldsymbol{R}}_i$	Normalized covariance matrix computed in the off-line phase from $\hat{\boldsymbol{R}}_i$
$\widehat{\boldsymbol{R}}$	Normalized covariance matrix computed in the on-line phase from $\hat{\boldsymbol{R}}$
T	Signal observation period ("snapshot" duration)

$\boldsymbol{V}_q$	Matrix including q eigenvectors
$a_i(\theta_k)$	Amplitude response of the i-th sensor to a wavefront impinging from direction θ_k
$a_{id}(\theta_k)$	Amplitude response of the i-th sensor to a wavefront impinging from direction θ_k at frequency $\omega_c + \omega_d$
$\boldsymbol{a}(\theta_k)$	Steering vector of the array towards direction θ_k at frequency ω_c
$\boldsymbol{a}_d(\theta_k)$	Steering vector of the array towards direction θ_k at frequency $\omega_c + \omega_d$
b	Feature vector dimension
d	Fourier coefficient index
$f(\mathbf{x})$	Decision function
$\boldsymbol{f}_i$	Similarity-profile of the i-th location
$\widehat{\boldsymbol{f}}$	Query similarity-profile obtained from the received signals
f_{ij}	Similarity between the data captured in the i-th location to the fingerprint of the j-th location
f_c	Center frequency of the transmitted signal $\tilde{s}(t)$ (Hz)
f_s	Sample frequency (Hz)
$g(t)$	Convolution of the transmit and receive filters
$g(\omega_d)$	Channel frequency response of the transmit and receive filters
$\hat{h}_i(t)$	Estimated channel impulse response corresponding to the i-th sensor
k	Signal reflection index
m, l	Signal "snapshot" index
$n_i(t)$	Additive noise at the i-th sensor
p	Number of antennas of an antenna array
$\hat{p}(\mathbf{x})$	Estimated measurement distribution
$p(\mathbf{x}\|\omega_i)$	Class-conditional density of $\mathbf{x}$
$p(\mathcal{D}_i, \omega_i)$	Statistical model (probability density) of the class ω_i obtained in the training stage from $\mathcal{D}_i$
q	Number of signal reflections (signal subspace dimension)
$\hat{q}$	Estimated signal subspace dimension
$\tilde{\boldsymbol{r}}_i, \widehat{\boldsymbol{r}}$	Vectorization of matrices $\widetilde{\boldsymbol{R}}_i$ and $\widehat{\boldsymbol{R}}$ respectively
$\tilde{s}(t)$	Transmitted signal
$s(t)$	Complex envelope of the transmitted signal $\tilde{s}(t)$
$s_t(\omega_d)$	Fourier coefficient
t_m, t_l	"Snapshot" time
$\boldsymbol{v}$	Eigenvector
$\mathbf{x}$	Random feature vector of length b
$x_i(t)$	Complex envelope of the signal received by the i-th antenna
$\boldsymbol{x}_{t_m}[\ell]$	Vector including ℓ-th sample of the received signal performed at time $(t_m + \ell T/N)$ at each antenna of the p-antenna array

$\boldsymbol{x}_{t_m}[\omega_d]$	Discrete Fourier Transform of the $\boldsymbol{x}_{t_m}[\ell]$
$\boldsymbol{x}(t)$	"Snapshot" vector of the size $pN \times 1$
$\boldsymbol{x}_{t_m}$	"Frequency domain snapshot", vector of the size $pN \times 1$
(x, y)	Point Cartesian coordinates
$\boldsymbol{\Gamma}$	Matrix including complex coefficients of q reflections from M "snapshots"
$\boldsymbol{\Sigma}$	Covariance matrix
α	Signal energy threshold
ψ	Principal angles between subspaces
$\gamma_k(t)$	Complex coefficient representing the phase shift and attenuation of the k-th reflection
$\boldsymbol{\gamma}(t)$	Vector of q complex coefficients
η	Rank of the matrix $\boldsymbol{\Gamma}$
$\boldsymbol{\theta}$	Vector of signal directions-of-arrival
θ_i	Direction-of-arrival of the i-th reflection
$\boldsymbol{\vartheta}_i$	Vector of unknown parameters of length β corresponding to a class i
ℓ	Signal sample index
λ	Eigenvalue
μ	Expected value (mean) of a random variable
σ	Standard deviation of a random variable
σ_i	Singular value of a matrix
$\boldsymbol{\tau}$	Vector of delays of signal reflections relative to the reference
τ_k	Delay of the k-th reflection relative to the reference
$\tau_i(\theta_k)$	Delay between the i-th sensor and the reference sensor of the k-th reflection
$\bar{\tau}$	Delay spread of multipath reflections
ω_i	Class i (State of nature i)
ω_c	Center frequency of the transmitted signal $\tilde{s}(t)$ (rads^{-1})
ω_c	Center frequency of the transmitted signal $\tilde{s}(t)$ (rads^{-1})
ω_d	Frequency of Fourier coefficients of the signal $s(t)$ (rads^{-1})
$\mathbb{D}(\mathbf{x}_1 \| \mathbf{x}_2)$	Distance measure between $\mathbf{x}_1$ and $\mathbf{x}_2$
$\det[\boldsymbol{A}]$	Determinant of the matrix $\boldsymbol{A}$
$\boldsymbol{A}^H$	Hermitian transpose of the matrix $\boldsymbol{A}$
$Tr\{\cdot\}$	Trace operator
$\mathrm{vec}(\cdot)$	Vectorization operator, which forms a column vector from the columns of a matrix by stacking them one under the other
$\|f\|$	Norm of f
$\otimes$	Kronecker product

Abbreviations

AMPS	**A**dvanced **M**obile **P**hone **S**ystem
ANN	**A**rtificial **N**eural **N**etworks
AP	**A**ccess **P**oint
BS	**B**ase **S**tation
BW	**B**and**w**idth
CDF	**C**umulative **D**istribution **F**unction
CDMA	**C**ode **D**ivision **P**ultiple **A**ccess
CFR	**C**channel **F**requency **R**esponse
CIR	**C**channel **I**mpulse **R**esponse
DFT	**D**iscrete **F**ourier **T**ransform
DOA	**D**irection **o**f **A**rrival
DTOA	**D**ifferential **T**ime **o**f **A**rrival
kNN	**k**-**N**earest-**N**eighbors
LF	**L**ocation **F**ingerprinting
LOS	**L**ine **o**f **S**ight
LTF	**L**ong **T**raining **F**ield
MAP	**M**aximum **a** **P**osteriori
MDM	**M**inimum **D**istance **M**easure
MIMO	**M**ultiple-**I**nput **M**ultiple-**O**utput
ML	**M**aximum **L**ikelihood
MLE	**M**aximum **L**ikelihood **E**stimator
MMSE	**M**inimum **M**ean **S**quare **E**rror
MSE	**M**ean **S**quare **E**rror
MT	**M**obile **T**erminal
NN	**N**eural **N**etworks
OFDM	**O**rthogonal **F**requency-**D**ivision **M**ultiplexing

PDF	**P**robability **D**istribution **F**unction
PDP	**P**ower **D**elay **P**rofile
RF	**R**adio **F**requency
RSS	**R**eceived **S**ignal **S**trength
RSSI	**R**eceived **S**ignal **S**trength **I**ndication
RT	**R**ay-**T**raicing
SNR	**S**ignal **t**o **N**oise **R**atio
SP	**S**imilarity-**P**rofile
SVD	**S**ingular **V**alue **D**ecomposition
TDOA	**T**ime **D**ifference **o**f **A**rrival
TOA	**T**ime **o**f **A**rrival
UWB	**U**ltra-**w**ide**b**and

Chapter 1

Introduction

1.1 Motivation and Goals

Determining the position or location of a wireless emitter is an old and well-investigated problem with both military and commercial applications. Many techniques have been developed to solve this problem over the last 60 years, most of them based on the assumption that the wireless signal travels from the source to the receiving antennas along the line-of-sight (LOS) path connecting them. The classical position location techniques, direction-of-arrival (DOA), time-of-arrival (TOA) and differential-time-of-arrival (DTOA), are all based on this assumption, with the localization carried out via triangulation, using several such measurements [1, 2].

In recent years there has been a growing interest in position location in shopping malls and in indoor venues, where LOS conditions usually do not exist. In these cases, the propagation from the source to the receiving antennas is usually made through reflections from buildings and walls, referred to as multipath. Consequently, the multipath signals arriving at the receiving antennas may be very different from the LOS path. As a result, the the classical position location techniques are not valid in such scenarios.

Fingerprinting techniques have been recently developed [3–57] to overcome this multipath problem. Fingerprinting techniques are based on the premise that there is a one-to-one relation between the characteristics of the multipath signals received at the base stations and the emitter location, i.e., that a fingerprint can be extracted from the received signals and serve as a unique identifier of the emitter location. The problem

is casted as a pattern recognition problem, namely, a database of fingerprints is pre-collected in the desired coverage area, and the location is determined by matching the extracted fingerprint to the fingerprint database.

Two types of fingerprinting techniques have been developed about the same time. The first, developed by Wax et al. [3–6] and further investigated by Nezafat et al. [7–9], is based on using the multipath characteristics, derived from the signals coherently received by a multiple-antenna base station (BS), as the location fingerprint. A review of this technique, referred to as "Location Fingerprinting", was first presented by Koshima and Hoshen [10]. The second technique, developed by Bahl and Padmanabhan [11] and by Laitinen, Lahteenmaki, and Nordstrom [12], is based on using the received signal strength (RSS) obtained at several base stations as the location fingerprint.

The RSS fingerprint suffers from dependence on many irrelevant parameters such as the orientation of the transmitter and body shadowing, but more critically, it suffers from high signal strength variability along a short distance of wavelength caused by constructive and destructive interference between the multipath signals. As a result, the accuracy of this technique is limited and requires signal strength measurements from multiple BSs to assure an acceptable accuracy. In many cases, however, multiple BSs may not be able to receive the signals, in which case the accuracy is very low. The coherently received multipath-based fingerprint, on the other hand, exploits the multipath to its advantage, rather than suffers from it, thus enabling a much higher accuracy.

The work of Wax, Hilsenrath, and Meng [3–5] was focused on the outdoor environment and confined to narrowband signals of the advanced mobile phone system (AMPS) and used a fingerprint based on the directions-of-arrival of the multipath signals. In [6] Wax, Hilsenrath, and Bar extended their work to wideband signals used in code division multiple access (CDMA) systems by adding another, separate fingerprint based on the power delay profile (PDP) of the multipath signals. The idea of using the PDP as a fingerprint was also investigated by Nypan, Gade, and Hallingstad [13], Ahonen and Laitinen [14] and Ahonen and Eskelinen [15]. Meurer et al. [16] proposed using the covariance matrix of the channel impulse response (CIR) as a location fingerprint rather than the power delay profile. Triki, Oktem and Slock [17–19] have extended the PDP fingerprinting in several aspects, including adding to the fingerprint the spatial information of the antenna array, in both receive and transmit (MIMO), as well as the Doppler

shifts of the different reflections, for the case that the mobile terminal is moving. The asymptotic performance of the PDP method was investigated under various statistical models by Oktem and Slock [20, 21]. The applicability of PDP fingerprinting for UWB localization was investigated by Altahus, Troesch, and Wittneben [22] and by Steiner and Wittneben [23, 24].

The current work extends the work of Wax et al. [3–6] in several aspects. First, it presents a novel and more powerful fingerprint that exploits both the directions-of-arrival and the differential-delays of the multipath signals. This novel fingerprint is derived from a lower dimensional subspace of the spatial-temporal covariance matrix in which the multipath signals reside, also referred to as the signal subspace. The subspace estimation does not require estimation of the directions-of-arrival and differential-delays of the multipath reflections, which is both difficult and computationally intensive problem in rich multipath environments. Moreover, the subspace preferable includes only the dominant reflections, thus forming a rich and robust fingerprint that is used in conjunction with a powerful similarity-profile matching criterion to provide accurate single-site localization. Second, it presents necessary and sufficient conditions that guarantee unique localization. Third, unlike the method proposed in [6], our method is applicable to any wideband signal, provided the signal has a repeatable segment. As such, it is applicable to most modern communication techniques, since they all use a fixed and repeatable segment of the signal (i.e., a preamble) for synchronization and channel estimation purposes. As shown in the Sections 3.5 and 4.6, our method is applicable also to localization using the array channel impulse response (CIR) and channel frequency response (CFR). In addition, unlike [3–6], our work is focused on the indoor environment, yet applicable also to outdoor environments. Even though both environments are characterized by rich multipath, the indoors multipath environment is typically richer and characterized by a larger angle spread and smaller delay spread. Last, but not least, the time domain and the frequency domain approaches to the multipath fingerprinting are investigated in this thesis.

1.2 Organization

The outline of the rest of the thesis is as follows. In Chapter 2, we present the location fingerprinting as a classification problem and give the relevant background of

classification techniques. Then, we review the most important and common location fingerprinting techniques. The original contribution of this thesis starts from Chapter 3, where we present a time domain problem formulation and the conditions for unique localization. Then, in Sections 3.3 and 3.4 we present the similarity-metric derivation and the signal subspace based localization method. In Chapter 4, we present the frequency domain approach to the multipath fingerprinting problem. Finally, in Chapter 5 we conclude with a summary and discussion on future research directions.

Chapter 2

Background and Overview of Location Fingerprinting Techniques

2.1 Introduction

Location Fingerprinting (LF) is a localization technique that is based on the identification of location dependent signal characteristics like the received signal strength (RSS), power delay profile (PDP), direction of arrival (DOA), time difference of arrival (TDOA), channel impulse response (CIR) and etc. These characteristics – known as "fingerprints" or position signatures – are pre-calculated or pre-measured for the entire coverage area and stored in a database, and then matched or correlated to the characteristics of a measured signal.

A general view of location fingerprinting techniques is presented in Figure 2.1. The technique consists of two phases: an off-line phase (learning or training phase) and an on-line phase (positioning). During the off-line phase, a database of "location fingerprints" is collected in the desired coverage area, with the fingerprint extracted from signals received by the BS antenna array or/and by multiple BSs. In the on-line phase, the location fingerprint is extracted from signals received by the BS antenna array or/and by multiple BSs and matched to the fingerprints stored in the database. The location whose fingerprint best matches the extracted fingerprint is selected as the emitter location.

Therefore, LF can be considered as a pattern recognition problem and numerous machine learning techniques can be applied to this problem [11, 26, 27, 41–44, 58–60].

The critical element of LF techniques is the creation and maintenance of the database, which is often called a *radio map*. There are two major approaches to a database creation. The first, is based on an extensive measurements of signal characteristics in the coverage area, and is carried out either by the mobile terminals (MT) (client-based systems) or by the base station/s (infrastructure-based and client-assisted systems) [2, 11, 29–32, 61]. The second, is based on computing of signal characteristics using radio propagation models [11, 32, 33, 38, 40, 41] or/and ray tracing simulators [17, 34–37, 43, 44]. The accuracy of LF techniques is highly dependent on the database creation procedure and in particular on the resolution of database points, and the database complexity.

In the following sections of this chapter we first overview the major classification techniques used in location fingerprinting and then the most important and common LF techniques.

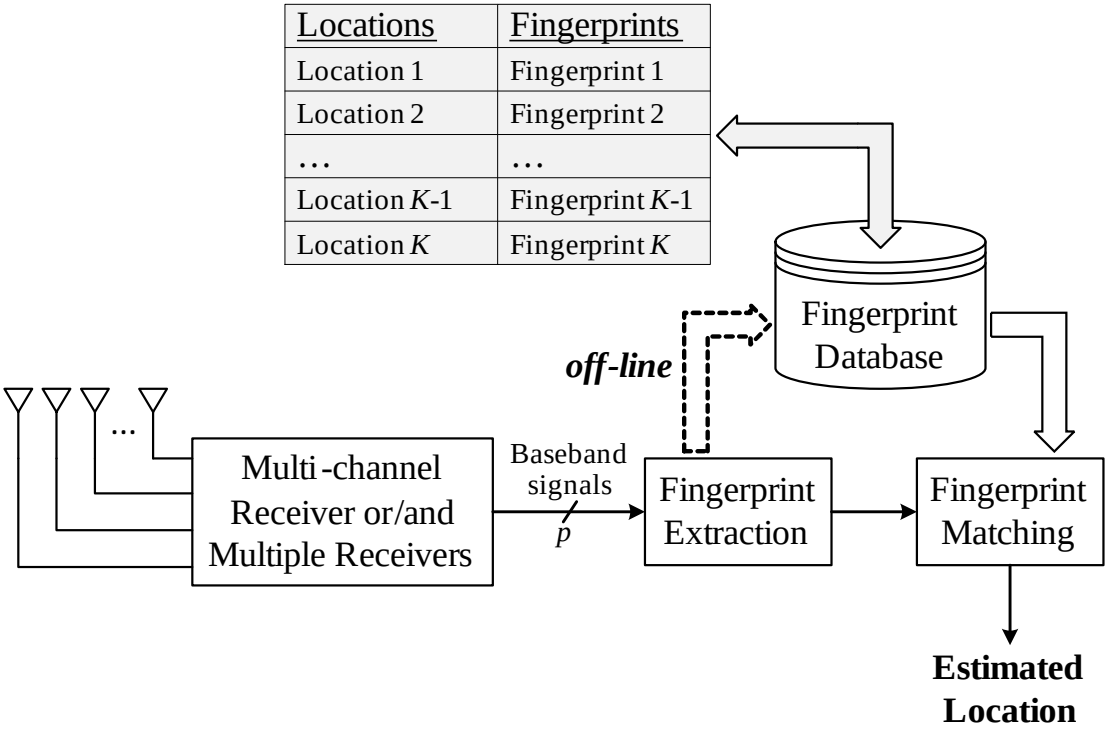

FIGURE 2.1: General block diagram of location fingerprinting techniques.

2.2 LF Classification Techniques

2.2.1 Probabilistic Methods: The General Principle

Most probabilistic methods rely on the Bayesian decision theory which is a fundamental statistical approach to the problem of pattern classification. This approach is based on quantifying the tradeoffs between various classification decisions using probability and the costs that accompany such decisions. The decision problem requires that all of the relevant probability values are known. Unfortunately, this is usually not the case and we need to estimate the unknown probabilities and probability densities using our general knowledge about the problem and/or *training data* — particular representatives of the patterns we want to classify [58].

The optimal Bayesian classifier minimizing the average probability of error for zero-one loss function is given by

$$f(\mathbf{x}) = \underset{i=1,\ldots,K}{\arg\max}\, P(\omega_i|\mathbf{x}) \tag{2.1}$$

where ω_i denotes the *state of nature* or simply the *class* i, $\mathbf{x} = (x_1, \ldots, x_b)^T \in \mathcal{C}^{b\times 1}$ is a random *feature vector*, $P(\omega_i|\mathbf{x})$ is *a posteriori* probability (or *posterior*) and $f(\mathbf{x})$ is a decision function. Using Bayes' formula we can rewrite (2.1) as

$$f(\mathbf{x}) = \underset{i=1,\ldots,K}{\arg\max}\, p(\mathbf{x}|\omega_i)P(\omega_i) \tag{2.2}$$

where $P(\omega_i)$ and $p(\mathbf{x}|\omega_i)$ are *a priori probability* of the class ω_i (or *prior*) and the class-conditional density of $\mathbf{x}$, respectively.

Another possible, yet less common in the location fingerprinting field, approaches are the minimum mean square error (MMSE) estimator [39, 42] and the minimum distance measure (MDM) [40] classifier. Let ω_i denote the coordinate tuple of the location i. The MMSE location estimation minimizing the localization mean square error (MSE), then, is given by

$$\hat{\omega} = E(\omega|\mathbf{x}) = \sum_{i=1}^{K} \omega_i P(\omega_i|\mathbf{x}) \tag{2.3}$$

The MDM classification (location estimation) is performed by minimizing the distance measure between the estimated measurement distribution $\hat{p}(\mathbf{x})$ and the statistical models

obtained in the training stage $p(\mathcal{D}_i, \omega_i)$

$$f(\mathbf{x}) = \arg\min_{i=1,\ldots,K} \mathbb{D}\big(\hat{p}(\mathbf{x}) \| p(\mathcal{D}_i|\omega_i)\big) \tag{2.4}$$

where $\mathcal{D}_i$ is the training samples of the class ω_i and $\mathbb{D}$ is the distance measure. Numerous distance measures have been proposed to evaluate the similarity between statistical models. For example, ISE distance, Kullback-Leibler divergence (KLD) (also information divergence, relative entropy), Hellinger (or Bhattacharyya) distance [40], Minkowski distance, earth mover distance (EMD), Hausdorff distance (HD) [45] and etc. The main advantage of the MDM method is its robustness to modeling errors, unlike the Bayesian classifier, which is known to be very sensitive to modeling errors [40].

The problem, then, is to estimate the unknown *a priori probabilities* $P(\omega_i)$ and the class-conditional densities $p(\mathbf{x}|\omega_i)$. Note that $p(\mathbf{x}|\omega_i)$ is a probability density function when $\mathbf{x}$ is a continuous random vector, and a probability mass function in case of a discrete random vector.

Usually the estimation of the prior probability $P(\omega_i)$ presents no serious difficulties. However, estimation of the class-conditional densities is a quite complex problem. Let us call $\mathcal{D}_i = \{\mathbf{x}_k^i\}_{k=1}^{n_i}$ the set of n_i independent samples drawn according to the probability $p(\mathbf{x}|\omega_i)$, $i = 1, \ldots, K$. We assume the *separability condition* supposing that the learning set $\mathcal{D}_i$ have no influence on $p(\mathbf{x}|\omega_j, \mathcal{D}_j)$ if $i \neq j$. Several approaches to the problem of probability/probability density estimation, utilizing the training data $\mathcal{D}_i$, can be distinguished: parametric against non-parametric and Bayesian against non-Bayesian (Maximum Likelihood).

Concerning location fingerprinting techniques, the class ω_i denotes the emitter location i (coordinate tuple i), the random vector $\mathbf{x}$ denotes the signal characteristics or the received signal itself and the training data $\mathcal{D}_i$ denote the signal characteristics or the signal itself measured and calculated during the off-line phase at the location i. Position location, in the on-line phase, is performed using the classifiers (2.1)–(2.4). These classifiers assume that all of the relevant probability values are known. Estimation of these probability values is performed during the off-line phase using various techniques described further.

2.2.1.1 Parametric Techniques

The parametric approach assumes that the *location-conditional* PDF $p(\mathbf{x}|\omega_i)$ has a known form and can be parametrized using a vector of unknown location-specific parameters $\boldsymbol{\vartheta}_i$, i.e. $p(\mathbf{x}|\omega_i) = p(\mathbf{x}|\omega_i, \boldsymbol{\vartheta}_i)$, where $\boldsymbol{\vartheta}_i = (\vartheta_1^i, \ldots, \vartheta_\beta^i)^T \in \mathcal{C}^{\beta\times 1}$. For example, we can assume that $p(\mathbf{x}|\omega_i, \boldsymbol{\vartheta}_i)$ is a normal density with unknown mean μ_i and covariance matrix $\boldsymbol{\Sigma}_i$. In this case the vector $\boldsymbol{\vartheta}_i$ includes the mean μ_i and the elements of the covariance matrix $\boldsymbol{\Sigma}_i$. As a result, the problem of estimating an unknown function $p(\mathbf{x}|\omega_i)$ is reduced to one of estimating the parameters μ_i and $\boldsymbol{\Sigma}_i$ from the learning set $\mathcal{D}_i$ corresponding to the location i (class i). Two common and reasonable approaches to this problem, known as *parameter estimation* problem, shall be considered: *maximum likelihood* estimation and *Bayesian* estimation.

Maximum Likelihood Maximum likelihood method treats $\boldsymbol{\vartheta}_i$ as unknown, but fixed model parameters. The best estimate of their value produces a distribution that maximizes the probability of obtaining the observed data. Thus, the Maximum Likelihood Estimator (MLE) of the unknown vector of parameters $\boldsymbol{\vartheta}_i$, following [58], is given by

$$\hat{\boldsymbol{\vartheta}}_i = \arg\max_{\boldsymbol{\vartheta}_i} p(\mathcal{D}_i|\boldsymbol{\vartheta}_i) \tag{2.5}$$

We should point out that the estimated vector of parameters $\hat{\boldsymbol{\vartheta}}_i$ can be used as the fingerprint of the location i, while the fingerprint matching procedure can be derived from the Bayesian decision rule (Bayesian Classifier)

$$f(\mathbf{x}) = \arg\max_{i=1,\ldots,K} p(\mathbf{x}|\omega_i, \hat{\boldsymbol{\vartheta}}_i)P(\omega_i) \tag{2.6}$$

Bayesian Bayesian methods consider the parameters $\boldsymbol{\vartheta}_i$ as random variables having a priori distribution $p(\boldsymbol{\vartheta}_i)$ that is assumed to be known and represents our initial knowledge about $\boldsymbol{\vartheta}_i$. Observation of the samples from the training set $\mathcal{D}_i$ allows us to convert a distribution $p(\boldsymbol{\vartheta}_i)$ into a posterior distribution $p(\boldsymbol{\vartheta}_i|\mathcal{D}_i)$.

The classical Bayesian approach, in contrast to the ML, does not assume a single parametric model of the $p(\mathbf{x}|\omega_i)$ and averages it over the possible values of $\boldsymbol{\vartheta}_i$. Thus, the location-conditional density $p(\mathbf{x}|\omega_i)$, following [58], is given by

$$p(\mathbf{x}|\omega_i, \mathcal{D}_i) = \int p(\mathbf{x}|\omega_i, \boldsymbol{\vartheta}_i)p(\boldsymbol{\vartheta}_i|\mathcal{D}_i)d\boldsymbol{\vartheta}_i \tag{2.7}$$

The simplified Bayesian approach assumes a fixed parametric model of the $p(\mathbf{x}|\omega_i)$, i.e. $p(\mathbf{x}|\omega_i, \mathcal{D}_i) = p(\mathbf{x}|\omega_i, \hat{\boldsymbol{\vartheta}}_i)$; however, the estimation of $\boldsymbol{\vartheta}_i$ is based on the assumption that it is a random vector, and can be performed, for example, using well-known parameter estimation algorithms MAP or MMSE [59]

- MMSE is a Minimum Mean Square Error estimator that minimizes the mean square error (MSE) $E(\|\hat{\boldsymbol{\vartheta}}_i - \boldsymbol{\vartheta}_i\|^2|\mathcal{D}_i)$ and given by

$$\hat{\boldsymbol{\vartheta}}_i = E(\boldsymbol{\vartheta}_i|\mathcal{D}_i) \tag{2.8}$$

- MAP is a Maximum a Posteriori (MAP) estimator given by

$$\hat{\boldsymbol{\vartheta}}_i = \arg\max_{\boldsymbol{\vartheta}_i} p(\boldsymbol{\vartheta}_i|\mathcal{D}_i) = \arg\max_{\boldsymbol{\vartheta}_i} p(\mathcal{D}_i|\boldsymbol{\vartheta}_i)p(\boldsymbol{\vartheta}_i) \tag{2.9}$$

2.2.1.2 Non-parametric Techniques

Non-parametric techniques make few assumptions about density form and can be used with arbitrary distributions. There are several simple methods for estimating an unknown density function like *histogram*, *kernel density estimators* (and in particular a *Parzen window* approach), and a *k-nearest neighbors* (kNN). A detailed description of these techniques and examples of their usage may be found in [39, 42, 58, 60].

2.2.2 Non-parametric Classification: the Nearest Neighbor Algorithm

The *nearest neighbor* algorithm is conceptually and computationally simple technique with sub-optimal performance relative to the Bayesian classifier [58]. Consider the learning set $\mathcal{D} = \{\mathbf{x}_1, \ldots, \mathbf{x}_K\}$ obtained during the off-line phase, where $\mathbf{x}_i \in \mathcal{C}^{b\times 1}$ is a vector of signal characteristics or the signal itself corresponding to the location i. In addition, consider the vector of measurements $\mathbf{x} \in \mathcal{C}^{b\times 1}$ obtained during the on-line phase at the unknown location. Then the nearest neighbor location estimation is given by

$$\hat{i} = \arg\min_{i=1,\ldots,K} \mathbb{D}(\mathbf{x}\|\mathbf{x}_i) \tag{2.10}$$

where $\mathbb{D}(\mathbf{x}\|\mathbf{x}_i)$ is a general metric or "distance" function between $\mathbf{x}$ and $\mathbf{x}_i$. Numerous distance measures can be used to evaluate the similarity between the vectors $\mathbf{x}$ and $\mathbf{x}_i$. For example, Minkowski distance (including the Euclidean distance as a special case),

Kullback-Leibler divergence (KLD) (or information divergence, relative entropy), earth mover distance (EMD), Hausdorff distance (HD), peak-to-peak distance [45, 58], etc.

The kNN algorithm is an extension of the nearest neighbor algorithm (2.10). To estimate/calculate the emitter coordinates the kNN algorithm uses coordinates of k locations in the database having the smallest distance $\mathbb{D}(\mathbf{x}\|\mathbf{x}_i)$. The common kNN approach is an averaging of these k location coordinates [27, 49]

$$\hat{\boldsymbol{\omega}} = \frac{1}{k}\sum_{i=1}^{k}\boldsymbol{\omega}_i \tag{2.11}$$

where $\boldsymbol{\omega}$ denotes the coordinate tuple of the emitter location.

The weighted version of kNN algorithm, following [11, 26], is given by

$$\hat{\boldsymbol{\omega}} = \frac{\sum_{i=1}^{k} \mathrm{w}_i\boldsymbol{\omega}_i}{\sum_{i=1}^{k} \mathrm{w}_i} \tag{2.12}$$

where w_i is a weight of the i-th location that can be, for example, the function of the distance measure, i.e., $\mathrm{w}_i = \mathrm{func}\big(\mathbb{D}(\mathbf{x}\|\mathbf{x}_\mathrm{i})\big)$.

2.2.3 SVM Method

Support Vector Machine (SVM) is a classification technique used in the machine learning and statistical analysis fields, and having a wide variety of applications in science, engineering and medicine [62, 63]. SVM theoretical background can be found in [58, 60, 62] and its application to LF in [26, 54, 55].

2.2.4 Artificial Neural Networks

An artificial neural networks (ANN), often called a neural network (NN), is a mathematical model allowing to construct an effective non-linear input-output mapping and have been used in a variety of applications including location fingerprinting [26, 56, 57]. Usually, a multilayer perceptron (MLP) [58] network with one or more hidden layers is used for NN-based localization. During the offline phase, location-based fingerprints and the corresponding location coordinates are used as the inputs and the targets respectively for the NN training purpose. During the on-line phase the measured fingerprint is entered to the trained NN leading to estimated coordinate tuple at the output of the system.

2.3 RSS-based Localization

RSS stands for Received Signal Strength indication, also denoted as RSSI, and available in most off the shelf wireless devices. Due to this fact and to its relatively simple algorithm implementation the RSS-based localization techniques gained popularity and currently are among the most common LF techniques. The RSS-based techniques use location fingerprints derived from RSS of a mobile terminal (MT) measured by multiple BSs or vice versa, the RSS of the BSs measured by the MT.

2.3.1 Probabilistic Approach

The probabilistic approach discussed in [27, 46, 49], assumes the parametric distribution of the conditional density $p(\mathbf{x}|\omega_i)$, where $\mathbf{x}$ denotes RSS measurements from b BSs and ω_i denotes coordinates of the i-th database point ($i = 1, \ldots, K$). The non-parametric approaches investigated in [42] estimated the location-conditional density $p(\mathbf{x}|\omega_i)$ of RSS using the histogram method and the kernel method, with the Gaussian kernel. To simplify $p(\mathbf{x}|\omega_i)$ estimation the BSs are commonly assumed to be independent [27, 42, 46], so the conditional density estimation is calculated by

$$p(\mathbf{x}|\omega_i) = \prod_{j=1}^{b} p(x_j|\omega_i) \tag{2.13}$$

where x_j denotes the RSS measured by the j-th BS.

In case of parametric approach the signal strength PDF is often assumed to be the Gaussian distribution [27, 46] and as a result, only the mean μ_{ij} and the standard deviation σ_{ij} are estimated for each database point $i \in [1, K]$ and for each BS $j \in [1, b]$. The vector of parameters $\vartheta_{ij} = [\mu_{ij}, \sigma_{ij}]$ is estimated during the off-line phase, from the sample data $\mathcal{D}_{ij} = \{x_k^{ij}\}_{k=1}^{n_{ij}}$, using one of the techniques discussed in the Section 2.2.1.

After the database construction, the online determination phase uses the classifiers (2.1)–(2.4) to locate the mobile terminal. Although the prior probability $P(\omega_i)$ is determined by a specific indoor area and the mobile subscribers' habits, commonly all database points are assumed to be equiprobable [27, 42, 46]. Thus, the Bayesian location estimation (2.2) can be reduced to the ML classifier. For the parametric approach,

following [27, 46], the ML classifier is given by

$$\hat{i} = \underset{i=1,\ldots,K}{\arg\max} \prod_{j=1}^{b} p(x_j|\omega_i, \hat{\vartheta}_{ij}) \tag{2.14}$$

where $p(x_j|\omega_i, \hat{\vartheta}_{ij})$ is the *likelihood function* that has the Gaussian distribution with the mean μ_{ij} and the standard deviation σ_{ij}.

The disadvantage of RSS-based techniques is the dependence of RSS fingerprints on many irrelevant parameters such as the orientation of the transmitter and body shadowing, but more critically, they suffers from high signal strength variability along a short distance of wavelength caused by constructive and destructive interference between the multipath signals. Additional problem arises when the signal transmit power and/or antenna gain of the equipment used in the off-line (calibration) phase differ from the ones used in the on-line phase. As a result, the accuracy of this technique is limited and requires signal strength measurements from multiple BSs to assure an acceptable accuracy. Usually it requires, a very dense BS (AP) deployment, especially in the indoor environment. In many cases, however, multiple BSs may not be able to receive the signals, in which case the accuracy is very low.

To enhance the robustness of the RSS-based methods, Shih-Hau Fang, Tsung-Nan Lin, and Kun-Chou Lee [46] proposed a fading correction technique that mitigates multipath disturbance of a RSS. The key idea was to use instead of the original RSS indication a "filtered" RSS derived by averaging the logarithmic power spectrum of the RSS with respect to frequency. The proposed technique significantly reduced the level of RSS variations resulted from the multipath.

2.3.2 The kNN Approach

The kNN approach, presented in a general form in the Section 2.2.2, exploits the vector $\mathbf{x} \in \mathcal{C}^{b\times 1}$ of RSS measurements from multiple base stations (BS) as a location fingerprint. Bahl and Padmanabhan [11, 64] used the vector of mean RSS values from each AP and the kNN algorithm with the Euclidean distance measure. Their results indicate that using more RSS samples in the averaging process and a higher number b of APs yields better accuracy. However, increasing the number of APs above 3 yields a little benefit due to the inherent noise in the RSS measurements imposing a limitation on the localization accuracy [64].

Battiti [26] suggested weighted kNN algorithm with weights proportional to the inverse of the distance between signal strengths

$$\hat{\boldsymbol{\omega}} = \frac{\sum_{i=1}^{k} \frac{1}{\mathbb{D}(\mathbf{x}\|\mathbf{x}_i) + d_0} \cdot \boldsymbol{\omega}_i}{\sum_{i=1}^{k} \frac{1}{\mathbb{D}(\mathbf{x}\|\mathbf{x}_i) + d_0}} \tag{2.15}$$

where $\mathbb{D}(\mathbf{x}\|\mathbf{x}_i)$ is a distance measure between the RSS vector $\mathbf{x}$ measured in the on-line phase and the database RSS vectors $\mathbf{x}_i$, and d_0 is a small real constant used to avoid division by zero.

2.4 Signal Subspace Fingerprinting

The subspace-based localization techniques have been developed by Wax et al. [3–6] and further investigated by Nezafat et al. [7–9], and Cherntanomwong et al. [47, 48]. These techniques exploit the multipath characteristics, derived from the signals coherently received by a multiple-antenna base station (BS), as the location fingerprint. The multipath characteristics, like DOA and TOA, are obtained using the subspace structure of observations [3, 4].

The problem formulation used by the subspace-based localization techniques relies on the multichannel model [65] commonly used in the sensor array processing [66–77]. Consider an array composed of p sensors receiving a wideband signal $s(t)$ impinging on the array through q reflections from directions $\boldsymbol{\theta} = \{\theta_1, \cdots, \theta_q\}$. Using the narrowband assumption [72] and complex envelope representation, the $p \times 1$ vector received by the array is given by

$$\boldsymbol{x}(t) = \boldsymbol{A}(\boldsymbol{\theta})\boldsymbol{s}(t) + \boldsymbol{n}(t) \tag{2.16}$$

where $\boldsymbol{s}(t)$ is the $q \times 1$ vector of received multipath reflections and $\boldsymbol{A}(\boldsymbol{\theta})$ is the $p \times q$ matrix of *steering vectors* [72].

Suppose that the received vector $\boldsymbol{x}(t)$ is sampled at M time instants $t_1, \ldots, t_M$. The sampled data can then be expressed as

$$\boldsymbol{X} = \boldsymbol{A}(\boldsymbol{\theta})\boldsymbol{S} + \boldsymbol{N} \tag{2.17}$$

where $\boldsymbol{X}$ and $\boldsymbol{N}$ are the $p \times M$ matrices

$$\boldsymbol{X} = \left[\boldsymbol{x}(t_1), \ldots, \boldsymbol{x}(t_M)\right] \tag{2.18}$$

$$\boldsymbol{N} = \left[\boldsymbol{n}(t_1), \ldots, \boldsymbol{n}(t_M)\right] \tag{2.19}$$

Note that the matrix $\boldsymbol{A}(\boldsymbol{\theta})$ captures all the direction-of-arrival information of the multipath reflections and can be used as the basis for location fingerprint.

2.4.1 Probabilistic Approach

Wax et al. [3–6] proposed to use the following fingerprint matching criteria (classifier decision function), developed using the deterministic ML framework [74]

$$\hat{i} = \arg\max_{\boldsymbol{A}_i(\boldsymbol{\theta})} Tr\left\{\boldsymbol{P}_{\boldsymbol{A}_i}\widetilde{\boldsymbol{R}}\right\} \tag{2.20}$$

where $\boldsymbol{P}_{\boldsymbol{A}_i}$ is the projection operator onto the space spanned by the columns of the matrix $\boldsymbol{A}_i(\boldsymbol{\theta})$

$$\boldsymbol{P}_{\boldsymbol{A}_i} = \boldsymbol{A}_i\left(\boldsymbol{\theta}\right)\left(\boldsymbol{A}_i^H(\boldsymbol{\theta})\boldsymbol{A}_i(\boldsymbol{\theta})\right)^{-1}\boldsymbol{A}_i^H(\boldsymbol{\theta}) \tag{2.21}$$

where H denotes the Hermitian conjugate, $Tr\left\{\cdot\right\}$ is the trace operator, and $\widetilde{\boldsymbol{R}}$ is the sample-covariance matrix estimated in the on-line phase

$$\widetilde{\boldsymbol{R}} = \frac{1}{M}\sum_{m=1}^{M}\boldsymbol{x}\left(t_m\right)\boldsymbol{x}^H\left(t_m\right) \tag{2.22}$$

According to the ML criterion (2.20), the localization is carried out by searching in the database for the location i that maximizes the $Tr\left\{\boldsymbol{P}_{\boldsymbol{A}_i}\widetilde{\boldsymbol{R}}\right\}$ expression [4, 5]. The projection matrix at each database point is estimated during the off-line phase using the eigenvectors of the sample-covariance matrix. The selected eigenvectors correspond to the dominant eigenvalues of the sample-covariance matrix [3, 4, 66, 72].

In [6] Wax, Hilsenrath, and Bar extended their work to wideband signals used in code division multiple access (CDMA) systems by adding another, separate fingerprint based on the power delay profile (PDP) of the multipath signals and described in the Section 2.5.

2.4.2 The Nearest Neighbor Approach

A different approach mentioned by Wax, Meng, and Hilsenrath [4] and investigated by Nezafat et al. [7–9] uses a distance measure based on *principal angles* between the database subspaces and the subspace obtained in the on-line phase. The *principal angles* (or *canonical angles*), following [78, 79], are defined recursively by

$$\begin{aligned} \cos(\psi_1) &= \max_{\mathbf{u}\in\boldsymbol{A}_1} \max_{\mathbf{v}\in\boldsymbol{A}_2} \mathbf{u}^H\mathbf{v} = \mathbf{u}_1^H\mathbf{v}_1 \\ \cos(\psi_i) &= \max_{\mathbf{u}\in\boldsymbol{A}_1} \max_{\mathbf{v}\in\boldsymbol{A}_2} \mathbf{u}^H\mathbf{v} = \mathbf{u}_i^H\mathbf{v}_i, \quad i = 2,\ldots,q \end{aligned} \tag{2.23}$$

with

$$\begin{aligned} \mathbf{u}^H\mathbf{u}_j &= 0, \quad j = 1,\ldots,i-1 \\ \mathbf{v}^H\mathbf{v}_j &= 0, \quad j = 1,\ldots,i-1 \end{aligned} \tag{2.24}$$

where $\boldsymbol{A}_1$ and $\boldsymbol{A}_2$ are subspaces in p-dimensional complex vector space, $r = \dim \boldsymbol{A}_1 \geq \dim \boldsymbol{A}_2 = q \geq 1$, the angles $\psi_1,\ldots,\psi_q \in [0,\pi/2]$ between $\boldsymbol{A}_1$ and $\boldsymbol{A}_2$ are defined recursively, and $\|\mathbf{u}\| = \|\mathbf{v}\| = 1$. For computing cosines of principal angles, a singular value decomposition (SVD)-based algorithm can be used [78, 79]. The algorithm can be formulated as follows. Let, columns of matrices $U \in \mathcal{C}^{p\times r}$ and $V \in \mathcal{C}^{p\times q}$ form orthonormal bases for the subspaces $\boldsymbol{A}_1$ and $\boldsymbol{A}_2$, respectively. Then the cosines of principal angles are given by

$$\cos(\psi_i) = \sigma_i, \quad i = 1,\ldots,q \tag{2.25}$$

where $1 \geq \sigma_1 \geq \ldots \geq \sigma_q \geq 0$ are the singular values of the matrix $U^H V$.

2.5 Power Delay Profile Fingerprinting

The Power Delay Profile Fingerprinting (PDP-F) is a class of kNN techniques using fingerprints based on the channel impulse response [6, 13–19]. The idea of using the PDP as a fingerprint was first presented by Wax, Hilsenrath, and Bar in [6] for CDMA signal and also investigated by Nypan, Gade, and Hallingstad [13], Ahonen and Laitinen [14] and Ahonen and Eskelinen [15] for GSM and UMTS systems.

Nypan, Gade, and Hallingstad [13], Ahonen and Laitinen [14] suggested to use as a fingerprint the absolute value of the CIR $\|h_i(t)\|$ between the BS and a mobile terminal (MT) at every location i. To reduce the influence of fading, the PDP is usually estimated

by averaging the square of the CIR taps [13, 18]

$$\widehat{PDP}_i(\tau) = \frac{1}{M} \sum_{m=1}^{M} \left\| h_i(t_m, \tau) \right\|^2 \tag{2.26}$$

where $h_i(t_m, \tau)$ is the CIR at the location i estimated at the time t_m. The PDP matching can be performed using the distance measures presented in the Section 2.2.2.

Meurer et al. [16] proposed using the covariance matrix of the CIR as a location fingerprint rather than the absolute value of the CIR (PDP). Triki, Oktem and Slock [17, 19] have extended the PDP fingerprinting in several aspects, including adding to the fingerprint the spatial information of the antenna array, in both receive and transmit (MIMO), as well as the Doppler shifts of the different reflections, for the case that the mobile terminal is moving. The asymptotic performance of the PDP method was investigated under various statistical models by Oktem and Slock [20, 21]. The applicability of PDP fingerprinting for UWB localization was investigated by Altahus, Troesch, and Wittneben [22], Steiner and Wittneben [23, 24].

An improved version of the power delay profile with higher time domain resolution capability and higher noise immunity, based on the super resolution techniques like MUSIC and ESPRIT was investigated by Li and Pahlavan [53], and Godaliyadda and Garg [50–52].

Chapter 3

Single-Site Emitter Localization via Multipath Fingerprinting

3.1 Problem Formulation

Consider an array composed of p sensors with arbitrary locations and arbitrary directional characteristics receiving a wideband signal $s(t)$, centered at frequency $\omega_c = 2\pi f_c$, impinging on the array through q reflections with differential delays $\tau_1, \cdots, \tau_q$, and corresponding directions $\theta_1, \cdots, \theta_q$. The outputs of the antenna array are sampled simultaneously at N times ("taps"), with an interval of $D = 1/BW$ seconds, i.e., each sensor is sampled at times $(t + \ell D)$, $\ell = 0, \ldots, N-1$, where BW is a signal bandwidth. We refer to the collection of these pN samples as a "snapshot".

We assume that the bandwidth of the signal $s(t)$ is small compared to the size of the antenna array, i.e., that the propagation delays across the array are much smaller than the inverse bandwidth of the signal, so that the narrow-band array representation is applicable. This assumption is definitely valid for the bandwidth and antenna array size in modern communication techniques such as Wi-Fi.

We further assume that the antenna array is sampled M times at $\{t_m\}$, $m = 1, \ldots, M$, forming M snapshots, and that the following conditions hold regarding the signals and the noise:

A.1 The signal is identical for all snapshots.

A.2 The directions-of-arrival and the differential-delays of the multipath reflections are identical for all the M snapshots.

A.3 The noise samples $n_i(t_m + \ell D)$; $\ell = 0, \ldots, N-1$; $m = 1, \ldots, M$; $i = 1, \ldots, p$ are i.i.d. Gaussian random variables with zero mean and unknown variance σ^2.

A.1 is valid for most modern wireless communication systems, such as Wi-Fi, since these communication systems have a repeatable signal part for synchronization and channel estimation purposes. Consequently, we can confine the sampling times to this repeatable signal part using the synchronization capabilities of the receiver. A.2 is valid provided that the M snapshots are sampled in a close vicinity of each other and consequently capture the same physical environment, i.e., the same directions-of-arrival and differential-delays.

Following [69, 73], and using complex envelope representation, the ℓ-th sample of the i-th sensor can be expressed as

$$x_i(t + \ell D) = \sum_{k=1}^{q} \gamma_k(t)\, a_i(\theta_k)\, s(t + \ell D - \tau_k)\, e^{-j\omega_c \tau_i(\theta_k)} + n_i(t + \ell D) \tag{3.1}$$

where

$s(t)$	is the complex envelope of the signal,
τ_k	is the delay of the k-th reflection relative to the reference,
$\tau_i(\theta_k)$	is the delay between the i-th sensor and the reference sensor of the k-th reflection,
$a_i(\theta_k)$	is the amplitude response of the i-th sensor to a wavefront impinging from direction θ_k,
$\gamma_k(t)$	is the complex coefficient representing the phase shift and attenuation of the k-th reflection,
$n_i(t)$	is the additive noise at the i-th sensor.

It should be pointed out that our formulation assumes that (i) $\gamma_k(t)$ is fixed during a snapshot, and (ii) $\gamma_k(t)$ may vary from snapshot to snapshot. (i) is a valid assumption since the time it takes for an indoor channel to change significantly is of the order of milliseconds [80, 81], whereas the sampling duration of a snapshot $D(N-1)$ is of the order of microseconds. (ii) is a valid assumption since the time between the snapshots is of the order of milliseconds, and hence slight emitter movement or channel variations may change from snapshot to snapshot.

Using vector notation, we can rewrite (3.1) as follows

$$\boldsymbol{x}_i(t) = \boldsymbol{A}_i \boldsymbol{\gamma}(t) + \boldsymbol{n}_i(t), i = 1, \ldots, p \tag{3.2}$$

where $\boldsymbol{x}_i(t)$ and $\boldsymbol{n}_i(t)$ are the $N \times 1$ vectors

$$\boldsymbol{x}_i(t) = [x_i(t),\ x_i(t+D),\ \ldots,\ x_i(t+(N-1)D)]^T \tag{3.3}$$

$$\boldsymbol{n}_i(t) = [n_i(t),\ n_i(t+D),\ \ldots,\ n_i(t+(N-1)D)]^T \tag{3.4}$$

$\boldsymbol{\gamma}(t)$ is the $q \times 1$ vector

$$\boldsymbol{\gamma}(t) = [\gamma_1(t),\ \ldots,\ \gamma_q(t)]^T \tag{3.5}$$

and $\boldsymbol{A}_i$ is the $N \times q$ matrix

$$\boldsymbol{A}_i = \left[a_i(\theta_1)\, e^{-j\omega_c \tau_i(\theta_1)} \boldsymbol{s}(t-\tau_1),\ \ldots,\ a_i(\theta_q)\, e^{-j\omega_c \tau_i(\theta_q)} \boldsymbol{s}(t-\tau_q)\right] \tag{3.6}$$

with $\boldsymbol{s}(t-\tau_i)$ being the $N \times 1$ vector

$$\boldsymbol{s}(t-\tau_i) = [s(t-\tau_i),\ \ldots,\ s(t+(N-1)D-\tau_i)]^T \tag{3.7}$$

Combining the $\boldsymbol{x}_i(t)$ vectors $(i = 1, \ldots, p)$ into the $pN \times 1$ "snapshot" vector $\boldsymbol{x}(t)$, we can rewrite (3.2) as

$$\boldsymbol{x}(t) = \boldsymbol{A}\boldsymbol{\gamma}(t) + \boldsymbol{n}(t) \tag{3.8}$$

where $\boldsymbol{x}(t)$ and $\boldsymbol{n}(t)$ are the $pN \times 1$ vectors

$$\boldsymbol{x}(t) = \left[\boldsymbol{x}_1^T(t),\ \ldots,\ \boldsymbol{x}_p^T(t)\right]^T \tag{3.9}$$

$$\boldsymbol{n}(t) = \left[\boldsymbol{n}_1^T(t),\ \ldots,\ \boldsymbol{n}_p^T(t)\right]^T \tag{3.10}$$

and $\boldsymbol{A}$ is the $pN \times q$ matrix

$$\boldsymbol{A} = \left[\boldsymbol{a}(\theta_1) \otimes \boldsymbol{s}(t-\tau_1),\ \ldots,\ \boldsymbol{a}(\theta_q) \otimes \boldsymbol{s}(t-\tau_q)\right] \tag{3.11}$$

with $\otimes$ denoting the Kronecker product, and $\boldsymbol{a}(\theta_k)$ is the steering vector of the array towards direction θ_k, given by

$$\boldsymbol{a}(\theta_k) = \left[a_1(\theta_k)\, e^{-j\omega_c \tau_1(\theta_k)},\ \ldots,\ a_p(\theta_k)\, e^{-j\omega_c \tau_p(\theta_k)}\right]^T \tag{3.12}$$

We shall refer to the columns of matrix $\boldsymbol{A}$ as the *direction-delay vectors* and to the span of the columns of the matrix $\boldsymbol{A}$ as the *spatial-temporal signal subspace*. Note that

the matrix $\boldsymbol{A}$ captures all the direction-of-arrival and the differential-delay information of the multipath reflections.

As will become clear in the sequel, this spatial-temporal signal subspace will be the basis for our location fingerprint.

3.2 Conditions for Unique Localization

In this section, we present necessary and sufficient conditions that guarantee unique localization.

The following conditions, characterizing the array and the propagation environment, are assumed for the analysis:

B.1 Any pN distinct direction-delay vectors are linearly independent.

B.2 The number of reflections is smaller than the length of *direction-delay vectors*, namely $q < pN$.

We should point out that these conditions are mild and are obeyed in most practical cases.

Following (3.8) and ignoring the noise, since the noise is decoupled from the uniqueness problem by its nature, the M snapshots of the vector $\boldsymbol{x}(t)$ taken at $t_1, \ldots, t_M$ can be expressed as

$$\boldsymbol{X} = \boldsymbol{A}(\boldsymbol{\theta}, \boldsymbol{\tau})\, \boldsymbol{\Gamma} \tag{3.13}$$

where $\boldsymbol{X}$ is the $pN \times M$ matrix

$$\boldsymbol{X} = \left[\boldsymbol{x}(t_1), \ \ldots \ , \boldsymbol{x}(t_M)\right] \tag{3.14}$$

$\boldsymbol{\Gamma}$ is the $q \times M$ matrix of the reflections' coefficients

$$\boldsymbol{\Gamma} = \left[\boldsymbol{\gamma}(t_1), \ \ldots \ , \boldsymbol{\gamma}(t_M)\right] \tag{3.15}$$

and $\boldsymbol{A}(\boldsymbol{\theta}, \boldsymbol{\tau}) \equiv \boldsymbol{A}$ is the $pN \times q$ matrix defined in (3.11), with $\boldsymbol{\theta} = \{\theta_1, \ldots, \theta_q\}$ and $\boldsymbol{\tau} = \{\tau_1, \ldots, \tau_q\}$ denoting the directions-of-arrival and differential-delays of emitter reflections. Note that $\boldsymbol{\theta}$ and $\boldsymbol{\tau}$ are the only parameters characterizing the emitter location.

Our objective is to specify necessary and sufficient conditions under which the solution $(\boldsymbol{\theta}, \boldsymbol{\tau}, \boldsymbol{\Gamma})$ of the set of equations (3.13) is unique for every batch $\boldsymbol{X}$. To this end, let η

denote the rank of the $q \times M$ matrix $\mathbf{\Gamma}$

$$\eta = rank\left(\mathbf{\Gamma}\right) = rank\left(\mathbf{\Gamma}\mathbf{\Gamma}^{H}\right) \tag{3.16}$$

Following [71, 76], we can state the following:
An array satisfying conditions B.1-B.2 can uniquely localize sources having q reflections if

$$q < \frac{pN + \eta}{2} \tag{3.17}$$

The line of proof is analogous to [71, 76] and is based on establishing that if (3.17) holds true then for every $\boldsymbol{X}$ we have

$$\boldsymbol{X} = \boldsymbol{A}\left(\boldsymbol{\theta}, \boldsymbol{\tau}\right)\mathbf{\Gamma} \neq \boldsymbol{A}\left(\boldsymbol{\theta}', \boldsymbol{\tau}'\right)\mathbf{\Gamma'} \tag{3.18}$$

for any $\left(\boldsymbol{\theta}', \boldsymbol{\tau}'\right) \neq \left(\boldsymbol{\theta}, \boldsymbol{\tau}\right)$ and any set of Γ'. Namely, that the set of directions-of-arrival and differential-delays uniquely specifies the obtained data $\boldsymbol{X}$.

Two special cases are of the particular interest. The first case is $\eta = q$, occurring when the multipath coefficients are uncorrelated. In this case, the necessary and sufficient condition for unique localization (3.17) is $q < pN$. By B.2, this implies that uniqueness is always assured in this case. The second case is $\eta = 1$, occurring either when the multipath coefficients are fully correlated or in case when $M = 1$. In this case, the necessary and sufficient condition for unique localization is $q < \left(pN + 1\right)/2$.

These results show that the higher is the size pN of the spatial-temporal covariance matrix, and the higher is the rank η of the multipath coefficients matrix $\mathbf{\Gamma}$, the higher is the number q of multipath reflections the array can uniquely localize.

3.3 The ML Spatial-Temporal Similarity Metric

To derive a similarity-metric for the fingerprint matching, we resort to the estimation of the matrix $\boldsymbol{A}$ using the Maximum Likelihood (ML) criterion.

To this end, we assume that the complex attenuations $\boldsymbol{\gamma}\left(t\right)$ are unknown deterministic quantities that need to be estimated in conjunction with the spatial-temporal matrix $\boldsymbol{A}$. Assuming that the received vector $\boldsymbol{x}(t)$ is sampled at times $t_1, \ldots, t_M$, yielding M i.i.d

snapshots by A.3, the conditional p.d.f. of the sampled data is given by

$$p\left(\boldsymbol{x}\left(t_1\right),\ldots,\boldsymbol{x}\left(t_M\right)\left|\boldsymbol{A},\boldsymbol{\Gamma},\sigma^2\right.\right)=\prod_{m=1}^{M}\frac{1}{\pi^{pN}\det\left[\sigma^2\boldsymbol{I}\right]}\cdot\exp\left(-\frac{1}{\sigma^2}\left\|\boldsymbol{x}\left(t_m\right)-\boldsymbol{A}\boldsymbol{\gamma}\left(t_m\right)\right\|^2\right) \tag{3.19}$$

The ML estimator (MLE), following [74], is given by

$$\left[\hat{\sigma}^2,\hat{\boldsymbol{A}},\hat{\boldsymbol{\Gamma}}\right]=\underset{\sigma^2,\boldsymbol{A},\boldsymbol{\Gamma}}{\arg\max}\left\{-MpN\log\sigma^2-\frac{1}{\sigma^2}\sum_{m=1}^{M}\left\|\boldsymbol{x}\left(t_m\right)-\boldsymbol{A}\boldsymbol{\gamma}\left(t_m\right)\right\|^2\right\} \tag{3.20}$$

After straightforward derivation and elimination of constant terms, we get

$$\left[\hat{\boldsymbol{A}},\hat{\boldsymbol{\Gamma}}\right]=\underset{\boldsymbol{A},\,\boldsymbol{\Gamma}}{\arg\min}\sum_{m=1}^{M}\left\|\boldsymbol{x}\left(t_m\right)-\boldsymbol{A}\boldsymbol{\gamma}\left(t_m\right)\right\|^2 \tag{3.21}$$

Minimization now with respect to $\boldsymbol{\Gamma}$, yields

$$\hat{\boldsymbol{\gamma}}\left(t_m\right)=\left(\boldsymbol{A}^H\boldsymbol{A}\right)^{-1}\boldsymbol{A}^H\boldsymbol{x}\left(t_m\right) \tag{3.22}$$

where H denotes the Hermitian conjugate.

Substituting (3.22) back into (3.21), yields

$$\hat{\boldsymbol{A}}=\underset{\boldsymbol{A}}{\arg\min}\sum_{m=1}^{M}\left\|\boldsymbol{x}\left(t_m\right)-\boldsymbol{P}_A\boldsymbol{x}\left(t_m\right)\right\|^2=\underset{\boldsymbol{A}}{\arg\max}\sum_{m=1}^{M}\left\|\boldsymbol{P}_A\boldsymbol{x}\left(t_m\right)\right\|^2 \tag{3.23}$$

where $\boldsymbol{P}_A$ is the projection operator onto the space spanned by the columns of the matrix $\boldsymbol{A}$.

$$\boldsymbol{P}_A=\boldsymbol{A}\left(\boldsymbol{A}^H\boldsymbol{A}\right)^{-1}\boldsymbol{A}^H \tag{3.24}$$

It can be easily verified that (3.23) can also be written as

$$\hat{\boldsymbol{A}}=\underset{\boldsymbol{A}}{\arg\max}\,Tr\left\{\boldsymbol{P}_A\hat{\boldsymbol{R}}\right\} \tag{3.25}$$

where $Tr\left\{\cdot\right\}$ is the trace operator, and $\hat{\boldsymbol{R}}$ is the sample-covariance matrix

$$\hat{\boldsymbol{R}}=\frac{1}{M}\sum_{m=1}^{M}\boldsymbol{x}\left(t_m\right)\boldsymbol{x}^H\left(t_m\right) \tag{3.26}$$

It follows from (3.23) that the ML estimator of the spatial-temporal matrix $\boldsymbol{A}$ is obtained by searching for the spatial-temporal signal subspace projection matrix $\boldsymbol{P}_A$ that is closest to the sampled vectors $\left\{\boldsymbol{x}\left(t_m\right)\right\}$, $m=1,\ldots,M$, with the "closeness" measured by the modulus of the projection of the vectors onto this subspace.

3.4 Signal Subspace Based Localization

According to the ML criterion (3.25), the localization is carried out by searching in the database for the location i that maximizes the following expression

$$\hat{i} = \underset{\{\boldsymbol{P}_i\}}{\arg\max}\, Tr\left\{\boldsymbol{P}_i \hat{\boldsymbol{R}}\right\} \tag{3.27}$$

where $\hat{\boldsymbol{R}}$ is the sample-covariance matrix (3.26) and $\boldsymbol{P}_i$ is the projection operator onto the signal subspace corresponding to the i-th location.

3.4.1 The Generation of the Fingerprint Database

The fingerprint database is composed of the sample-covariance and projection matrices $\left\{\hat{\boldsymbol{R}}_i, \boldsymbol{P}_i\right\}$ of all the locations and is pre-computed in the off-line phase.

The sample-covariance matrix $\hat{\boldsymbol{R}}_i$ is computed from L snapshots of the received vector $\boldsymbol{x}(t)$, collected in the close vicinity of location i. In the close vicinity of a point the directions-of-arrival and the differential-delays of the multipath reflections are essentially the same. In contrast, the coefficients vector $\boldsymbol{\gamma}(t)$ varies from location to location and may vary from snapshot to snapshot. The spatial averaging in the close vicinity of a point therefore ensures that the matrix $\boldsymbol{\Gamma}$ becomes full rank and hence that the full dimension of the signal subspace is captured. The spatial averaging also helps in providing a more comprehensive and robust characterization of the multipath reflections.

The expected value of $\hat{\boldsymbol{R}}_i$, omitting the index i for clarity of the presentation, is given by

$$\boldsymbol{R} = E\left[\boldsymbol{x}(t)\,\boldsymbol{x}^H(t)\right] = \boldsymbol{A}\boldsymbol{\Sigma}\boldsymbol{A}^H + \sigma^2\boldsymbol{I} \tag{3.28}$$

where

$$\boldsymbol{\Sigma} = E\left[\boldsymbol{\gamma}(t)\,\boldsymbol{\gamma}^H(t)\right] \tag{3.29}$$

Recalling B.2 and assuming that the $q \times q$ matrix $\boldsymbol{\Sigma}$ has full rank, which is a valid assumption provided that the L snapshots are collected as described above, it can be easily verified [66, 72] that the eigenvalues and eigenvectors of $\boldsymbol{R}$, denoted by $\{\lambda_1 \geq \lambda_2 \geq \cdots \geq \lambda_{pN}\}$ and $\{\boldsymbol{v}_1, \boldsymbol{v}_2, \ldots, \boldsymbol{v}_{pN}\}$, respectively, have the following important property:

The subspace spanned by the eigenvectors $\boldsymbol{V}_q = \{\boldsymbol{v}_1, \boldsymbol{v}_2, \ldots, \boldsymbol{v}_q\}$ is identical to the subspace spanned by the columns of the matrix $\boldsymbol{A}$, i.e. $span\left(\boldsymbol{V}_q\right) = span\left(\boldsymbol{A}\right)$.

Based on this identity, the estimation of the projection matrix $\boldsymbol{P}_i$ of the i-th location is carried out as follows:

1) Calculate the sample-covariance matrix $\hat{\boldsymbol{R}}_i$ of location i by

$$\hat{\boldsymbol{R}}_i = \frac{1}{L}\sum_{l=1}^{L} \boldsymbol{x}\left(t_l\right)\boldsymbol{x}^H\left(t_l\right) \tag{3.30}$$

2) Perform an eigenvalue decomposition of $\hat{\boldsymbol{R}}_i$.

3) Estimate the signal subspace dimension $\hat{q}$.

4) Select the first $\hat{q}$ eigenvectors of $\hat{\boldsymbol{R}}_i$ corresponding to the signal subspace: $\boldsymbol{V}_{\hat{q}} = \{\boldsymbol{v}_1, \boldsymbol{v}_2, \ldots, \boldsymbol{v}_{\hat{q}}\}$.

5) Estimate the projection matrix by $\hat{\boldsymbol{P}}_i = \boldsymbol{V}_{\hat{q}}\left(\boldsymbol{V}_{\hat{q}}^H\boldsymbol{V}_{\hat{q}}\right)^{-1}\boldsymbol{V}_{\hat{q}}^H$.

3.4.2 Signal Subspace Dimension Estimation

The estimation of the signal subspace dimension is a well-known problem in array processing and numerous techniques have been developed to solve it [66, 72, 75].

The problem at hand, however, is different than the classical problem addressed in the literature. Here we are targeting a rich multipath environment, such as in indoor venues and shopping malls, where the number of reflections is usually very large, and want to ensure that the subspace dimension captures only the more dominant reflections in the environment and not the numerous low energy reflections. These low energy reflections may not be stable enough in real life scenarios because of movement of people and changing environment. To illustrate this point, refer to Figure 3.1, where a typical multipath, characterizing the indoor environment shown in Figure 3.2, is presented. The multipath signals originate from the location denoted by the green dot, $(x_i, y_i) = (34, 66)$, and captured by an antenna array at the orange dot. Figure 3.1 shows the two-dimensional plot of the power of the multipath signals, parameterized by the angle-of-arrival and time-of-arrival. Note the large number of reflections and their high dynamic range, and especially the large number of low energy reflections that are close to the noise floor.

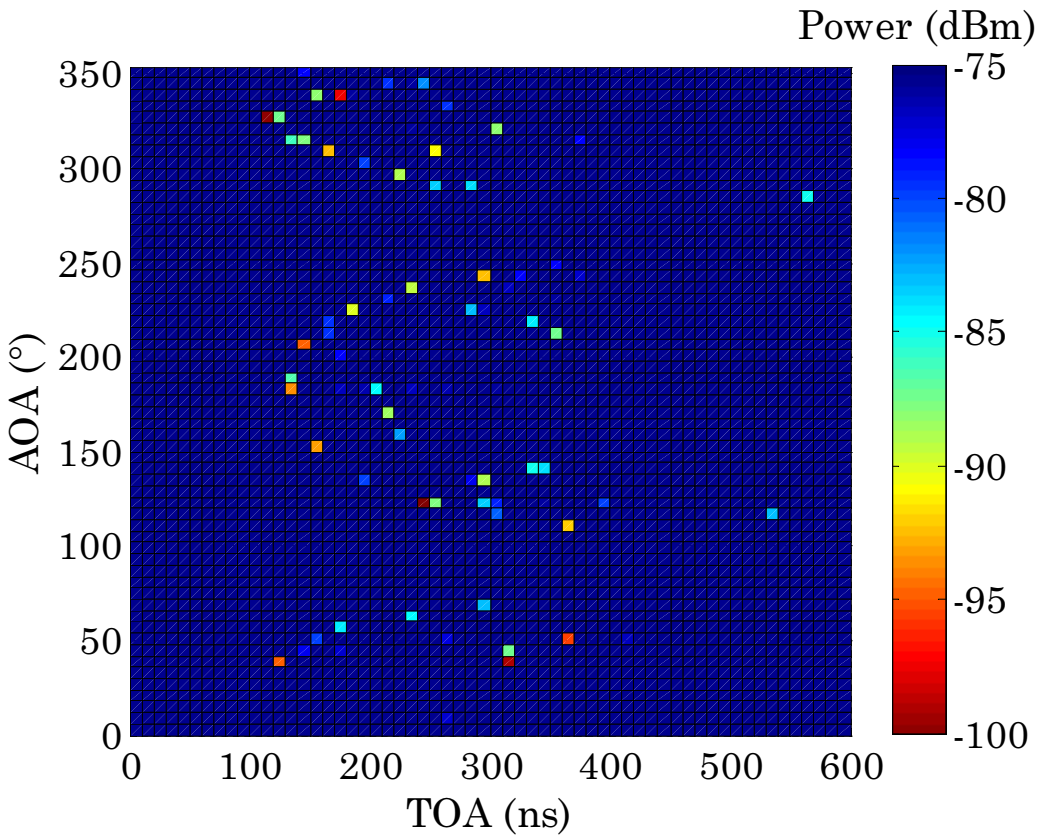

FIGURE 3.1: The spatial-temporal power profile of the multipath reflections corresponding to the location of green dot, $(x_i, y_i) = (34, 66)$m , in Figure 3.2.

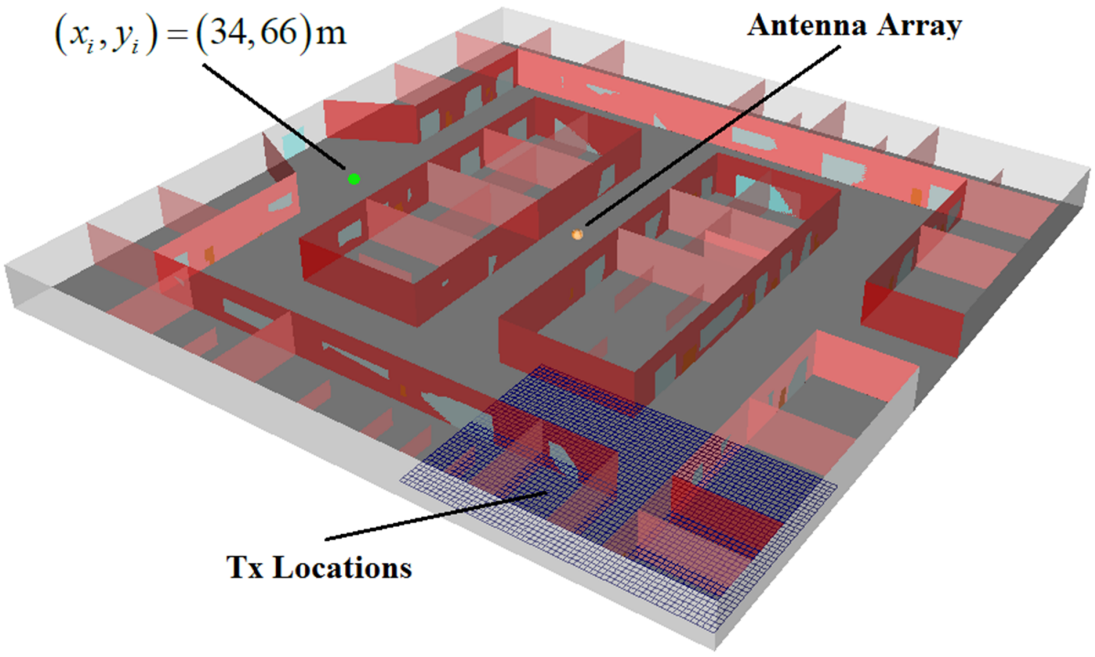

FIGURE 3.2: The simulation environment.

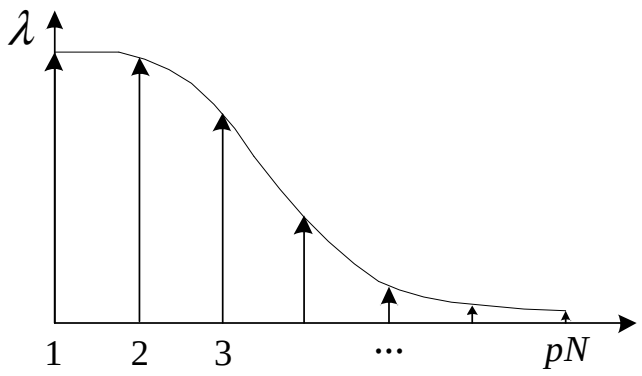

FIGURE 3.3: A typical eigenvalue profile of the signal covariance matrix.

A typical profile of the eigenvalues of the covariance matrix is shown in Figure 3.3. The small eigenvalues typically capture the low energy multipath reflections that should, as explained above, be excluded from the subspace formation. Based on this observation, we have disqualified the classical technique based on information theoretic criteria [70] that is sensitive to low energy signals, and selected a more robust technique that captures only the dominant reflections. Specifically, the signal subspace dimension $\hat{q}$ is estimated by the number of large eigenvalues that capture, say, 90% of the signal energy

$$\hat{q} = \left(\min Q,\ s.t.\ \frac{\sum_{i=1}^{Q} \lambda_i}{\sum_{i=1}^{pN} \lambda_i} \geq \alpha \;\middle|\; Q = 1, 2, \ldots, pN \right) \tag{3.31}$$

where $\{\lambda_1 \geq \lambda_2 \geq \cdots \geq \lambda_{pN}\}$ and $0 \leq \alpha \leq 1$ is a parameter set, say, to 0.9.

3.4.3 The Similarity-Profile Matching Criterion

As described above, the localization can be carried out by searching for the index i that maximizes the ML criterion (3.27). Yet, due to ambiguity inherent in the physical environment, some locations may have similar spatial-temporal fingerprints, and as a result give rise to a certain level of ambiguity error. To address this problem we next introduce a matching technique that better copes with these ambiguities.

To this end, following [4], we introduce the notion of similarity-profile (SP). The SP of the i-th location $\boldsymbol{f}_i$ captures the similarity of the received data at the i-th location

to the fingerprints in the database and is defined by

$$\boldsymbol{f}_i = [f_{i1}, \ \ldots \ , f_{iK}] \tag{3.32}$$

where K is the number of locations in the database and f_{ij} is the similarity between the data captured in the i-th location to the fingerprint of the j-th location

$$f_{ij} = Tr\left\{\boldsymbol{P}_j \widetilde{\boldsymbol{R}}_i\right\} \tag{3.33}$$

with

$$\widetilde{\boldsymbol{R}}_i = \hat{\boldsymbol{R}}_i \Big/ Tr\left\{\hat{\boldsymbol{R}}_i\right\} \tag{3.34}$$

Notice that the covariance matrices $\left\{\hat{\boldsymbol{R}}_i\right\}$ have been normalized to eliminate dependence on the power of the received signals. This is done to cope with potential power change of the source between the off-line and on-line phases.

The motivation for the SP matching is based on the observation that both similar and dissimilar fingerprints provide useful identification information on the query fingerprint. Consequently, it is beneficial to employ the whole similarity vector $\boldsymbol{f}_i$ as the i-th location identifier.

To better illustrate this point, we refer to Figure 3.4 showing the SP belonging to the green dot, $(x, y) = (34, 66)\, m$, in Figure 3.2. The SP vector (3.32) is presented as a two-dimensional plot, with color coding representing the level of similarity f_{ij} (3.33) between the i-th point and all the other points in the data-base. Note that this plot peaks at $(x, y) = (34, 66)\, m$, as expected, but also at another point $(x, y) = (33, 10)\, m$, reflecting a potential ambiguity point. To cope better with such potential ambiguities, we propose to use the whole similarity profile, with its peaks and valleys, as the fingerprint of the i-th location.

Using the SP notion we can represent the database, constructed during the off-line phase, by the similarity-matrix $\boldsymbol{F}$, given by

$$\boldsymbol{F} = \begin{bmatrix} \boldsymbol{f}_1 \\ \boldsymbol{f}_2 \\ \vdots \\ \boldsymbol{f}_K \end{bmatrix} \tag{3.35}$$

According to the SP criterion the localization is carried out by searching over the

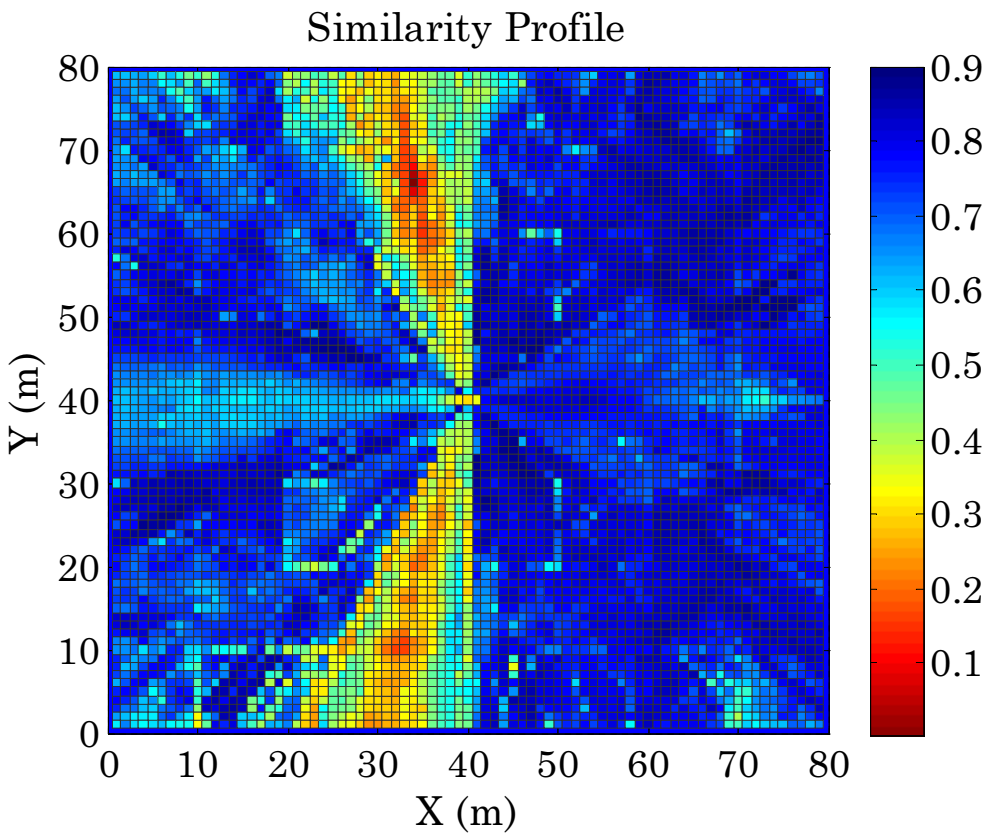

FIGURE 3.4: The similarity profile corresponding to the location of the green dot, $(x, y) = (34, 66)\, m$, in Figure 3.2.

database $\boldsymbol{F}$ for the SP that best matches the query SP obtained from the received signals. That is,

$$\hat{i} = \underset{\{\text{location } i\}}{\arg\min} \left\| \boldsymbol{f}_i - \widehat{\boldsymbol{f}} \right\|_2^2 \tag{3.36}$$

where $\widehat{\boldsymbol{f}}$ is the query SP obtained from the received signals,

$$\widehat{\boldsymbol{f}} = \left[\widehat{f}_1, \ \ldots \ , \widehat{f}_K\right] = \left[Tr\left\{\boldsymbol{P}_1\widehat{\boldsymbol{R}}\right\}, \ \ldots \ , Tr\left\{\boldsymbol{P}_K\widehat{\boldsymbol{R}}\right\}\right] \tag{3.37}$$

with

$$\widehat{\boldsymbol{R}} = \hat{\boldsymbol{R}} \Big/ Tr\left\{\hat{\boldsymbol{R}}\right\} \tag{3.38}$$

Note that projection matrices $\{\boldsymbol{P}_i\}$ and the similarity-matrix $\boldsymbol{F}$ are calculated during the off-line phase, whereas $\widehat{\boldsymbol{f}}$ is calculated in the on-line phase from the sample-covariance matrix $\hat{\boldsymbol{R}}$.

In the typical case, wherein $K \gg (pN)^2$, the computational load of (3.36) can be significantly reduced by leveraging the properties of the L_2 norm. Indeed, following

[28] and using the well-known vec(·) operator, which forms a column vector from the columns of a matrix by stacking them one under the other, we can write

$$\left\|\boldsymbol{f}_i - \widehat{\boldsymbol{f}}\right\|_2^2 = \left\|\boldsymbol{P}\left(\tilde{\boldsymbol{r}}_i - \widehat{\boldsymbol{r}}\right)\right\|_2^2 = \left(\tilde{\boldsymbol{r}}_i - \widehat{\boldsymbol{r}}\right)^H \boldsymbol{P}^H \boldsymbol{P}\left(\tilde{\boldsymbol{r}}_i - \widehat{\boldsymbol{r}}\right) \tag{3.39}$$

where

$$\left(\tilde{\boldsymbol{r}}_i - \widehat{\boldsymbol{r}}\right) = \left(\mathrm{vec}\left(\widetilde{\boldsymbol{R}}_{\mathrm{i}}\right) - \mathrm{vec}\left(\widehat{\boldsymbol{R}}\right)\right) \tag{3.40}$$

$$\boldsymbol{P} = \left[\mathrm{vec}\left(\boldsymbol{P}_1^{\mathrm{T}}\right), \ \ldots \ , \mathrm{vec}\left(\boldsymbol{P}_{\mathrm{K}}^{\mathrm{T}}\right)\right]^T \tag{3.41}$$

Assuming $\boldsymbol{P}^H\boldsymbol{P}$ has a full rank and denoting by $\boldsymbol{G}$ be the Cholesky factor of $\boldsymbol{P}^H\boldsymbol{P}$, i.e.,

$$\boldsymbol{P}^H\boldsymbol{P} = \boldsymbol{G}\boldsymbol{G}^H \tag{3.42}$$

we can rewrite (3.36) as

$$\hat{i} = \underset{\{\text{location i}\}}{\arg\min} \left\|\boldsymbol{G}^H\left(\tilde{\boldsymbol{r}}_i - \widehat{\boldsymbol{r}}\right)\right\|_2^2 \tag{3.43}$$

Now, since $\boldsymbol{G}$ is a $(pN)^2 \times (pN)^2$ matrix, as compared to $\boldsymbol{P}$ which is $K \times (pN)^2$, (3.43) provides significant computational saving compared to (3.36). Indeed, in a typical scenario, with $p = 6$, $N = 4$ and $K = 10,000$, this technique provides more than an order of magnitude savings in both the computational load and storage.

Note also that since $\boldsymbol{G}$ and $\{\tilde{\boldsymbol{r}}_i\}$ are pre-computed in the off-line phase, the on-line computation is rather mild and involves essentially only multiplication of $\boldsymbol{G}$ with $\widehat{\boldsymbol{r}}$, the $(pN)^2$ vector of the elements of the sample-covariance matrix $\widehat{\boldsymbol{R}}$, and a search over the data-base for the minimum of the L_2 norm (3.43). We would like to point out that the computational load involved in the search over the database can be significantly reduced, by organizing the search in a tree-structured manner and leveraging the triangular inequality the L_2 norm obeys, as in [28].

3.5 Channel Impulse Response Based Localization

In this section we show that our method is applicable also to localization using the array channel impulse response (CIR).

In modern communication systems the CIR is usually obtained by exploiting a known signal, referred to as training signal, specifically included in the transmitted signal for

this purpose. The CIR is obtained by de-convolution of the received signal with this training signal.

It follows from the problem formulation presented in Section 3.1 that the ℓ-th sample of the estimated CIR corresponding to the i-th sensor and m-th snapshot can be expressed by

$$\hat{h}_i\left(t_m+\ell D\right)=\sum_{k=1}^{q}\gamma_k\left(t_m\right)a_i\left(\theta_k\right)g\left(t_m+\ell D-\tau_k\right)e^{-j\omega_c\tau_i(\theta_k)}+n_i\left(t_m+\ell D\right) \tag{3.44}$$

where $g(t)$ is the convolution of the transmit and receive filters and $n_i(t+\ell D)$, $\ell=0,\ldots,N-1$ are samples of the CIR estimation noise. We assume that the estimation noise conforms to the assumption A.3.

Note that expression (3.1) and (3.44) are essentially identical, differing only in the signal part. Yet, since $g(t)$ is repeatable from snapshot to snapshot, A.1-A.2 apply here as well.

Stacking the estimated CIR samples in a vector form analogously to (3.9), we get

$$\hat{\boldsymbol{h}}\left(t\right)=\boldsymbol{A}\boldsymbol{\gamma}\left(t\right)+\boldsymbol{n}\left(t\right) \tag{3.45}$$

Since this expression is identical to our problem formulation (3.8), we can straightforwardly apply our localization method to the sample-covariance of the array CIR, given by

$$\hat{\boldsymbol{C}}=\frac{1}{M}\sum_{m=1}^{M}\hat{\boldsymbol{h}}\left(t_m\right)\hat{\boldsymbol{h}}^H\left(t_m\right) \tag{3.46}$$

Note that our localization method differs from the PDP methods in two aspects. First, its fingerprint is based on the signal subspace spanned by the dominant reflections. Second, its matching algorithm is based on the SP criterion.

The advantage of using the CIR for localization, as compared to using the received signals with a repeatable part, is the indifference of the localization algorithm to different repeatable parts (training signals). Yet, its computational load, in both the off-line and on-line phases, is higher because of the extra de-convolution step required to obtain the CIR estimates.

3.6 Simulation Results

In this section we present simulation results illustrating the performance of the proposed localization algorithm.

To simulate a typical indoor propagation environment we used the $80m \times 80m \times 5m$ shopping mall shown in Figure 3.2. The malls walls were constructed from typical materials having typical reflection and penetration coefficients. To simulate the electromagnetic propagation we used a 3D ray tracing radio wave propagation simulator. The system parameters receiver sensitivity, transmit power and antenna gains - have been set to those typically available in off-the-shelf Wi-Fi equipment. The orange point in the center of the mall denotes the location of the antenna array. The array was a uniform circular array, with a diameter of 25 cm, having $p = 6$ omni-directional antennas. To generate the data, emitters were distributed uniformly in the mall area with 0.1m separation. A sample of the emitter locations is shown in Figure 3.2 by the blue points grid. The antenna array and the emitters were placed at a height of 2.5m and 1.5m, respectively.

The database was built as a rectangular grid with 1m separation. The test points were selected by random shifts, in both axes, from the database points. That is, random shifts, Δx_i and Δy_i, were generated independently for each database point i according to a uniform distribution $U[-1/2, 1/2]m$. This was done in order to simulate a more realistic situation wherein the test points and the database points do not coincide. The sample-covariance matrices of the database and test point were constructed from L and M snapshots, respectively, captured in a close vicinity of the database/test point. The snapshots used for the database and for the test points were different.

The signal used in the simulations was the Long Training Field (LTF) of the preamble of the 802.11a/g/n Wi-Fi packet [82], which is present in each transmitted packet and is used for channel estimation, accurate frequency offset estimation and time synchronization.

The signal-to-noise ratio (SNR) varied from 0 to 60dB according to the path loss from the base station to the emitter location and was the same in the database generation and in the tests. The eigenvalue threshold α for subspace dimension estimation (3.31) was selected to be 0.9 in all simulations.

The localization performance was evaluated by computing the cumulative distribution

function (CDF) of the position location errors, with the position location error defined by the Euclidean distance between the location of the test point and the location of the most likely database grid point selected by the localization algorithm.

3.6.1 Simulation Scenario 1

In this simulation we present the achievable localization accuracy using the ML (3.27) and the SP (3.43) matching criteria, with a varying number of antennas. The number of samples (taps) per antenna was $N = 8$ and the signal bandwidth (BW) was 20MHz, while the number of signal snapshots used for each database and test location were $L = 60$ and $M = 55$, respectively. To vary the number of antennas we used 3 and 1 out of the 6 antennas of the array.

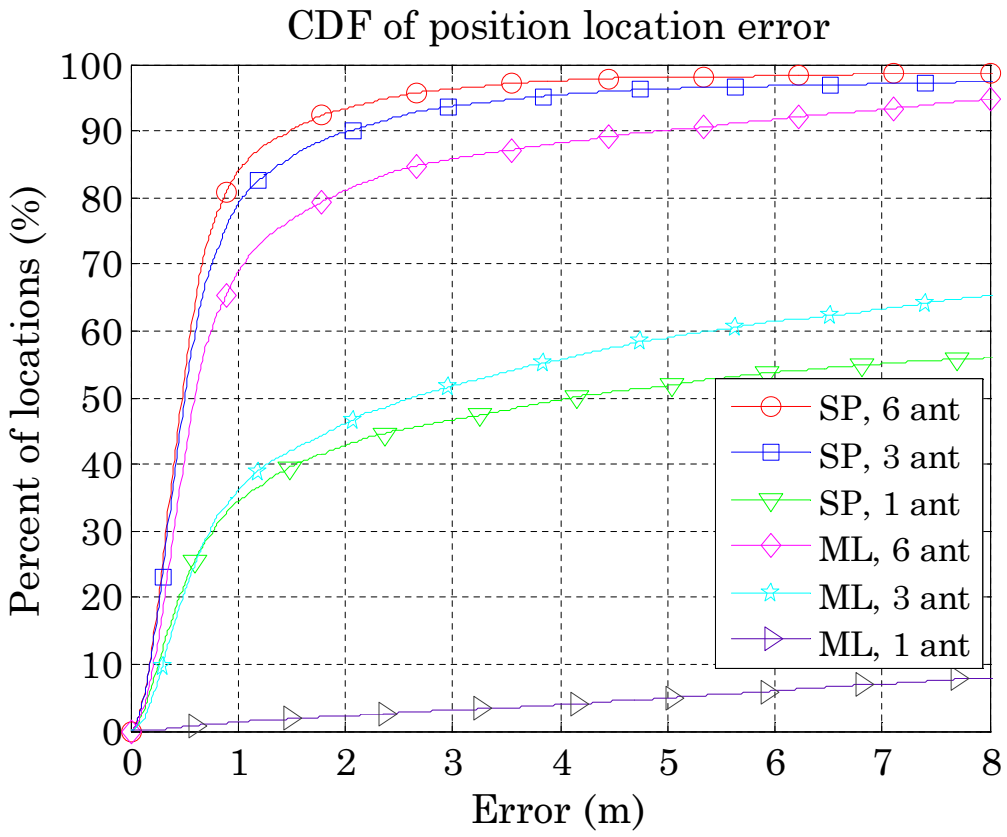

FIGURE 3.5: Performance of the SP and ML techniques for different number of antennas. The number of taps was $N = 8$, the BW=20MHz and the number of snapshots for the database and tests were $L = 60$ and $M = 55$, respectively.

As seen in Figure 3.5, the accuracy difference between the SP and the ML criteria is considerable, especially in more challenging scenarios wherein the level of ambiguity

increases, namely when the number of antennas is reduced from 6 to 3 and from 3 to 1. Since this advantage of the SP criterion was persistent in all the simulations, we have decided to omit the results of the ML criterion and concentrate on the SP in the sequel for clarity of the presentation.

Note also that though there is only marginal accuracy degradation when going from 6 antennas to 3, it is much more significant when going from 3 antennas to 1. This clearly demonstrates the crucial contribution of the spatial dimension in enabling high accuracy, especially at relatively law bandwidth of 20MHz.

3.6.2 Simulation Scenario 2

In this simulation we present the distribution of signal subspace dimension over the mall area as a function of the number of taps N. The number of antennas was $p = 6$, the BW=20MHz, and the number of database snapshots $L = 60$.

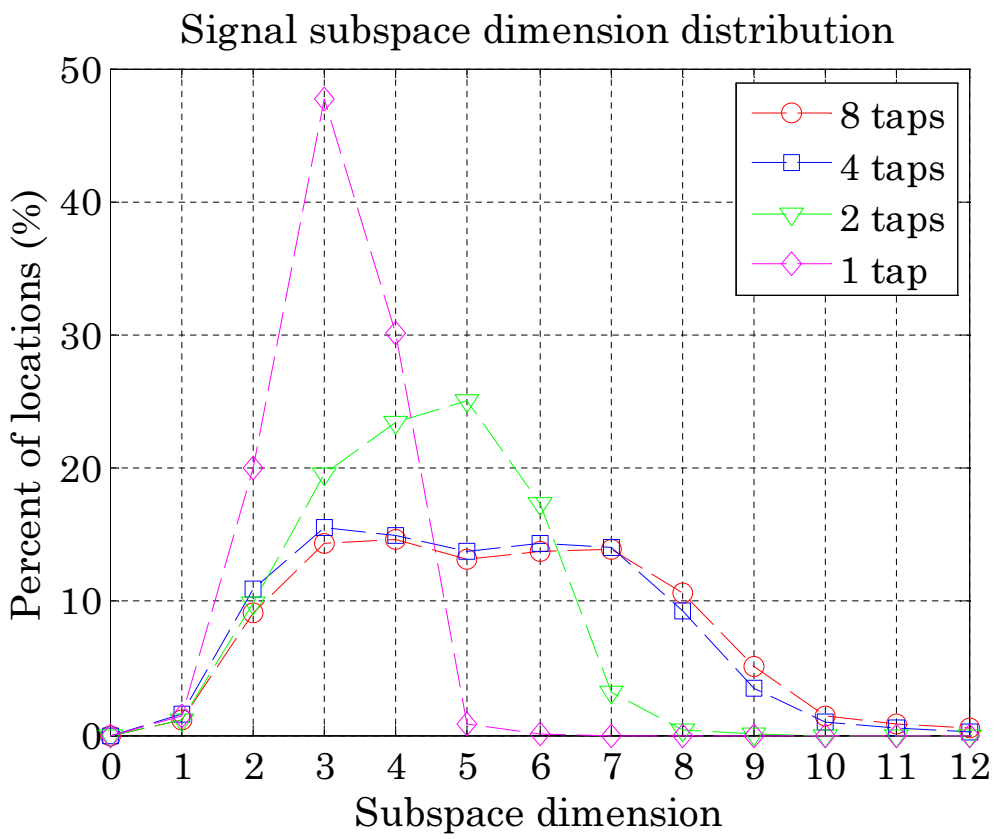

FIGURE 3.6: Signal subspace dimension distribution for different number of taps. The number of antennas was $p = 6$, the signal BW=20MHz, and the number of database snapshots $L = 60$.

As seen in Figure 3.6, the signal subspace dimension rises with the increase of the dimension pN of the snapshot vector but typically stays below 9, even when the dimension of the snapshot vector rises to 24 (for $N = 4$) and 48 (for $N = 8$).

3.6.3 Simulation Scenario 3

In this simulation we present the influence of the number of snapshots, L and M, on the localization accuracy. The signal bandwidth was 20MHz and the number of taps $N = 8$. In the first case (Figure 3.7), the number of antennas was $p = 6$ and the number of database snapshots $L = 60$, while the number of test point snapshots varied. In the second case (Figure 3.8), the number of antennas was $p = 3$ and the number of test point snapshots $M = 25$, while the number of database snapshots varied.

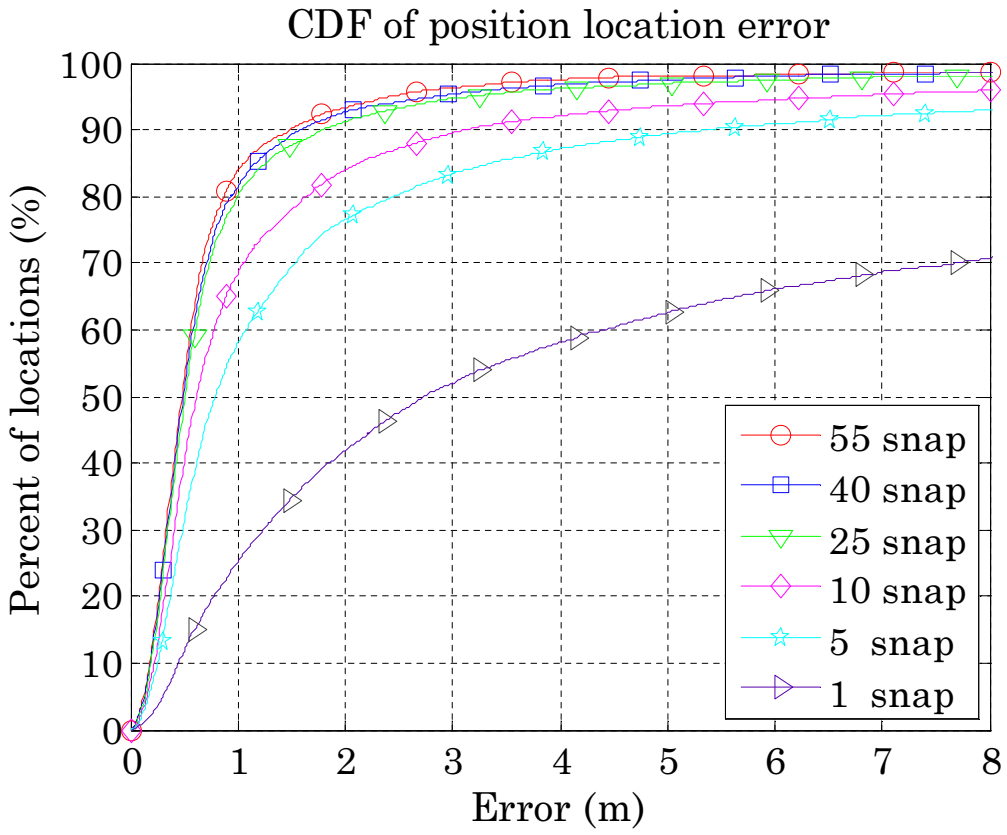

FIGURE 3.7: Performance of the SP criterion for different number of test point snapshots. The number of antennas was $p = 6$, the BW=20MHz, the number of taps $N = 8$, and the number of database snapshots $L = 60$.

As seen in Figure 3.7 and Figure 3.8, the higher the number of test point/database snapshots the higher is the accuracy. This can be attributed to the fact that the higher number of snapshots provides better covariance matrix estimation and consequently

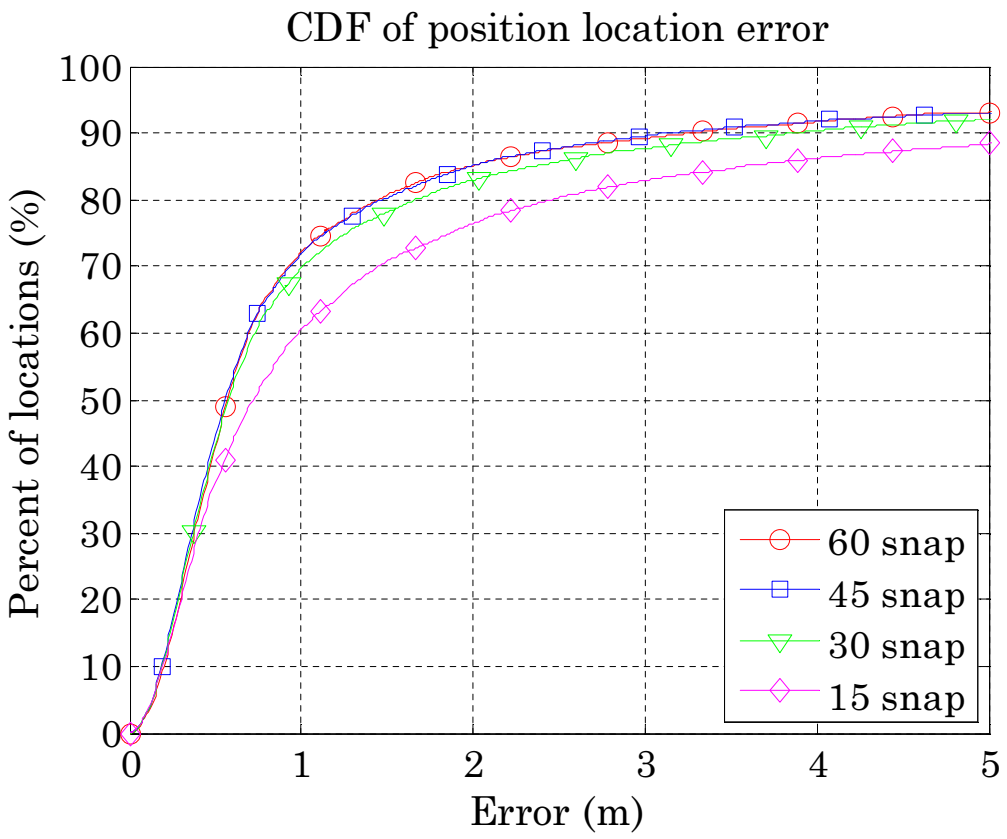

FIGURE 3.8: Performance of the SP criterion for different number of database snapshots. The number of antennas was $p = 3$, the BW=20MHz, the number of taps $N = 8$, and the number of test point snapshots $M = 25$.

better signal subspace estimation. Yet, beyond some number of snapshots, about 25-30, the improvement in accuracy is marginal. The fact that 25-30 snapshots are sufficient to fully characterize the signal subspace can be explained by the relatively low dimension of this subspace, as discussed above and shown in Figure 3.6. Since in practical applications the typical snapshot interval is of the order of milliseconds, this implies that the time necessary for localization is of the order of 100 milliseconds, which is definitely acceptable for most applications.

3.6.4 Simulation Scenario 4

In this simulation we present the influence of number of taps on the localization accuracy for a 6-antenna array and bandwidths of 20MHz and 80MHz. The number of database and test point snapshots was $L = 60$ and $M = 25$, respectively.

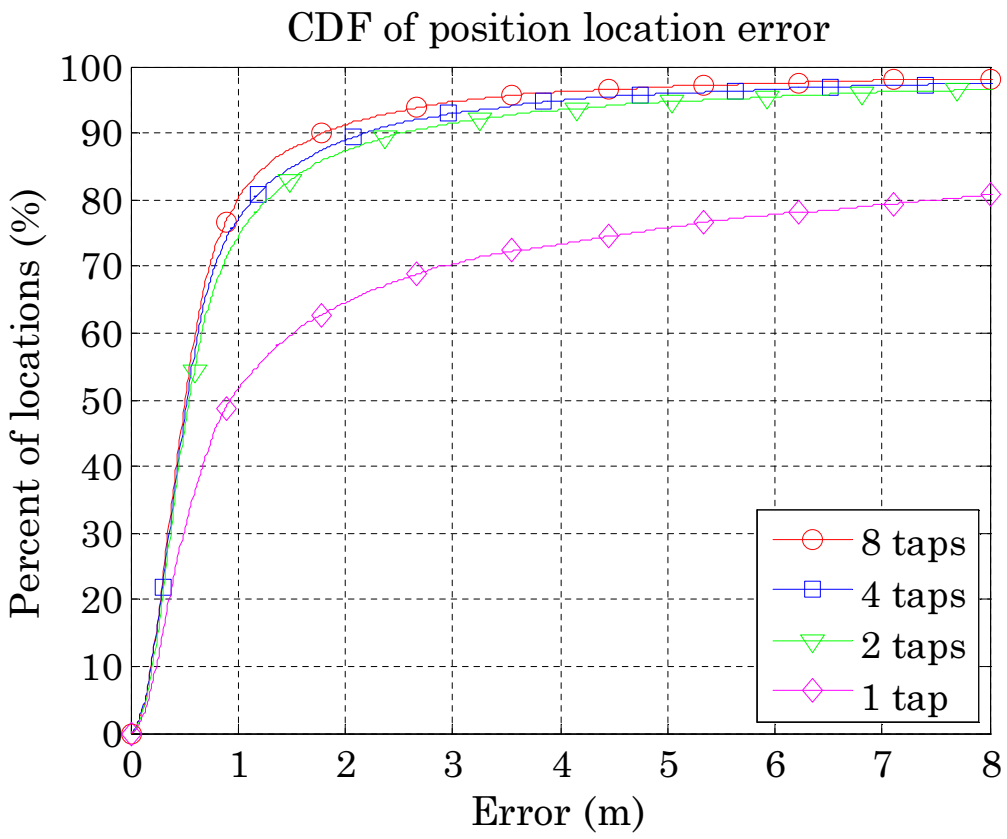

FIGURE 3.9: Performance of the SP criterion for different number of taps. The number of antennas was $p = 6$, the BW=20MHz, and the number of database and test point snapshots was $L = 60$ and $M = 25$, respectively.

As seen in Figure 3.9 and Figure 3.10, the higher is the number of taps the better is the accuracy. This can be attributed to the fact that the higher number of taps allows capturing longer-delay reflections and as a result to provide a more robust fingerprint with lower ambiguity. The improvement in accuracy for 20MHz occurs at lower number of taps than that for 80MHz since the sampling time for the 20MHz and 80MHz are 50ns and 12.5ns, respectively, implying that for a higher bandwidth a larger number of taps is required to capture the multipath delay spread.

Note also that in the case of a single tap there is a significant degradation in accuracy as well as much higher ambiguity level, reflected by the higher error in upper percentile of the CDF graph. This highlights the inability of spatial-only fingerprint to provide enough location distinction.

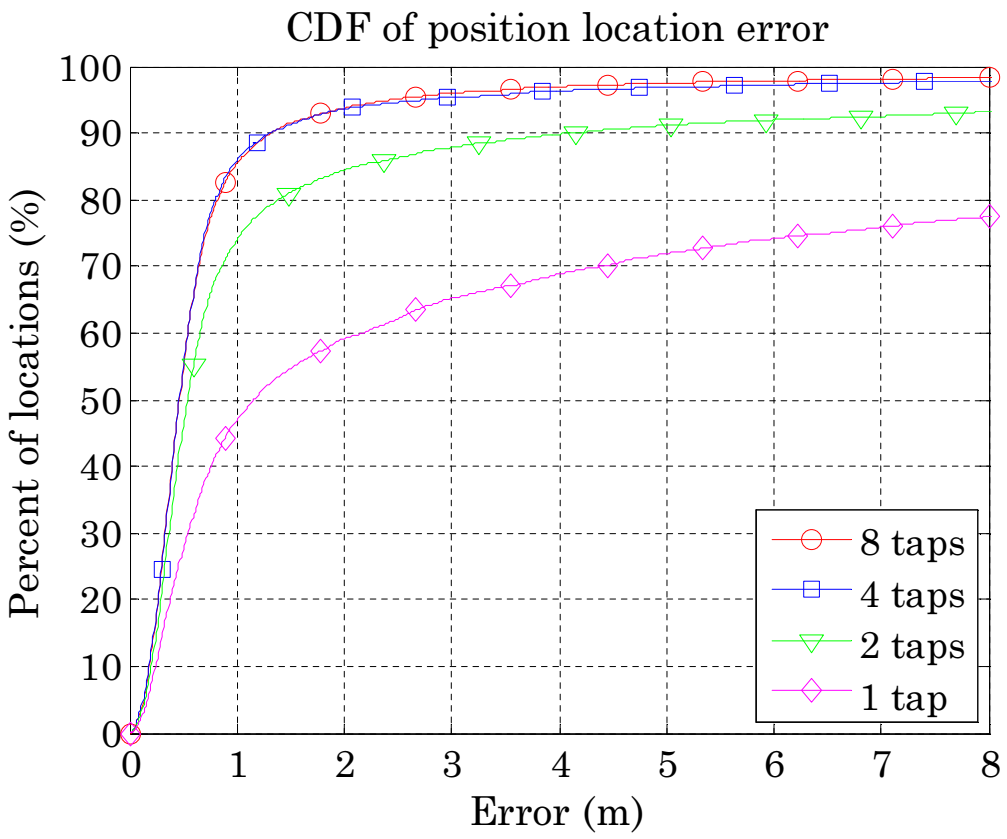

FIGURE 3.10: Performance of the SP criterion for different number of taps. The number of antennas was $p = 6$, the BW=80MHz, and the number of database and test point snapshots was $L = 60$ and $M = 25$, respectively.

3.6.5 Simulation Scenario 5

In this simulation we present the achievable accuracy for a 3-antenna array using different signal bandwidths, 20MHz, 40MHz, and 80MHz. The number of taps was $N = 8$, while the number of database and test point snapshots were $L = 60$ and $M = 10$, respectively.

As seen in Figure 3.11, the achievable accuracy improves as the bandwidth increases. Note that the effect of the larger bandwidth is more noticeable here, as compared to that between Figure 3.9 and Figure 3.10, since here the scenario is more challenging - a smaller number of antennas and test point snapshots.

3.6.6 Simulation Scenario 6

In this simulation we present the achievable accuracy in the case of $p = 1$ antenna using different signal bandwidths, 20MHz, 40MHz, and 80MHz. The simulation parameters were identical to those of scenario 1 except that here number of taps was $N = 32$.

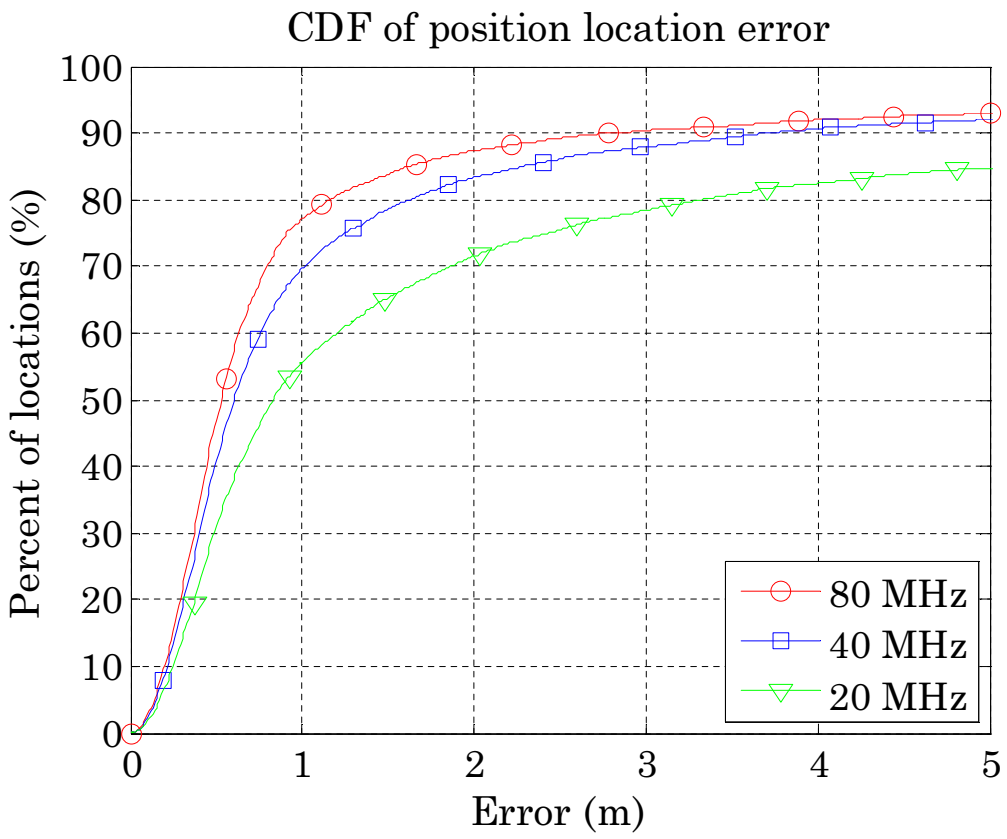

FIGURE 3.11: Performance of the SP criterion for different BWs. The number of antennas was $p = 3$, the number of taps $N = 8$, and the number of database and test point snapshots was $L = 60$ and $M = 10$, respectively.

As can be seen in Figure 3.12, there is a large improvement in accuracy as the bandwidth increases, demonstrating the importance of the improved time resolution resulting from the increased bandwidth in the case of single antenna.

Note also that the ambiguity level, reflected by the higher error in upper percentile of the CDF graph, is considerably higher than in the case of 6 and 3 antennas presented in Figure 3.5. This high level of ambiguity highlights the inability of temporal-only fingerprint to provide enough location distinction.

3.7 Real Data Results

In this section we present experimental results illustrating the performance of the proposed localization algorithm with real data.

The experiment was conducted at the $33m \times 33m \times 5m$ office floor shown in Figure 3.13. The BS was an 802.11g Wi-Fi access point (AP) having a uniform circular array,

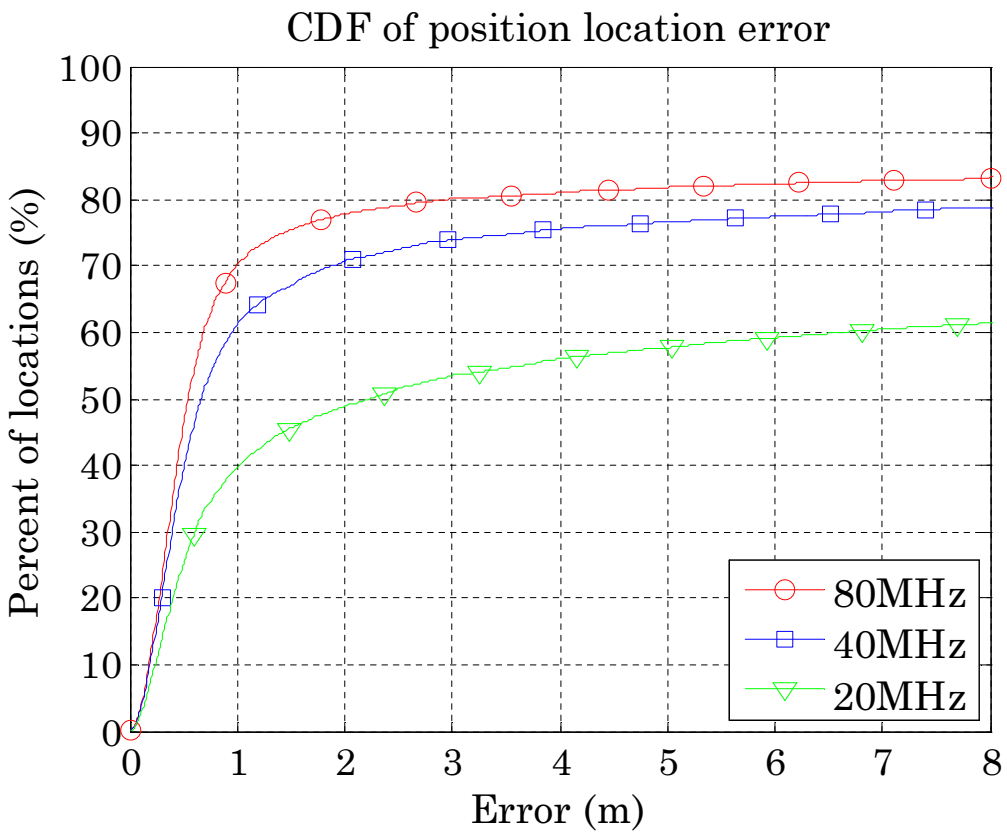

FIGURE 3.12: Performance of the SP criterion for different BWs. The number of antennas was $p = 1$, the number of taps $N = 32$, and the number of database and test point snapshots was $L = 60$ and $M = 25$, respectively.

with a diameter of 25cm and $p = 6$ omni-directional antennas. The antenna array was located at the red dot. The emitter was a laptop communicating with the BS over Wi-Fi. The antenna array and the emitter were placed at a height of 3m and 1.5m, respectively. The green square points, separated by 0.5m, denote locations of database points. The database covariance matrices were built by spatial averaging of the captured data in the vicinity of these points. The test point locations were selected by random shifts from the database points, in a similar way to the simulations.

To enable performance comparison with simulated data in both the experiment and simulation we used $p = 6$ antennas, BW of 20MHz, $N = 8$ taps, and $L = 30$ for the database and $M = 25$ for the test points. The eigenvalue threshold α for subspace dimension estimation (3.31) was selected to be 0.9. The signal used was the long training field (LTF) of the preamble of the 802.11g Wi-Fi packet [82] with BW=20MHz.

As seen in Figure 3.14, the accuracy achieved with real data is about 1m and closely matches that obtained with the simulated data. This clearly validates the proposed

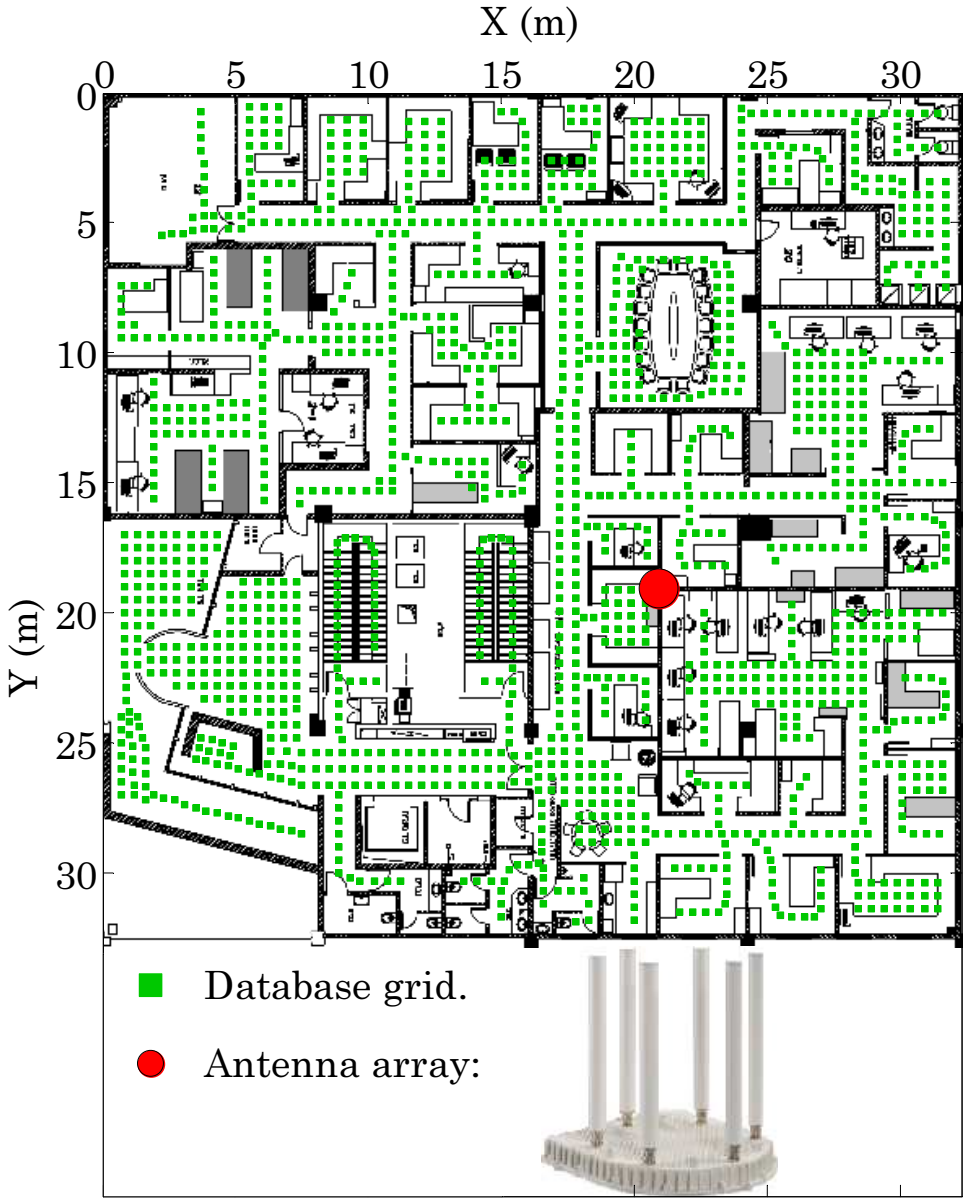

FIGURE 3.13: The office floor wherein the real data experiment was conducted.

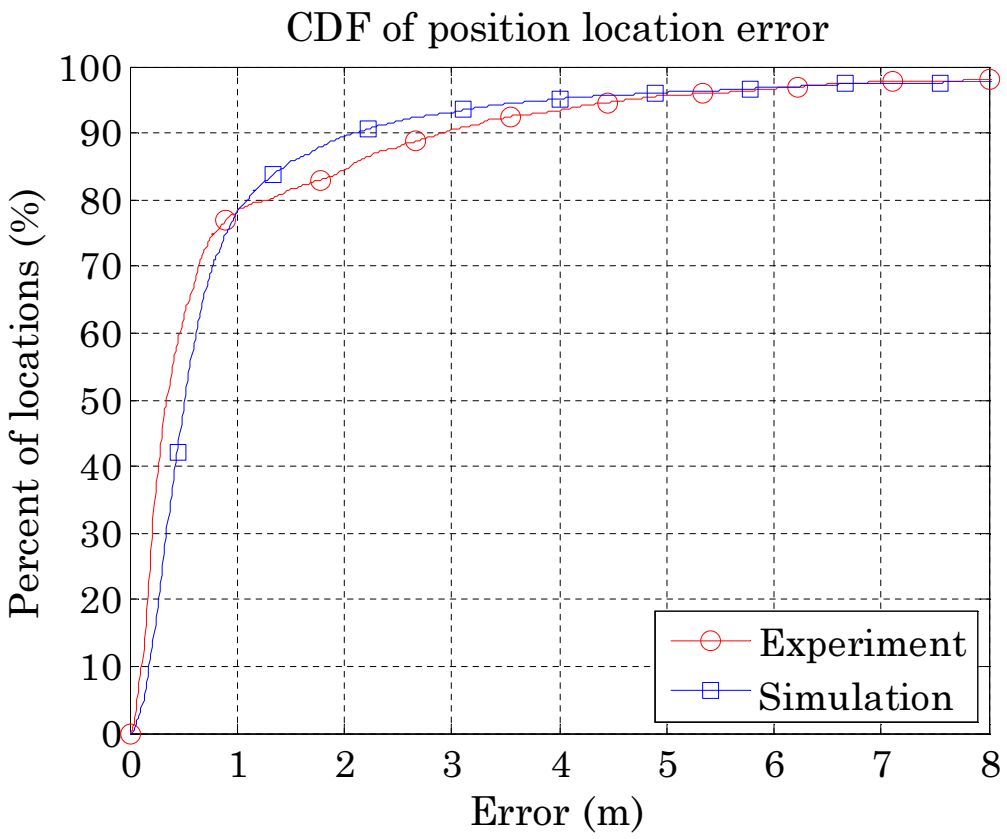

FIGURE 3.14: Performance of the SP criterion for real data compared to that of simulated data. In both we used $p = 6$ antennas, 20MHz BW, $N = 8$ taps, and the number of database and test point snapshots was $L = 30$ and $M = 25$ respectively.

method and the simulation results.

3.8 Discussion

In this section, we discuss several aspects affecting the localization accuracy.

It should be clear from the simulations that given a rich multipath environment, the localization accuracy is a function of many system parameters including the antenna array size, the number of antenna elements, the BW of the signal, the number of taps, the number of snapshots used for the database grid and the number of snapshots used for the test points. As seen in the simulations, these system parameters can be traded, up to a degree, to compensate for each other.

The localization accuracy can be improved by either using some sort of interpolation between the database grid points or by using a finer grid. Yet, the improvement

in accuracy has its limit, dictated by the system parameters and by the noise level characterizing the environment and the database generation.

The accuracy is affected also by the value of the parameter α used for the subspace dimension estimation. The higher is α the higher is the estimated dimension and hence the richness of the fingerprint. We have found that varying α in the range 0.8-0.9 has mild effect on the accuracy and that 0.9 presents overall the best performance, serving as a good compromise between the conflicting desires for enriching the fingerprint, on the one hand, and for robustness of the fingerprint, on the other hand.

Last, but not least, it should be clear that in case an area is covered by more than one base station, using all the information from the overlapping base stations should improve the localization accuracy. Naturally, there are several ways to exploit the overlapping coverage, with varying level of computational load and accuracy.

3.9 Summary

We have presented a novel method enabling single-site localization based on a spatial-temporal fingerprint of the multipath reflections. This spatial-temporal fingerprint is based on a lower dimensional subspace of the spatial-temporal covariance matrix - referred to as the signal subspace - capturing the directions-of-arrival and the differential-delays of the dominant multipath reflections. The fingerprint matching is based on the SP criterion, which outperforms considerably the conventional ML criterion, especially in challenging scenarios that are prone to ambiguity.

The high level of accuracy of this method, demonstrated by simulations and real data results, and its mild computational load make it a promising candidate for providing high quality and ubiquitous localization in indoor environments.

Chapter 4

Localization via Multipath Fingerprinting: A Frequency Domain Approach

4.1 Introduction

Most modern communication systems are based on the orthogonal frequency-division multiplexing (OFDM) modulation technique. In such systems, signal processing and channel estimation are carried out in the frequency domain. As a result, localization in the frequency domain is more natural and convenient than the time domain approach presented in Chapter 3. Furthermore, the repeatable signal part used for synchronization and channel estimation, and utilized by the time domain localization algorithm, in some communication systems, like LTE, may depend on system configurations. As a result, database must include different sets of data for each system configuration. The frequency domain approach eliminates this problem by using repeatable signal subcarriers – pilots – defined in the frequency domain.

In this chapter we present a multipath fingerprinting localization technique in the frequency domain. The fingerprint is based on a lower dimensional signal subspace which captures both the directions-of-arrival and the differential-delays of the dominant multipath signals.

4.2 Problem Formulation

Let the complex envelope $s(t)$ of the transmitted signal $\tilde{s}(t)$ over a finite interval $[t', t'+T]$ be approximated by a Fourier series

$$s\left(t\right) \approx \sum_{d=-N/2}^{N/2-1} s_{t'}\left(\omega_d\right) e^{j\omega_d t} \tag{4.1}$$

where $s_{t'}\left(\omega_d\right)$ are the Fourier coefficients, given by

$$s_{t'}\left(\omega_d\right) = \frac{1}{T} \int_{t'}^{t'+T} s(t) e^{-j\omega_d t} \mathrm{d}t \tag{4.2}$$

and

$$\omega_d = \frac{2\pi}{T} d, \qquad d = -N/2, \ldots, N/2-1 \tag{4.3}$$

where $\omega_{-N/2}$ and $\omega_{N/2-1}$ are the lowest and highest frequencies, respectively, included in the bandwidth B. For clarity of presentation we assume that the number of Fourier coefficients N is even. In addition, we assume that $N < \infty$, as the signal $s(t)$ is band-limited.

Consider an array composed of p sensors with arbitrary locations and arbitrary directional characteristics receiving a wideband signal $\tilde{s}(t)$, centered at frequency $\omega_c = 2\pi f_c$, impinging on the array through q reflections $(q < p)$ with time delays $\tau_1, \ldots, \tau_q$, and corresponding directions $\theta_1, \ldots, \theta_q$.

We assume that the bandwidth of the signal $s(t)$ is small compared to the size of the antenna array, i.e., that the propagation delays across the array are much smaller than the inverse bandwidth of the signal, so that the narrow-band array representation is applicable. This assumption is definitely valid for the bandwidth and antenna array size in modern communication techniques such as Wi-Fi.

Using complex envelop representation and formulation (4.1), the signal received at the i-th sensor during the interval $[t_m, t_m + T]$ can be approximately expressed as

$$x_i\left(t\right) = \sum_{k=1}^{q} \sum_{d=-N/2}^{N/2-1} \gamma_k\left(t_m\right) a_{id}\left(\theta_k\right) s_{t_m}\left(\omega_d\right) e^{j\omega_d(t-\tau_k)} e^{-j(\omega_c+\omega_d)\tau_i(\theta_k)} + n_i\left(t\right) \tag{4.4}$$

where $t \in [0, T]$ and

τ_k	is the delay of the k-th reflection relative to the reference,
$\tau_i(\theta_k)$	is the delay between the i-th sensor and the reference sensor of the k-th reflection,
$a_{id}(\theta_k)$	is the amplitude response of the i-th sensor to a wavefront impinging from direction θ_k at frequency $\omega_c + \omega_d$,
$\gamma_k(t)$	is the complex coefficient representing the phase shift and attenuation of the k-th reflection,
$n_i(t)$	is the additive noise at the i-th sensor.

It should be pointed out that in formulation (4.4) the delays of the multipath reflections were transformed to phase shifts. Rigorously, it is correct only for periodic signals, when signal delay is equivalent to a cyclic shift in time. Yet, it is a good approximation in case when the signal observation time T is much longer than the delay spread of multipath reflections $\bar{\tau} \ll T$. In many OFDM based communication techniques each transmitted symbol is prepended by the cyclic prefix consisting from the last part of the symbol. If the cyclic prefix is longer than the channel delay-spread, then a signal delay is equivalent to a cyclic time shift, which is transformed to a phase shift in the frequency domain [83].

In addition, our formulation assumes that (i) $\gamma_k(t)$ is fixed during a snapshot, and (ii) $\gamma_k(t)$ may vary from snapshot to snapshot. (i) is a valid assumption since the time it takes for an indoor channel to change significantly is of the order of milliseconds [80, 81], whereas the sampling duration of a snapshot T is of the order of microseconds. (ii) is a valid assumption since the time between the snapshots is of the order of milliseconds, and hence slight emitter movement or channel variations may change $\gamma_k(t)$ from snapshot to snapshot.

The signal received by the array can be expressed by

$$\boldsymbol{x}(t) = \sum_{k=1}^{q} \sum_{d=-N/2}^{N/2-1} \gamma_k(t_m)\, \boldsymbol{a}_d(\theta_k)\, s_{t_m}(\omega_d)\, e^{j\omega_d(t-\tau_k)} + \boldsymbol{n}(t) \tag{4.5}$$

where $\boldsymbol{x}(t)$ and $\boldsymbol{n}(t)$ are the $p \times 1$ vectors

$$\boldsymbol{x}(t) = [x_1(t), \ldots, x_p(t)]^T \tag{4.6}$$

$$\boldsymbol{n}(t) = [n_1(t), \ldots, n_p(t)]^T \tag{4.7}$$

and $\boldsymbol{a}_d(\theta_k)$ is the steering vector of the array towards direction θ_k at frequency $\omega_c + \omega_d$, given by

$$\boldsymbol{a}_d\left(\theta_k\right) = \left[a_{1d}\left(\theta_k\right) e^{-j(\omega_c+\omega_d)\tau_1(\theta_k)}, \ldots, a_{pd}\left(\theta_k\right) e^{-j(\omega_c+\omega_d)\tau_p(\theta_k)}\right]^T \tag{4.8}$$

The outputs of the antenna array are sampled simultaneously at N times, with an interval of T/N seconds, i.e., each sensor is sampled at times $(t_m + \ell T/N)$, $\ell = 0, \ldots, N-1$. We refer to the collection of these pN samples as a "snapshot", given by

$$\boldsymbol{X}\left(t_m\right) = \left[\boldsymbol{x}_{t_m}\left[0\right], \boldsymbol{x}_{t_m}\left[1\right], \ldots, \boldsymbol{x}_{t_m}\left[N-1\right]\right] \tag{4.9}$$

where

$$\boldsymbol{x}_{t_m}\left[\ell\right] = \sum_{k=1}^{q} \sum_{d=-N/2}^{N/2-1} \gamma_k\left(t_m\right) \boldsymbol{a}_d\left(\theta_k\right) s_{t_m}\left(\omega_d\right) e^{-j\omega_d \tau_k} e^{j\frac{2\pi}{N} d\ell} + \boldsymbol{n}_{t_m}\left[\ell\right] \tag{4.10}$$

We assume that the antenna array is sampled M times at $\{t_m\}$, $m = 1, \ldots, M$, forming M snapshots, and that the signals and the noise conform to the assumptions A.1–A.3 (defined in Chapter 3). Following the assumption A.1 that the transmitted signal $s(t)$ is identical for all snapshots, hereafter we omit the time dependence of the Fourier coefficients $s_t(\omega_d)$.

4.3 The ML Spatial-Temporal Similarity Metric in Frequency Domain

To derive a similarity-metric for the fingerprint matching, we resort to the estimation of the (θ_k, τ_k) using the Maximum Likelihood (ML) criterion.

To this end, we assume that the complex attenuations $\gamma_k(t_m)$ are unknown deterministic quantities that need to be estimated in conjunction with (θ_k, τ_k), whereas the transmitted signal $s(t)$ is identical for all snapshots.

Assuming that the received vector $\boldsymbol{x}(t)$ is sampled at $t_1, \ldots, t_M$, yielding M i.i.d. snapshots by A.3, the conditional p.d.f. of the sampled data is given by

$$p\left(\boldsymbol{X}\left(t_1\right), \ldots, \boldsymbol{X}\left(t_M\right) \middle| \boldsymbol{\theta}, \boldsymbol{\tau}, \boldsymbol{\Gamma}, \sigma^2\right) = \prod_{m=1}^{M} \prod_{\ell=0}^{N-1} \frac{1}{\pi^p \det\left[\sigma^2 \boldsymbol{I}\right]} \cdot \exp\left(-\frac{1}{\sigma^2}\left\|\boldsymbol{z}_{t_m}\left[\ell\right]\right\|^2\right) \tag{4.11}$$

where $\boldsymbol{\theta} = \{\theta_1, \ldots, \theta_q\}$ and $\boldsymbol{\tau} = \{\tau_1, \ldots, \tau_q\}$ and $\boldsymbol{\Gamma}$ is the $q \times M$ matrix

$$\boldsymbol{\Gamma} = \left[\boldsymbol{\gamma}\left(t_1\right), \ldots, \boldsymbol{\gamma}\left(t_M\right)\right] \tag{4.12}$$

where $\boldsymbol{\gamma}(t)$ is the $q \times 1$ vector

$$\boldsymbol{\gamma}\left(t\right) = \left[\gamma_1\left(t\right), \ldots, \gamma_q\left(t\right)\right]^T \tag{4.13}$$

and $\boldsymbol{z}_{t_m}\left[\ell\right]$ is the $p \times 1$ vector

$$\boldsymbol{z}_{t_m}\left[\ell\right] = \boldsymbol{x}_{t_m}\left[\ell\right] - \sum_{k=1}^{q} \sum_{d=-N/2}^{N/2-1} \gamma_k\left(t_m\right) \boldsymbol{a}_d\left(\theta_k\right) s\left(\omega_d\right) e^{-j\omega_d \tau_k} e^{j\frac{2\pi}{N} d\ell} \tag{4.14}$$

The ML estimator (MLE), following [73], is given by

$$\left[\hat{\boldsymbol{\theta}}, \hat{\boldsymbol{\tau}}, \hat{\boldsymbol{\Gamma}}, \hat{\sigma}^2\right] = \underset{\boldsymbol{\theta}, \boldsymbol{\tau}, \boldsymbol{\Gamma}, \sigma^2}{\arg\max} \left\{ -MNp \log \sigma^2 - \frac{1}{\sigma^2} \sum_{m=1}^{M} \sum_{\ell=0}^{N-1} \left\|\boldsymbol{z}_{t_m}\left[\ell\right]\right\|^2 \right\} \tag{4.15}$$

After straightforward derivation and elimination of constant terms, we get

$$\left[\hat{\boldsymbol{\theta}}, \hat{\boldsymbol{\tau}}, \hat{\boldsymbol{\Gamma}}\right] = \underset{\boldsymbol{\theta}, \boldsymbol{\tau}, \boldsymbol{\Gamma}}{\arg\min} \left\{ \sum_{m=1}^{M} \sum_{\ell=0}^{N-1} \left\|\boldsymbol{z}_{t_m}\left[\ell\right]\right\|^2 \right\} \tag{4.16}$$

Using the well-known Parseval identity for the discrete Fourier transform (DFT)

$$\sum_{\ell=0}^{N-1} \left\|\boldsymbol{z}_t\left[\ell\right]\right\|^2 = \frac{1}{N} \sum_{d=0}^{N-1} \left\|\boldsymbol{z}_t\left[\omega_d\right]\right\|^2 = \frac{1}{N} \sum_{d=-N/2}^{N/2-1} \left\|\boldsymbol{z}_t\left[\omega_d\right]\right\|^2 \tag{4.17}$$

we can rewrite (4.16) as

$$\left[\hat{\boldsymbol{\theta}}, \hat{\boldsymbol{\tau}}, \hat{\boldsymbol{\Gamma}}\right] = \underset{\boldsymbol{\theta}, \boldsymbol{\tau}, \boldsymbol{\Gamma}}{\arg\min} \left\{ \sum_{m=1}^{M} \sum_{d=-N/2}^{N/2-1} \left\|\boldsymbol{z}_{t_m}\left[\omega_d\right]\right\|^2 \right\} \tag{4.18}$$

where $\left\{\boldsymbol{z}_{t_m}[\omega_d]\right\}$ is the DFT of the $\left\{\boldsymbol{z}_{t_m}[\ell]\right\}$, given by

$$\boldsymbol{z}_{t_m}\left[\omega_d\right] = \boldsymbol{x}_{t_m}\left[\omega_d\right] - \sum_{k=1}^{q} \gamma_k\left(t_m\right) \boldsymbol{a}_d\left(\theta_k\right) N s\left(\omega_d\right) e^{-j\omega_d \tau_k} \tag{4.19}$$

and $\left\{\boldsymbol{x}_{t_m}[\omega_d]\right\}$ is the DFT of the $\left\{\boldsymbol{x}_{t_m}[\ell]\right\}$.

According to the well-known Discrete Fourier Transform (DFT) representation, the Fourier series coefficients of a periodic bandlimited signal $s(t)$ are given by the DFT of one period of the samples of $s(t)$, divided by N, where N is the DFT length. Hence, the $\left\{Ns(\omega_d)\right\}$ in (4.19) is the DFT of the $\left\{s[\ell]\right\}$, $\ell = 0, \ldots, N-1$, samples of the

transmitted signal $s(t)$.

Substituting (4.19) back into (4.18), yields

$$\left[\hat{\boldsymbol{\theta}}, \hat{\boldsymbol{\tau}}, \hat{\boldsymbol{\Gamma}}\right] = \underset{\boldsymbol{\theta},\boldsymbol{\tau},\boldsymbol{\Gamma}}{\arg\min} \left\{ \sum_{m=1}^{M} \sum_{d=-N/2}^{N/2-1} \left\| \boldsymbol{x}_{t_m}\left[\omega_d\right] - \sum_{k=1}^{q} \gamma_k\left(t_m\right) \boldsymbol{a}_d\left(\theta_k\right) N s\left(\omega_d\right) e^{-j\omega_d \tau_k} \right\|^2 \right\} \tag{4.20}$$

Using matrix notation, we can rewrite it as

$$\left[\hat{\boldsymbol{\theta}}, \hat{\boldsymbol{\tau}}, \hat{\boldsymbol{\Gamma}}\right] = \underset{\boldsymbol{\theta},\boldsymbol{\tau},\boldsymbol{\Gamma}}{\arg\min} \left\{ \sum_{m=1}^{M} \sum_{d=-N/2}^{N/2-1} \left\| \boldsymbol{x}_{t_m}\left[\omega_d\right] - \boldsymbol{A}\left(\omega_d\right) \boldsymbol{\gamma}\left(t_m\right) \right\|^2 \right\} \tag{4.21}$$

where $\boldsymbol{A}(\omega_d)$ is the $p \times q$ matrix

$$\boldsymbol{A}\left(\omega_d\right) = N s(\omega_d) \left[\boldsymbol{a}_d\left(\theta_1\right) e^{-j\omega_d \tau_1}, \ldots, \boldsymbol{a}_d\left(\theta_q\right) e^{-j\omega_d \tau_q}\right] \tag{4.22}$$

We can rewrite (4.21) more compactly as

$$\left[\hat{\boldsymbol{\theta}}, \hat{\boldsymbol{\tau}}, \hat{\boldsymbol{\Gamma}}\right] = \underset{\boldsymbol{\theta},\boldsymbol{\tau},\boldsymbol{\Gamma}}{\arg\min} \left\{ \sum_{m=1}^{M} \left\| \boldsymbol{x}_{t_m} - \boldsymbol{A}\boldsymbol{\gamma}\left(t_m\right) \right\|^2 \right\} \tag{4.23}$$

where $\boldsymbol{A}$ is the $pN \times q$ matrix

$$\boldsymbol{A} = \left[\boldsymbol{A}\left(\omega_{-N/2}\right)^T, \ldots, \boldsymbol{A}\left(\omega_{N/2-1}\right)^T\right]^T \tag{4.24}$$

and $\boldsymbol{x}_{t_m}$ is the $pN \times 1$ vector referred as the *frequency domain snapshot*

$$\boldsymbol{x}_{t_m} = \left[\boldsymbol{x}_{t_m}\left[\omega_{-N/2}\right]^T, \ldots, \boldsymbol{x}_{t_m}\left[\omega_{N/2-1}\right]^T\right]^T \tag{4.25}$$

Minimization of (4.23) with respect to $\boldsymbol{\Gamma}$, yields

$$\hat{\boldsymbol{\gamma}}\left(t_m\right) = \left(\boldsymbol{A}^H \boldsymbol{A}\right)^{-1} \boldsymbol{A}^H \boldsymbol{x}_{t_m} \tag{4.26}$$

Substituting (4.26) back into (4.23), yields

$$\left[\hat{\boldsymbol{\theta}}, \hat{\boldsymbol{\tau}}\right] = \underset{\boldsymbol{\theta},\boldsymbol{\tau}}{\arg\min} \left\{ \sum_{m=1}^{M} \left\| \boldsymbol{x}_{t_m} - \boldsymbol{P}_{\boldsymbol{A}} \boldsymbol{x}_{t_m} \right\|^2 \right\} = \underset{\boldsymbol{\theta},\boldsymbol{\tau}}{\arg\max} \left\{ \sum_{m=1}^{M} \left\| \boldsymbol{P}_{\boldsymbol{A}} \boldsymbol{x}_{t_m} \right\|^2 \right\} \tag{4.27}$$

where $\boldsymbol{P}_{\boldsymbol{A}}$ is the projection operator onto the space spanned by the columns of the matrix $\boldsymbol{A}$

$$\boldsymbol{P}_{\boldsymbol{A}} = \boldsymbol{A}\left(\boldsymbol{A}^H \boldsymbol{A}\right)^{-1} \boldsymbol{A}^H \tag{4.28}$$

It can be easily verified that (4.27) can also be written as

$$\left[\hat{\boldsymbol{\theta}}, \hat{\boldsymbol{\tau}}\right] = \arg\max_{\boldsymbol{\theta},\boldsymbol{\tau}} Tr\left\{\boldsymbol{P_A}\hat{\boldsymbol{R}}\right\} \tag{4.29}$$

where $Tr\{\cdot\}$ is the trace operator, and $\hat{\boldsymbol{R}}$ is the sample covariance matrix

$$\hat{\boldsymbol{R}} = \frac{1}{M}\sum_{m=1}^{M} \boldsymbol{x}_{t_m}\boldsymbol{x}_{t_m}^H \tag{4.30}$$

It should be pointed out that if $\omega_c \gg \omega_d$ and the sensor amplitude response $\left\{a_{id}(\theta_k)\right\}$, $i = 1, \ldots, p$ is constant over the signal bandwidth (BW), the matrix $\boldsymbol{A}$ has a Khatry-Rao structure and may be written as follows

$$\boldsymbol{A} = \left[\boldsymbol{s}\left(\tau_1\right) \otimes \boldsymbol{a}\left(\theta_1\right), \ldots, \boldsymbol{s}\left(\tau_q\right) \otimes \boldsymbol{a}\left(\theta_q\right)\right] \tag{4.31}$$

where $\boldsymbol{a}(\theta_k)$ is the $p \times 1$ vector given by

$$\boldsymbol{a}\left(\theta_k\right) = \left[a_1\left(\theta_k\right) e^{-j\omega_c\tau_1(\theta_k)}, \ldots, a_p\left(\theta_k\right) e^{-j\omega_c\tau_p(\theta_k)}\right]^T \tag{4.32}$$

and $\boldsymbol{s}(\tau_k)$ is the $N \times 1$ vector given by

$$\boldsymbol{s}\left(\tau_k\right) = N\left[s\left(\omega_{-N/2}\right) e^{-j\omega_{-N/2}\tau_k}, \ldots, s\left(\omega_{N/2-1}\right) e^{-j\omega_{N/2-1}\tau_k}\right]^T \tag{4.33}$$

Note that the matrix $\boldsymbol{A}$ captures all the direction-of-arrival and the differential-delay information of the multipath reflections. Similarly to the time domain approach in Chapter 3, we refer to the span of the columns of the matrix $\boldsymbol{A}$ as the *spatial-temporal signal subspace* and use this spatial-temporal signal subspace as the location fingerprint.

4.4 Signal Subspace Based Localization

According to the ML criterion (4.29), the localization is carried out by searching in the database for the location i that maximizes the following expression

$$\hat{i} = \arg\max_{\{\boldsymbol{P_i}\}} Tr\left\{\boldsymbol{P_i}\hat{\boldsymbol{R}}\right\} \tag{4.34}$$

where $\hat{\boldsymbol{R}}$ is the sample-covariance matrix (4.30) and $\boldsymbol{P_i}$ is the projection operator onto the signal subspace corresponding to the i-th location. Yet, due to ambiguity inherent in the physical environment, some locations may have similar spatial-temporal fingerprints, and

as a result give rise to a certain level of ambiguity error. To address this problem we use the similarity-profile matching criteria (3.36) that better copes with these ambiguities.

The generation of the fingerprint database, the signal subspace estimation and the localization, including the similarity-profile matching, are performed analogously to Chapter 3 and are summarized in the following subsections 4.4.1–4.4.2.

4.4.1 The Generation of the Fingerprint Database

For each location $i \in [1, K]$, where K is the number of locations in the database, perform the following steps 1–8:

1. Sample the antenna array L times at $t_1, \ldots, t_L$, to form L snapshots $\{\boldsymbol{X}(t_l)\}$ (4.9) that include the same repeatable signal part.

2. Convert each snapshot $\boldsymbol{X}(t_l)$ to the frequency domain using Discrete Fourier Transform (DFT):
$$\boldsymbol{x}_{t_l}[\omega_d] = \sum_{n=0}^{N-1} \boldsymbol{x}_{t_l}[n] e^{-j\frac{2\pi d}{N}n} \tag{4.35}$$

3. For each $l \in [1, L]$, combine the $\{\boldsymbol{x}_{t_l}[\omega_d]\}$, $d = -N/2, \ldots, N/2 - 1$ vectors into the $pN \times 1$ frequency domain snapshot $\boldsymbol{x}_{t_l}$ according to (4.25).

4. Calculate the sample-covariance matrix $\hat{\boldsymbol{R}}_i$ of location i by
$$\hat{\boldsymbol{R}}_i = \frac{1}{L} \sum_{l=1}^{L} \boldsymbol{x}_{t_l} \boldsymbol{x}_{t_l}^H \tag{4.36}$$

5. Perform an eigenvalue decomposition of $\hat{\boldsymbol{R}}_i$.

6. Estimate the signal subspace dimension $\hat{q}$ according to (3.31).

7. Select the first $\hat{q}$ eigenvectors of $\hat{\boldsymbol{R}}_i$ corresponding to the signal subspace: $\boldsymbol{V}_{\hat{q}} = \{\boldsymbol{v}_1, \boldsymbol{v}_2, \ldots, \boldsymbol{v}_{\hat{q}}\}$.

8. Estimate the projection matrix by $\hat{\boldsymbol{P}}_i = \boldsymbol{V}_{\hat{q}} \left(\boldsymbol{V}_{\hat{q}}^H \boldsymbol{V}_{\hat{q}}\right)^{-1} \boldsymbol{V}_{\hat{q}}^H$.

For each location $i \in [1, K]$

9. Calculate the similarity-profile (SP) by
$$\boldsymbol{f}_i = \left[Tr\{\hat{\boldsymbol{P}}_1 \widetilde{\boldsymbol{R}}_i\}, Tr\{\hat{\boldsymbol{P}}_2 \widetilde{\boldsymbol{R}}_i\}, \ldots, Tr\{\hat{\boldsymbol{P}}_K \widetilde{\boldsymbol{R}}_i\}\right] \tag{4.37}$$

with $\widetilde{\boldsymbol{R}}_i$ given by

$$\widetilde{\boldsymbol{R}}_i = \hat{\boldsymbol{R}}_i \Big/ Tr\left\{\hat{\boldsymbol{R}}_i\right\} \tag{4.38}$$

4.4.2 Localization using the similarity-profile matching criterion

1. Sample the antenna array M times at $t_1, \ldots, t_M$, to form M snapshots $\left\{\boldsymbol{X}(t_m)\right\}$ (4.9) that include the same repeatable signal part.

2. Convert each snapshot $\boldsymbol{X}(t_m)$ to the frequency domain using Discrete Fourier Transform (DFT) (4.35).

3. For each $m \in [1, M]$, combine the $\left\{\boldsymbol{x}_{t_m}[\omega_d]\right\}$, $d = -N/2, \ldots, N/2 - 1$ vectors into the $pN \times 1$ frequency domain snapshot $\boldsymbol{x}_{t_m}$ according to (4.25).

4. Calculate the sample-covariance matrix $\hat{\boldsymbol{R}}$ of the received signal by

$$\hat{\boldsymbol{R}} = \frac{1}{M} \sum_{m=1}^{M} \boldsymbol{x}_{t_m} \boldsymbol{x}_{t_m}^H \tag{4.39}$$

5. Calculate the similarity-profile $\widehat{\boldsymbol{f}}$ of the received signal by

$$\widehat{\boldsymbol{f}} = \left[Tr\{\hat{\boldsymbol{P}}_1 \widehat{\boldsymbol{R}}\}, \ \ldots \ , Tr\{\hat{\boldsymbol{P}}_K \widehat{\boldsymbol{R}}\}\right] \tag{4.40}$$

   with $\widehat{\boldsymbol{R}}_i$ given by

$$\widehat{\boldsymbol{R}}_i = \hat{\boldsymbol{R}} \Big/ Tr\left\{\hat{\boldsymbol{R}}\right\} \tag{4.41}$$

6. Following (3.36), search over the database for the SP that best matches the query SP obtained from the received signals.

4.4.3 Pilot Based Localization

A special and important case of the frequency domain approach is localization based on pilots - known signals occupying particular subcarriers in the transmitted signal and used for channel estimation, phase and frequency tracking [82].

The pilot based localization algorithm is similar to the original algorithm with the only difference that instead of using frequency domain snapshots comprising of all subcarriers, the processing is confined to the relevant pilot subcarriers. That is, the frequency domain snapshot $\boldsymbol{x}_{t_m}$ (4.25) are confined to only J pilot subcarriers so that the spatial-temporal signal subspace $\boldsymbol{A}$ (4.24) is based only on the pilot subcarriers.

The advantage of this approach is its applicability to signals that do not include a repeatable signal part but only repeatable subcarriers (frequency bins). Modern communication systems based on the OFDM modulation technique include known pilots in each transmitted symbol.

In addition, we can apply the pilot based approach to signals that include a repeatable part but and use only part of subcarriers of the received signal $\boldsymbol{x}_{t_m}$ (4.25).

Exploiting only part of signal subcarriers allows significant reduction in the size $pJ \times pJ$ of the projection $\boldsymbol{P}_i$ and the sample-covariance $\hat{\boldsymbol{R}}$ matrices, and as a result, reduce the database size and the computational load. Note that proper selection of the subcarriers, i.e., have them uniformly spread over the signal bandwidth and include the edge subcarriers, assures full exploitation of the signal bandwidth. The maximal difference between the subcarriers' frequencies determines the minimal differential-delay of the multipath signals that is captured by the signal subspace.

4.5 Conditions for Unique Localization

In this section we present necessary and sufficient conditions that guarantee unique localization.

Following the problem formulation and the development presented in Sections 4.2 and 4.3 respectively, the m-th frequency domain snapshot is given by

$$\boldsymbol{x}_{t_m} = \boldsymbol{A}\boldsymbol{\gamma}(t_m) + \boldsymbol{n}_{t_m} \tag{4.42}$$

where

$$\boldsymbol{n}_{t_m} = \left[\boldsymbol{n}_{t_m}\left[\omega_{-N/2}\right]^T, \ldots, \boldsymbol{n}_{t_m}\left[\omega_{N/2-1}\right]^T\right]^T \tag{4.43}$$

and $\left\{\boldsymbol{n}_{t_m}\left[\omega_d\right]\right\}$ is the DFT of the $\left\{\boldsymbol{n}_{t_m}\left[\ell\right]\right\}$.

Assuming that the conditions B.1–B.2 are obeyed the problem at hand is identical to that discussed in the Section 3.2, with $\boldsymbol{X}$, the $pN \times M$ matrix, given by

$$\boldsymbol{X} = \left[\boldsymbol{x}_{t_1}, \ldots, \boldsymbol{x}_{t_M}\right] \tag{4.44}$$

Therefore, the condition 3.17 for unique localization is applicable as well to the frequency domain approach.

4.6 Localization Using the Array Channel Frequency Response

In this section, we show that our method is applicable also to localization using the array channel frequency response (CFR).

In modern communication systems the CFR is usually obtained by exploiting a known signal, referred to as training signal, specifically included in the transmitted signal for this purpose. Moreover, in systems based on the OFDM modulation technique channel estimation is usually performed in frequency domain using frequency domain sequence. The channel estimate for each frequency (subcarrier/frequency bin) is obtained by division of the received signal by the corresponding known training symbol.

Following the problem formulation and the development presented in Sections 4.2 and 4.3 respectively, the estimated CFR corresponding to the m-th snapshot is given by

$$\hat{\boldsymbol{h}}_{t_m}\left[\omega_d\right] = \sum_{k=1}^{q} \gamma_k(t_m)\boldsymbol{a}_d(\theta_k)g(\omega_d)e^{-j\omega_d\tau_k} + \boldsymbol{n}_{t_m}\left[\omega_d\right] \tag{4.45}$$

where $g(\omega_d)$ is the CFR of the transmit and receive filters and $\boldsymbol{n}_{t_m}\left[\omega_d\right]$ is the CFR estimation noise, and $\omega_d = \frac{2\pi}{T}d = \frac{2\pi f_s}{N}d$, and $f_s = \frac{N}{T}$ is the sample frequency. We assume that the estimation noise conforms to the assumption A.3.

Note that expression (4.19) and (4.45) are essentially identical, differing only in the signal part. Yet, since $g(\omega_d)$ is repeatable from snapshot to snapshot, A.1-A.2 apply here as well.

Stacking the estimated CFR subcarriers/frequency bins in a vector form analogously to (4.25), we get

$$\hat{\boldsymbol{h}}_t = \boldsymbol{A}\boldsymbol{\gamma}\left(t\right) + \boldsymbol{n}_t \tag{4.46}$$

where $\boldsymbol{A}$ is defined by (4.24).

Since this expression is identical to problem formulation (3.8), we can straightforwardly apply our localization method to the sample-covariance of the array CFR, given by

$$\hat{\boldsymbol{C}} = \frac{1}{M}\sum_{m=1}^{M} \hat{\boldsymbol{h}}_{t_m}\hat{\boldsymbol{h}}_{t_m}^H \tag{4.47}$$

The advantage of using the CFR for localization, as compared to using the received signals with a repeatable part, is the indifference of the localization algorithm to different

repeatable parts (training signals).

4.7 Simulation Results

In this section we present simulation results illustrating the performance of the proposed localization algorithm. The simulation environment and parameters are identical to those described in Section 3.6.

Similarly to the Section 3.6, we used the Long Training Field (LTF) of the preamble of the 802.11a/g/n Wi-Fi packet [82], which is present in each transmitted packet and is used for channel estimation, accurate frequency offset estimation and time synchronization. One symbol of the LTF consists of 64, 128 and 256 samples/subcarriers, corresponding to signal bandwidths of 20MHz, 40MHz and 80MHz, respectively (subcarrier spacing is 312.5kHz). The subcarrier indexes of the 20MHz signal are $-32, -31, \ldots, -1, 0, 1, \ldots, 31$, with the populated (nonzero) ones being $-26, -25, \ldots, -2, -1, 1, 2, \ldots, 25, 26$. The populated subcarriers of the 40MHz signal are $-58, \ldots, -2, 2, \ldots, 58$, while the populated subcarriers of the 80MHz signal are $-122, \ldots, -2, 2, \ldots, 122$. In each of the simulation scenarios the used subcarriers were uniformly and maximally spread over the signal bandwidth. For example, the indexes of used subcarriers for BW=20MHz and $J = 4$ were [-26, -9, 8, 26].

4.7.1 Simulation Scenario 1

In this simulation we present the achievable localization accuracy using the ML (4.34) and the SP (3.43) matching criteria, with a varying number of antennas. The number of used subcarriers per antenna was $J = 8$ and the signal bandwidth (BW) was 20MHz, while the number of signal snapshots used for each database and test location were $L = 60$ and $M = 55$, respectively. To vary the number of antennas we used 3 and 1 out of the 6 antennas of the array. The indexes of used subcarriers were: $\pm 26, \pm 19, \pm 11, -4, 3$.

As seen in Figure 4.1, the accuracy difference between the SP and the ML criteria is considerable, especially in more challenging scenarios wherein the level of ambiguity increases, namely when the number of antennas is reduced from 6 to 3 and from 3 to 1. Since this advantage of the SP criterion was persistent in all the simulations, we have

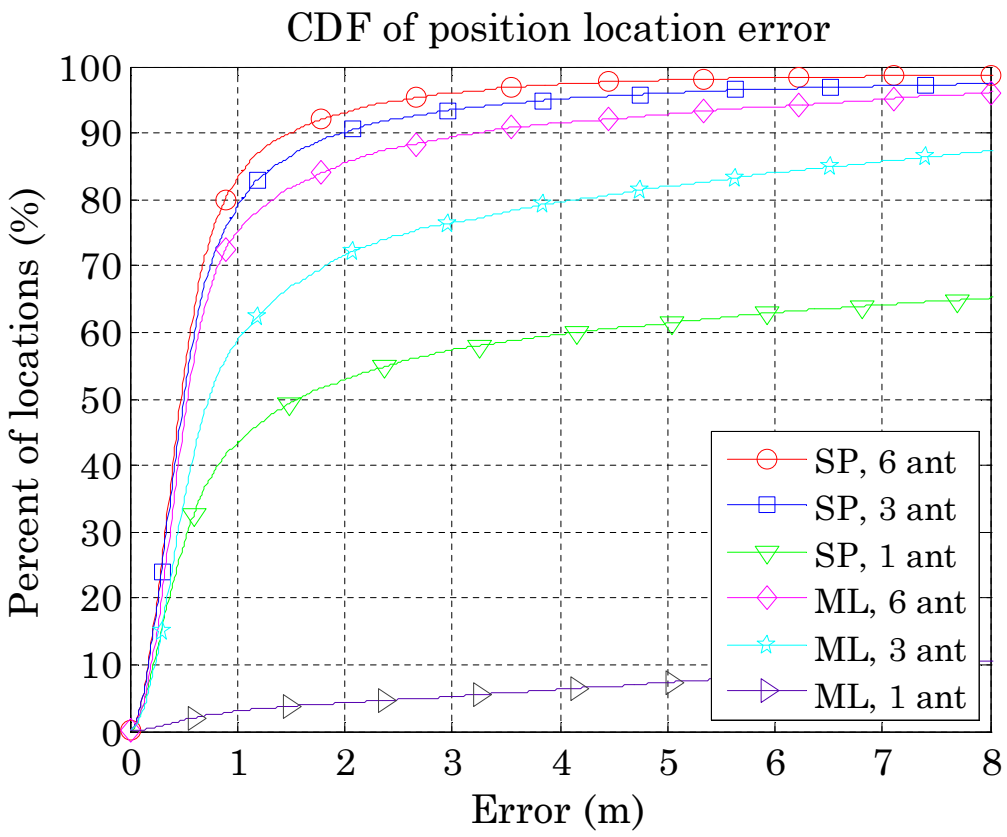

FIGURE 4.1: Performance of the SP and ML techniques for different number of antennas. The number of used subcarriers was $J = 8$, the BW=20MHz and the number of snapshots for the database and tests were $L = 60$ and $M = 55$, respectively.

decided to omit the results of the ML criterion and concentrate on the SP in the sequel for clarity of the presentation.

Note also that though there is only marginal accuracy degradation when going from 6 antennas to 3, it is much more significant when going from 3 antennas to 1. This clearly demonstrates the crucial contribution of the spatial dimension in enabling high accuracy, especially at relatively law bandwidth of 20MHz.

As seen in Figure 3.5 and Figure 4.1, localization accuracy of time and frequency domain techniques using the SP criteria is similar.

4.7.2 Simulation Scenario 2

In this simulation we present the distribution of signal subspace dimension over the mall area as a function of the number of subcarriers (frequency bins) J. The number of

antennas was $p = 6$, the bandwidth was 20MHz and 80MHz, and the number of database snapshots $L = 60$.

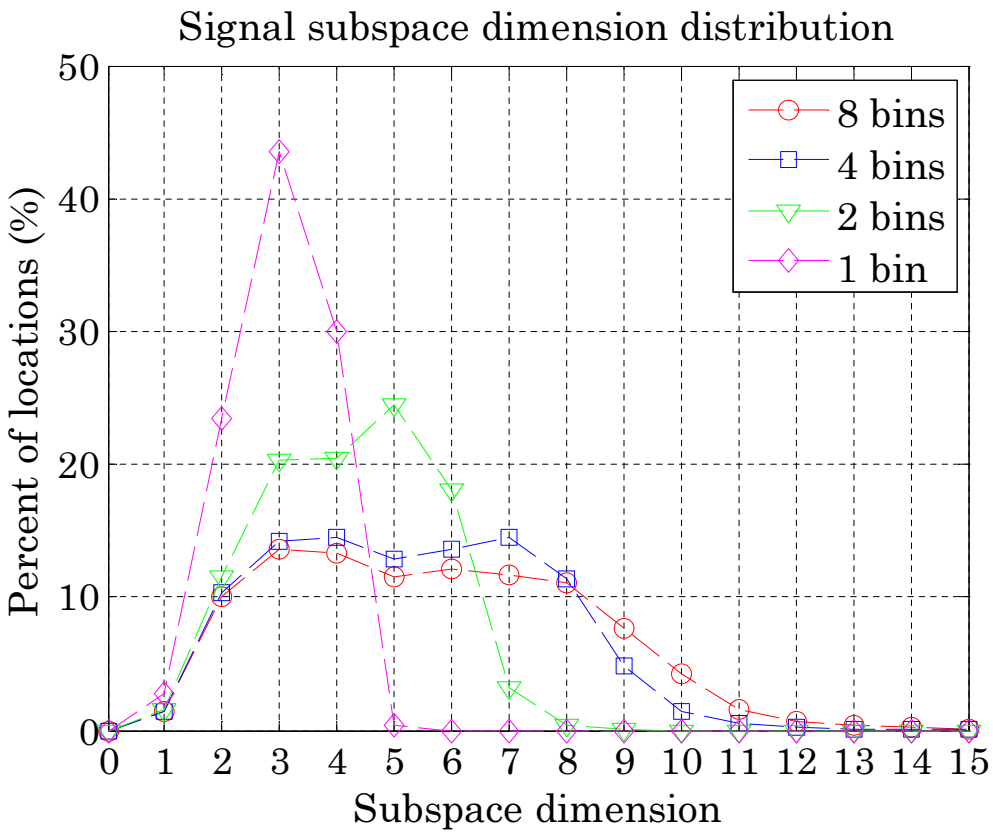

FIGURE 4.2: Signal subspace dimension distribution for different number of subcarriers (frequency bins). The number of antennas was $p = 6$, the signal BW=20MHz, and the number of database snapshots $L = 60$.

As seen in Figure 4.2 and 4.3, the signal subspace dimension rises with the increase of the dimension pJ of the snapshot vector but typically stays below 11, even when the dimension of the snapshot vector rises to 24 (for $J = 4$) and 48 (for $J = 8$). Not surprisingly, the time (Figure 3.6) and the frequency (Figure 4.2) localization techniques have similar subspace dimension distributions.

Higher signal BW allows capturing a larger number of signal reflections due to a better reflection differentiation in time. Hence, as seen in Figure 4.3 in case of BW=80MHz the dimension distribution mean is higher and includes more high-dimensional subspaces as compared to the 20MHz signals.

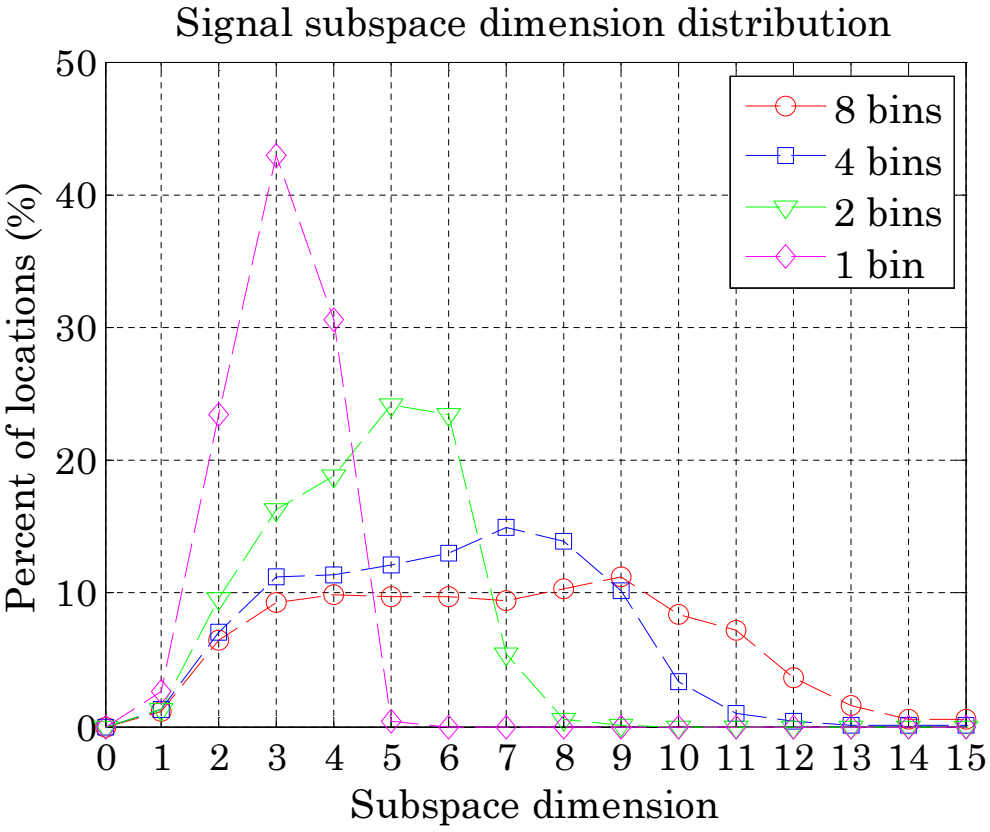

FIGURE 4.3: Signal subspace dimension distribution for different number of subcarriers (frequency bins). The number of antennas was $p = 6$, the signal BW=80MHz, and the number of database snapshots $L = 60$.

4.7.3 Simulation Scenario 3

In this simulation we present the influence of the number of snapshots, L and M, on the localization accuracy. The signal bandwidth was 20MHz and the number of subcarriers $J = 8$. The indexes of the used subcarriers were: $\pm 26, \pm 19, \pm 11, -4, 3$. In the first case (Figure 4.4), the number of antennas was $p = 6$ and the number of database snapshots $L = 60$, while the number of test point snapshots varied. In the second case (Figure 4.5), the number of antennas was $p = 3$ and the number of test point snapshots $M = 25$, while the number of database snapshots varied.

As seen in Figures 4.4 and 4.5, the higher the number of test point/database snapshots the higher is the accuracy. This can be attributed to the fact that the higher number of snapshots provides better covariance matrix estimation and consequently better signal subspace estimation. Yet, beyond some number of snapshots, about 25-30, the improvement in accuracy is marginal. The fact that 25-30 snapshots are sufficient to

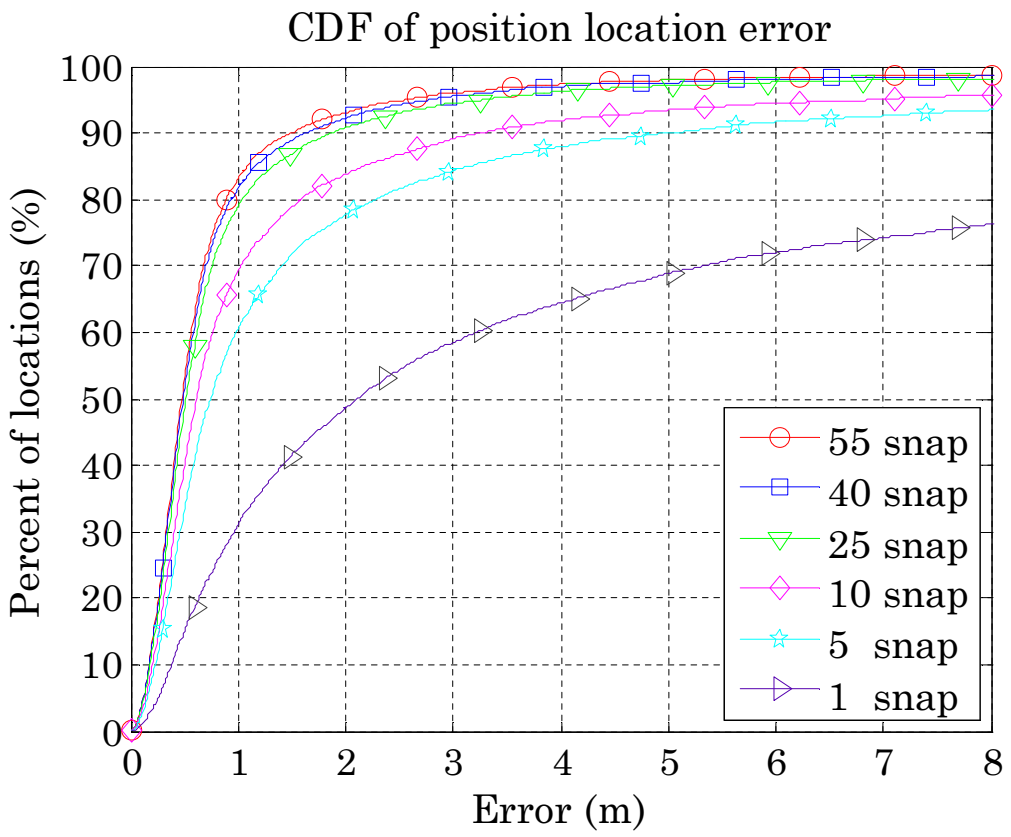

FIGURE 4.4: Performance of the SP criterion for different number of test point snapshots. The number of antennas was $p = 6$, the BW=20MHz, the number of subcarriers $J = 8$, and the number of database snapshots $L = 60$.

fully characterize the signal subspace can be explained by the relatively low dimension of this subspace, as discussed above and shown in Figure 4.2.

4.7.4 Simulation Scenario 4

In this simulation we present the influence of number of subcarriers on the localization accuracy for a 6-antenna array and bandwidth of 20MHz. The number of database and test point snapshots was $L = 60$ and $M = 25$, respectively.

As seen in Figure 4.6, the higher is the number of subcarriers the better is the accuracy. This can be attributed to the fact that according to 3.17 the higher number of subcarriers allows capturing a higher number of reflections and as a result to provide a more robust fingerprint with lower ambiguity.

Note also that in the case of a single subcarrier there is a significant degradation in accuracy as well as much higher ambiguity level, reflected by the higher error in upper

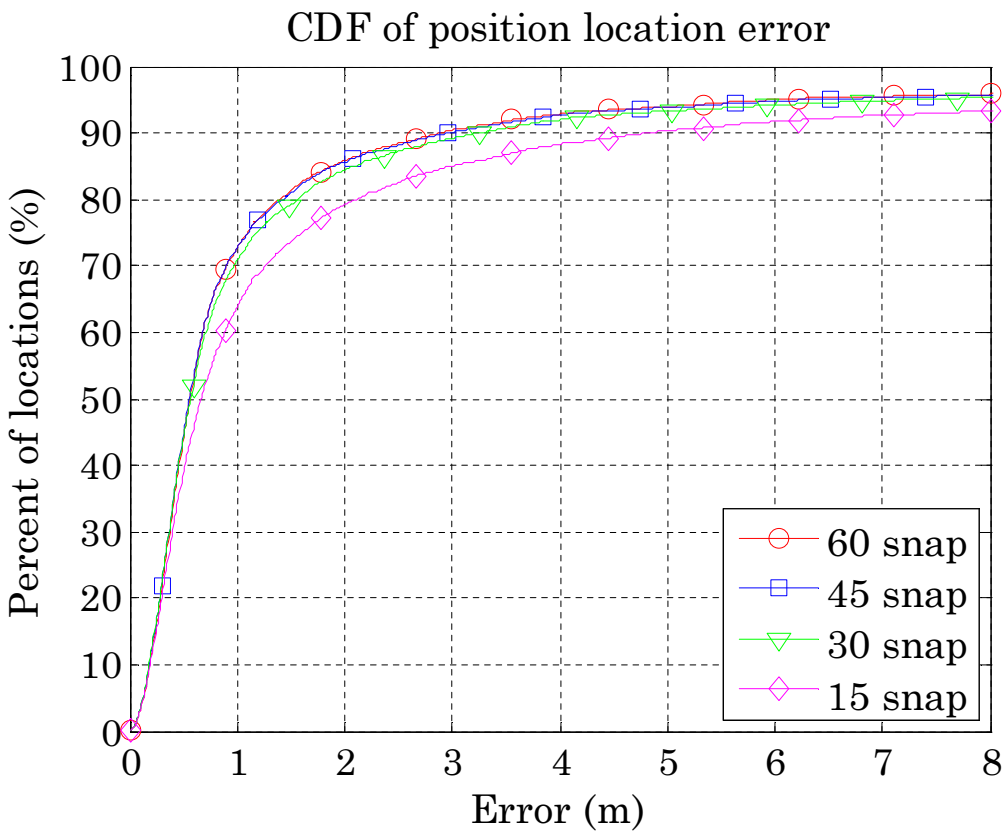

FIGURE 4.5: Performance of the SP criterion for different number of database snapshots. The number of antennas was $p = 3$, the BW=20MHz, the number of subcarriers $J = 8$, and the number of test point snapshots $M = 25$.

percentile of the CDF graph. This highlights the inability of spatial-only fingerprint to provide enough location distinction.

4.7.5 Simulation Scenario 5

In this simulation we present the influence of subcarrier spacing on the localization accuracy for a 3-antenna array and $J = 4$ subcarriers. The number of database and test point snapshots was $L = 30$ and $M = 25$, respectively.

As seen in Figure 4.7, the higher is the subcarriers spacing the better is the accuracy. This can be attributed to the fact that the higher subcarrier spacing provides better reflection differentiation, allowing to capture a higher number of reflection and as a result, to build a more robust fingerprint.

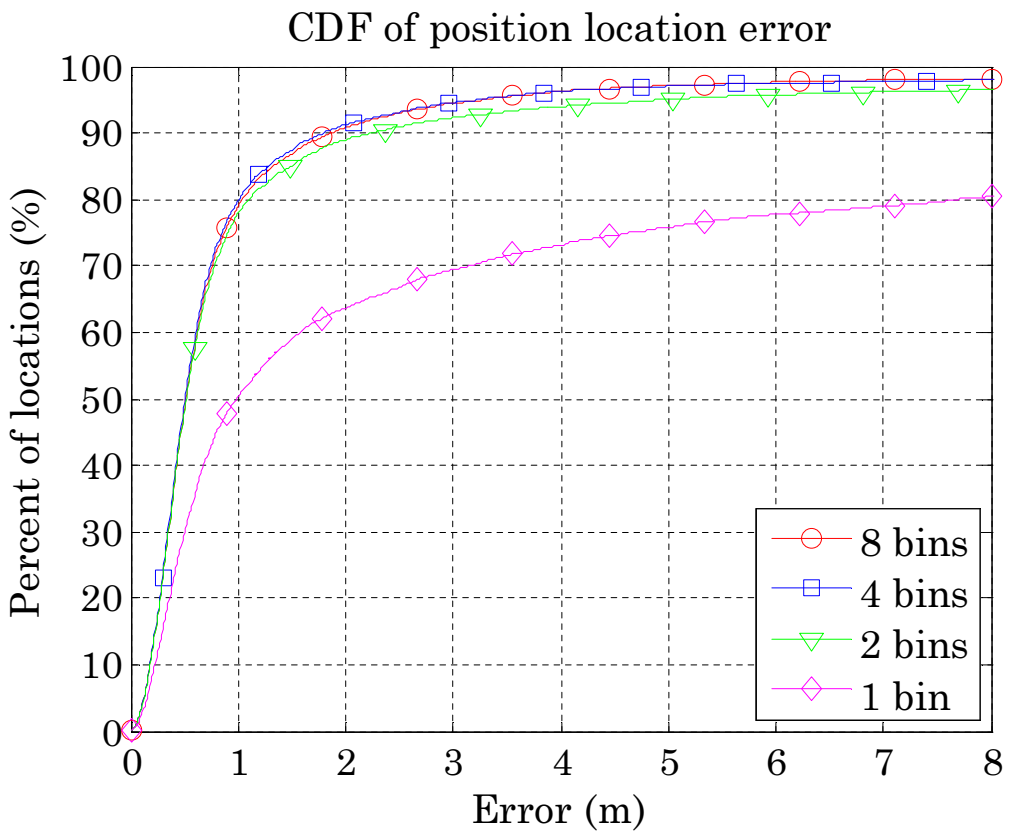

FIGURE 4.6: Performance of the SP criterion for different number of subcarriers (frequency bins). The number of antennas was $p = 6$, the BW=20MHz, and the number of database and test point snapshots was $L = 60$ and $M = 25$, respectively.

4.7.6 Simulation Scenario 6

In this simulation we present the achievable accuracy in the case of $p = 1$ antenna using different signal bandwidths, 20MHz, 40MHz, and 80MHz. The simulation parameters were identical to those of scenario 1 except that here number of subcarriers was $J = 32$ that were spread uniformly over the bandwidth.

As can be seen in Figure 4.8, there is a large improvement in accuracy as the bandwidth increases, demonstrating the importance of the improved time resolution resulting from the increased bandwidth in the case of single antenna.

Note also that the ambiguity level, reflected by the higher error in upper percentile of the CDF graph, is considerably higher than in the case of 6 and 3 antennas presented in Figure 4.1. This high level of ambiguity highlights the inability of temporal-only fingerprint to provide enough location distinction.

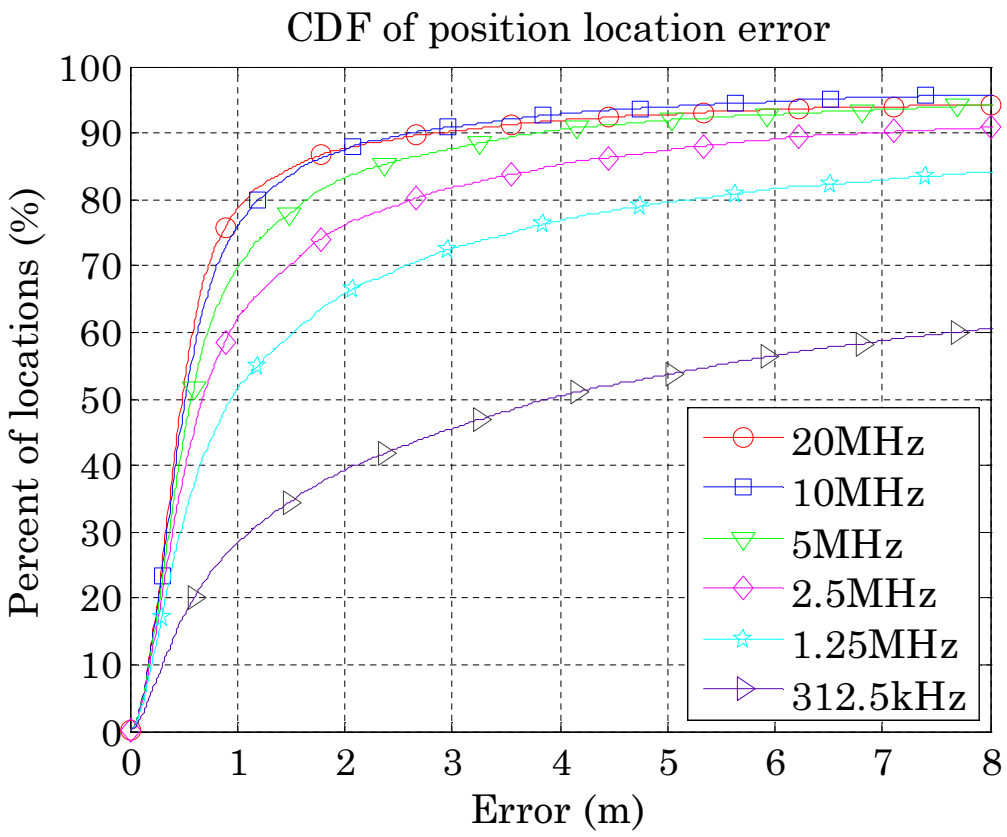

FIGURE 4.7: Performance of the SP criterion for different subcarrier spacing. The number of antennas was $p = 3$, the number of subcarriers was $J = 4$, and the number of database and test point snapshots was $L = 30$ and $M = 25$, respectively.

4.7.7 Simulation Scenario 7

In this simulation we present the achievable localization accuracy of the pilot-based technique with WLAN systems based on the 802.11n/ac standards. The number of used antennas was $p = 6$, and the number of signal snapshots used for each database and test location were $L = 60$ and $M = 25$, respectively. The indexes of used subcarriers were: [±21, ±7], [±53, ±25, ±11], [±103, ±75, ±39, ±11] for BWs of 20MHz, 40MHz, and 80MHz respectively.

As seen in Figure 4.9, the achievable localization accuracy is high for all BWs. This demonstrates applicability and a great potential of the pilot-based localization technique to the popular WiFi and LTE systems.

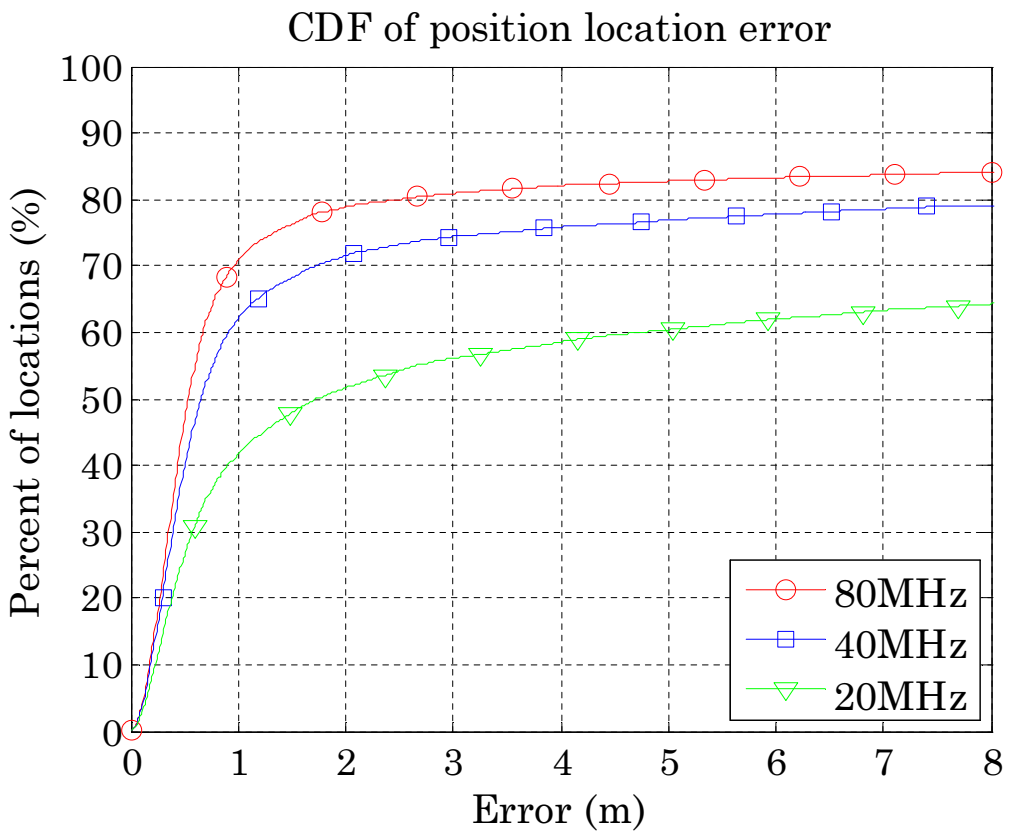

FIGURE 4.8: Performance of the SP criterion for different BWs. The number of antennas was $p = 1$, the number of subcarriers $J = 32$, and the number of database and test point snapshots was $L = 60$ and $M = 25$, respectively.

4.8 Summary

We have presented a novel method enabling single-site localization based on a spatial-temporal fingerprint of the multipath reflections. The fingerprint is based on a lower dimensional signal subspace estimated in the frequency domain.

The level of accuracy achieved by this method is high and similar to that of the time domain technique presented in Chapter 3. The main advantage of this technique is that it can suffice with repeatable subcarriers - pilots – eliminating the need for a repeatable signal part (packet preamble, demodulation reference signal). Though most modern communication systems have both reference signals and pilots, the big advantage of pilots are that they are embedded in the whole duration of the transmitted signal and thus enable exploiting the whole signal duration for localization. Furthermore, the repeatable signal part used for synchronization and channel estimation, and utilized by the time domain localization algorithm, in some communication systems, like LTE, may

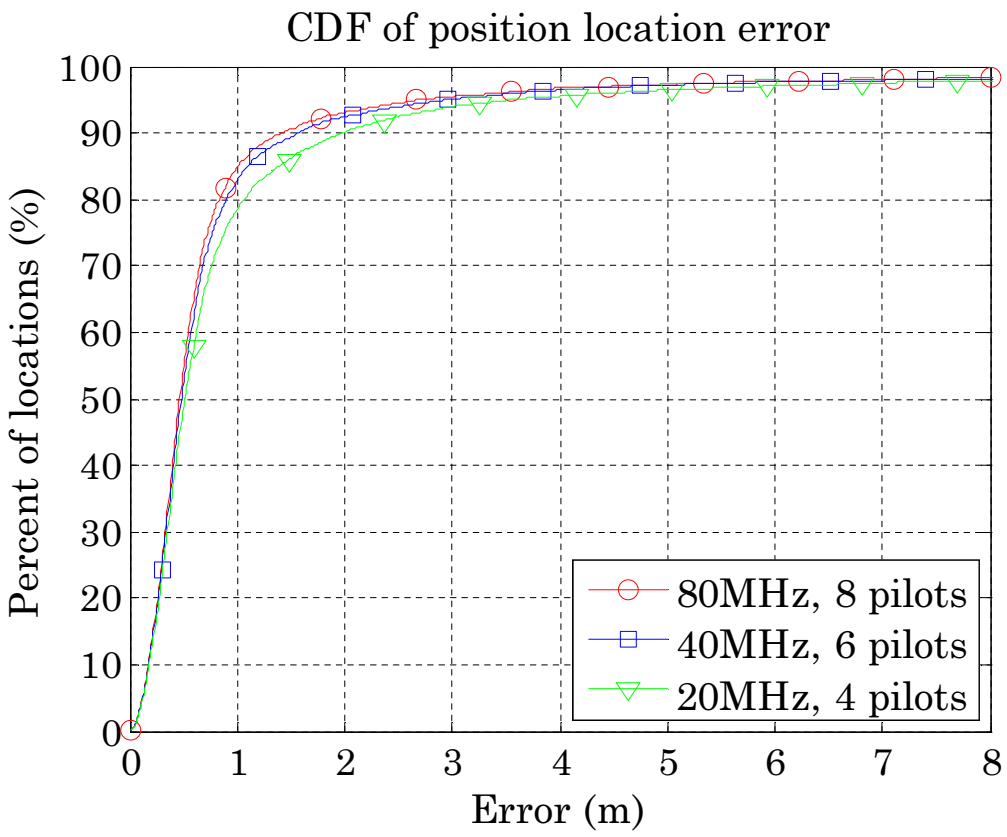

FIGURE 4.9: Performance of the pilot-based localization with the SP criterion in WLAN systems. The number of antennas was $p = 6$, the number of database and test point snapshots was $L = 60$ and $M = 25$, respectively.

depend on system configurations. As a result, database must include different sets of data for each system configuration. The frequency domain approach eliminates this problem by using signal pilots.

The high level of accuracy of this method, demonstrated by simulations, its mild computational load and convenient frequency domain processing make it a promising candidate for providing high quality and ubiquitous localization in indoor environments.

Chapter 5

Conclusion

5.1 Summary

We have presented a new localization method for rich multipath environments in both indoors and outdoors, based on a spatial-temporal fingerprint of the multipath reflections and a novel similarity-profile (SP) matching criterion. The spatial-temporal fingerprint is based on a lower dimensional subspace of the spatial-temporal covariance matrix – referred to as the signal subspace – capturing the directions-of-arrival and the differential-delays of the dominant multipath reflections. Rejection of low-energy reflections by proper subspace dimension selection was used to enhance the robustness of the algorithm. The fingerprint matching is based on the SP criterion, which outperforms considerably the conventional ML criterion, especially in challenging scenarios that are prone to ambiguity.

The presented fingerprinting technique was investigated in the time and frequency domains showing a similar level of accuracy. The frequency domain approach, has the advantage that it can work only with repeatable subcarriers – pilots – eliminating the need for a repeatable signal part (packet preamble). Though most modern communication systems have both preambles and pilots, the big advantage of pilots are that they are embedded in the whole duration of the transmitted signal and thus enable exploiting the whole signal duration for localization. Moreover, localization in the frequency domain is more natural and convenient than the time domain approach as long as signal processing and channel estimation in most modern OFDM-based communication systems are performed in the frequency domain.

The resultant algorithm includes several complexity reduction techniques providing significant savings in the computational load, storage and searching over the database.

The method enables high accuracy localization even with a single base station and signal bandwidth of 20 MHz. The accuracy can be further improved by using higher bandwidth, multiple BS with overlapping coverage, as well as by incorporating well known tracking techniques in the case of moving users. In addition, the presented fingerprinting technique can be applied to the popular WLAN and 3G/4G communication standards supported by most modern smartphones, tablets, laptops and etc. As a result, no new hardware is required in mobile terminals (MT).

The high level of accuracy of this method, demonstrated by simulations and real data results, its mild computational load, good coverage and the absence of additional hardware in the MT make it a promising candidate for providing high quality, cost-effective and ubiquitous localization in indoor environments.

5.2 Future Research

The work presented in this thesis opens a number of research topics that can be further investigated:

1. Our work uses the projection matrix $\boldsymbol{P}_{A_i}$ onto the spatio-temporal signal subspace $\boldsymbol{A}_i$ as a fingerprint of the i-th location, and the expression (3.25) as the similarity metric. The projection matrix and the similarity metric exploit only the i-th location data. A different approach, with potentially better performance, can exploit the data from all database points to construct the fingerprint and the similarity metric. Such an approach may have better fingerprint discrimination and hence better performance.

2. Model-based Localization.

   The "problematic point" of Location Fingerprinting techniques is the lengthy and often challenging training phase (off-line phase) required for the fingerprint database generation. One way to solve this problem is to use signal propagation modeling based on statistical or/and ray-tracing (RT) analysis.

   The basic idea of statistical modeling approach is to construct a fingerprint database using statistical propagation models eliminating on-site measurements

and describing the distribution of signal characteristics like RSS [11, 41, 44] or AOA, TOA [40] at any given location. An alternative approach is to use ray-tracing analysis of radiowave propagation for predicting the site-specific signal characteristics [17, 34, 43, 44].

3. Stochastic Maximum Likelihood Method.

   To derive a similarity-metric for the fingerprint matching we used the deterministic ML method, assuming that the complex attenuations $\boldsymbol{\gamma}(t)$ are unknown deterministic quantities. An alternative approach is modeling the complex attenuations $\boldsymbol{\gamma}(t)$ as stationary jointly Gaussian stochastic process, which leads the received signal to be a stationary, zero-mean, Gaussian process completely described by its second-order covariance matrix.

4. Similarity-Profile Criterion.

   The similarity-profile matching criterion was shown to provide excellent results. A mathematical analysis and a more axiomatic derivation of this criterion are desired, as well as its application to different machine learning problems.

5. Signal Subspace Dimension Estimation.

   Signal subspace dimension estimation plays a key role in the reliable and robust fingerprint formation. Developing and investigating new signal subspace dimension estimation techniques appropriate to the multipath fingerprinting can significantly improve the performance of the developed algorithms.

Bibliography

[1] A. H. Sayed, A. Tarighat, and N. Khajehnouri. Network-based wireless location: challenges faced in developing techniques for accurate wireless location information. *IEEE Signal Processing Magazine*, 22(4):24–40, July 2005. URL http://ieeexplore.ieee.org/xpl/articleDetails.jsp?arnumber=1458275.

[2] G. Sun, J. Chen, W. Guo, and K. J. R. Liu. Signal processing techniques in network-aided positioning: a survey of state-of-the-art positioning designs. *IEEE Signal Processing Magazine*, 22(4):12–23, July 2005. URL http://ieeexplore.ieee.org/xpl/articleDetails.jsp?arnumber=1458273.

[3] O. Hilsenrath and M. Wax. Radio transmitter location finding for wireless communication network services and management. *US Patent 6,026,304*, February 2000. URL http://www.patentlens.net/patentlens/patent/US_6026304/en/.

[4] M. Wax, Y. Meng, and O. Hilsenrath. Subspace signature matching for location ambiguity resolution in wireless communication systems. *US Patent 6,064,339*, May 2000. URL http://www.patentlens.net/patentlens/patent/US_6064339/en/.

[5] M. Wax and O. Hilsenrath. Signature matching for location determination in wireless communication systems. *US Patent 6,112,095*, August 2000. URL http://www.patentlens.net/patentlens/patent/US_6112095/en/.

[6] M. Wax, O. Hilsenrath, and A. Bar. Radio transmitter location finding in CDMA wireless communication systems. *US Patent 6,249,680*, June 2001. URL http://www.patentlens.net/patentlens/patent/US_6249680/en/.

[7] M. Nezafat, M. Kaveh, H. Tsuji, and T. Fukagawa. Localization of wireless terminals using subspace matching with ray-tracing-based simulations. *Sensor Array and Multichannel Signal Processing Workshop Proceedings*, pages 623–627, July

2004. URL http://ieeexplore.ieee.org/xpl/articleDetails.jsp?arnumber=1503024.

[8] M. Nezafat, M. Kaveh, H. Tsuji, and T. Fukagawa. Subspace matching localization: a practical approach to mobile user localization in microcellular environments. *Vehicular Technology Conference*, 7:5145–5149, September 2004. URL http://ieeexplore.ieee.org/xpl/articleDetails.jsp?arnumber=1405081.

[9] M. Nezafat, M. Kaveh, and H. Tsuji. Indoor localization using a spatial channel signature database. *IEEE Antennas and Wireless Propagation Letters*, 5(1):406–409, December 2006. URL http://ieeexplore.ieee.org/xpl/articleDetails.jsp?arnumber=1703945.

[10] H. Koshima and J. Hoshen. Personal locator services emerge. *IEEE Spectrum*, 37(2):41–48, February 2000. URL http://ieeexplore.ieee.org/xpl/articleDetails.jsp?arnumber=819928.

[11] P. Bahl and V. N. Padmanabhan. RADAR: an in-building RF-based user location and tracking system. *Proceedings of IEEE INFOCOM*, 2:775–784, 2000. URL http://ieeexplore.ieee.org/xpl/articleDetails.jsp?arnumber=832252.

[12] H. Laitinen, J. Lahteenmaki, and T. Nordstrom. Database correlation method for GSM location. *IEEE VTC*, 4:2504–2508, 2001. URL http://ieeexplore.ieee.org/xpl/articleDetails.jsp?arnumber=944052.

[13] T. Nypan, K. Gade, and O. Hallingstad. Vehicle positioning by database comparison using the Box-Cox metric and Kalman filtering. *IEEE VTC*, 4:1650–1654, May 2002. URL http://ieeexplore.ieee.org/xpl/articleDetails.jsp?arnumber=1002900.

[14] S. Ahonen and H. Laitinen. Database correlation method for UMTS location. *IEEE VTC*, 4:2696–2700, April 2003. URL http://ieeexplore.ieee.org/xpl/articleDetails.jsp?arnumber=1208882.

[15] S. Ahonen and P. Eskelinen. Mobile terminal location for UMTS. *IEEE Aerospace and Electronic Systems Magazine*, 18(2):23–27, February 2003. URL http://ieeexplore.ieee.org/xpl/articleDetails.jsp?arnumber=1183866.

[16] M. Meurer, S. Heilmann, D. Reddy, T. Weber, and P.W. Baier. A signature based localization technique relying on covariance matrices of channel impulse responses. *Proceedings of WPNC & UET*, pages 31–40, 2005. URL http://www.wpnc.net/60.html.

[17] M. Triki, D. T. M. Slock, V. Rigal, and P. Francois. Mobile terminal positioning via power delay profile fingerprinting: reproducible validation simulations. *IEEE VTC*, pages 1–5, September 2006. URL http://ieeexplore.ieee.org/xpl/articleDetails.jsp?arnumber=4109848.

[18] M. Triki and D. T. M. Slock. Mobile localization for NLOS propagation. *IEEE PIMRC*, pages 1–4, September 2007. URL http://ieeexplore.ieee.org/xpl/articleDetails.jsp?arnumber=4394714.

[19] T. Oktem and D. T. M. Slock. Power delay Doppler profile fingerprinting for mobile localization in NLOS. *IEEE PIMRC*, pages 876–881, September 2010. URL http://ieeexplore.ieee.org/xpl/articleDetails.jsp?arnumber=5672046.

[20] T. Oktem and D. T. M. Slock. Cramer-rao bounds for power delay profile fingerprinting based positioning. *IEEE ICASSP*, pages 2484–2487, May 2011. URL http://ieeexplore.ieee.org/xpl/articleDetails.jsp?arnumber=5946988.

[21] T. Oktem and D. T. M. Slock. Pairwise error probability analysis for power delay profile fingerprinting based localization. *IEEE VTC*, pages 1–5, May 2011. URL http://ieeexplore.ieee.org/xpl/articleDetails.jsp?arnumber=5956780.

[22] F. Althaus, F. Troesch, and A. Wittneben. UWB geo-regioning in rich multipath environment. *IEEE VTC*, 2:1001–1005, September 2005. URL http://ieeexplore.ieee.org/xpl/articleDetails.jsp?arnumber=1558076.

[23] C. Steiner and A. Wittneben. Low complexity location fingerprinting with generalized UWB energy detection receivers. *IEEE Transactions on Signal Processing*, 58(3):1756–1767, March 2010. URL http://ieeexplore.ieee.org/xpl/articleDetails.jsp?arnumber=5313944.

[24] C. Steiner and A. Wittneben. Efficient training phase for ultrawideband–based location fingerprinting systems. *IEEE Transactions on Signal Processing*, 59(12):6021–6032, December 2011. URL http://ieeexplore.ieee.org/xpl/articleDetails.jsp?arnumber=6004843.

[25] R. Talmon, I. Cohen, and S. Gannot. Supervised source localization using diffusion kernels. *IEEE WASPAA*, pages 245–248, October 2011. URL http://ieeexplore.ieee.org/xpl/articleDetails.jsp?arnumber=6082267.

[26] R. Battiti, M. Brunato, and A. Villani. Statistical learning theory for location fingerprinting in wireless LANs. Technical Report DIT-02-0086, Dept. Inform. Telecomun., Universita di Trento, October 2002. URL http://eprints.biblio.unitn.it/238/1/86.pdf.

[27] Hui Liu, H. Darabi, P. Banerjee, and Jing Liu. Survey of wireless indoor positioning techniques and systems. *IEEE Transactions on Systems, Man and Cybernetics, Part C: Applications and Reviews*, 37(6):1067–1080, November 2007. URL http://ieeexplore.ieee.org/xpl/articleDetails.jsp?arnumber=4343996.

[28] M. Wax, S. Jayaraman, V. Radionov, G. Lebedev, and O. Hilsenrath. Efficient storage and fast matching of wireless spatial signatures. *US Patent 6,104,344*, August 2000. URL http://www.patentlens.net/patentlens/patent/US_6104344/en/.

[29] M. Youssef and A. Agrawala. The Horus WLAN location determinatioin system. *Proc. third Intl Conf. Mobile Systems, Applications and Services*, pages 205–218, June 2005. URL http://64.238.147.56/citation.cfm?id=1067193.

[30] Huimin Wang, Lin Ma, Yubin Xu, and Zhian Deng. Dynamic radio map construction for WLAN indoor location. *Intelligent Human-Machine Systems and Cybernetics (IHMSC)*, 2:162–165, August 2011. URL http://ieeexplore.ieee.org/xpl/articleDetails.jsp?arnumber=6038240.

[31] Lang Peng, Junyi Han, Weixiao Meng, and Jingyu Liu. Research on radio-map construction in indoor WLAN positioning system. *Pervasive Computing Signal Processing and Applications (PCSPA)*, pages 1073–1077, September 2010. URL http://ieeexplore.ieee.org/xpl/articleDetails.jsp?arnumber=5635875.

[32] Minkyu Lee and Dongsoo Han. Voronoi tessellation based interpolation method for Wi-Fi radio map construction. *IEEE Communications Letters*, 16(3):404–407, March 2012. URL http://ieeexplore.ieee.org/xpl/articleDetails.jsp?arnumber=6150651.

[33] L. F. M. de Moraes and B. A. A. Nunes. Calibration-free WLAN location system based on dynamic mapping of signal strength. *in Proc. 2006 ACM MOBIWAC*, pages 92–99, 2006. URL http://dl.acm.org/citation.cfm?id=1164799.

[34] P. S. Maher and R. A. Malaney. A novel fingerprint location method using ray-tracing. *IEEE GLOBECOM*, pages 1–5, 2009. URL http://ieeexplore.ieee.org/xpl/articleDetails.jsp?arnumber=5425231.

[35] S. Ahonen and P.V. Eskelinen. Performance estimations of mobile terminal location with database correlation in UMTS networks. *4th International Conference on 3G Mobile Communication Technologies*, pages 400–403, June 2003. URL http://ieeexplore.ieee.org/xpl/articleDetails.jsp?tp=&arnumber=1350694.

[36] C.J. Debono and C. Calleja. The application of database correlation methods for location detection in GSM networks. *3rd International Symposium on Communications, Control and Signal Processing, ISCCSP*, pages 1324–1329, March 2008. URL http://ieeexplore.ieee.org/xpl/articleDetails.jsp?arnumber=4537431.

[37] G. Wolfe, R. Hoppe, D. Zimmermann, and F. M. Landstorfer. Enhanced localization technique within urban and indoor environments based on accurate and fast propagation models. *European Wireless 2002*, February 2002. URL http://docenti.ing.unipi.it/ew2002/proceedings/179.pdf.

[38] H. Lim, L.-C. Kung, J. C. Hou, and H. Luo. Zero-configuration, robust indoor localization: theory and experimentation. *IEEE INFOCOM*, pages 1–12, April 2006. URL http://ieeexplore.ieee.org/lpdocs/epic03/wrapper.htm?arnumber=4146876.

[39] M. McGuire, K.N. Plataniotis, and A.N. Venetsanopoulos. Location of mobile terminals using time measurements and survey points. *IEEE Transactions on Vehicular Technology*, 52(4):999–1011, July 2003. URL http://ieeexplore.ieee.org/xpl/articleDetails.jsp?arnumber=1224556.

[40] E. Tsalolikhin, I. Bilik, and N. Blaunstein. A single-base-station localization approach using a statistical model of the NLOS propagation conditions in urban terrain. *IEEE Transactions on Vehicular Technology*, 60(3):1124–1137, March 2011. URL http://ieeexplore.ieee.org/xpl/login.jsp?tp=&arnumber=5708185.

[41] T. Roos, P. Myllymaki, and H. Tirri. A statistical modeling approach to location estimation. *IEEE Transactions on Mobile Computing*, 1(1):59–69, Jan-Mar 2002. URL http://ieeexplore.ieee.org/xpl/articleDetails.jsp?tp=&arnumber=1011059.

[42] T. Roos, P. Myllymaki, H. Tirri, P. Misikangas, and J. Sievnen. A probabilistic approach to WLAN user location estimation. *International Journal of Wireless Information Networks*, 9(3):155–164, July 2002. URL http://dx.doi.org/10.1023/A:1016003126882.

[43] S. Kikuchi, A. Sano, and H. Tsuji. Blind mobile positioning in urban environment based on ray-tracing analysis. *EURASIP Journal on Applied Signal Processing*, 2006:1–12, January 2006. URL http://dl.acm.org/citation.cfm?id=1288397.

[44] A. Hatami and K. Pahlavan. Comparative statistical analysis of indoor positioning using empirical data and indoor radio channel models. *Processing of the IEEE CCNC*, 2:1018–1022, January 2006. URL http://ieeexplore.ieee.org/xpl/articleDetails.jsp?arnumber=1593192.

[45] K. Sayrafian-Pour and D. Kaspar. Application of beamforming in wireless location estimation. *EURASIP Journal on Applied Signal Processing*, 2006:1–13, January 2006. URL http://dl.acm.org/citation.cfm?id=1288401.

[46] Shih-Hau Fang, Tsung-Nan Lin, and Kun-Chou Lee. A novel algorithm for multipath fingerprinting in indoor WLAN environments. *IEEE Transactions on Wireless Communications*, 7(9):3579–3588, September 2008. URL http://ieeexplore.ieee.org/xpl/articleDetails.jsp?arnumber=4626331.

[47] P. Cherntanomwong, J.-I. Takada, H. Tsuji, and D. Gray. New radio source localization using array antennas based on fingerprinting techniques in outdoor environment. *Proceedings of Asia-Pacific Microwave Conference*, pages 1–4, December 2007. URL http://ieeexplore.ieee.org/xpl/articleDetails.jsp?arnumber=4554585.

[48] P. Cherntanomwong, J.-I. Takada, and H. Tsuji. Signal subspace interpolation from discrete measurement samples in constructing a database for location fingerprint technique. *IEICE transactions on communications*, E92-B(9):2922–2930,

September 2009. URL http://search.ieice.org/bin/summary.php?id=e92-b_9_2922&category=B&year=2009&lang=E&abst=.

[49] Tsung-Nan Lin and Po-Chiang Lin. Performance comparison of indoor positioning techniques based on location fingerprinting in wireless networks. *International Conference on Wireless Networks, Communications and Mobile Computing*, 2:1569–1574, June 2005. URL http://ieeexplore.ieee.org/xpl/articleDetails.jsp?arnumber=1549647.

[50] G.M.R.I. Godaliyadda and H. K. Garg. Analysis of super resolution spectral estimation techniques for indoor positioning applications. *Proc. 9th International Conference on Signal Processing*, pages 2538–2541, October 2008. URL http://ieeexplore.ieee.org/xpl/articleDetails.jsp?arnumber=4697666.

[51] G.M.R.I. Godaliyadda and H. K. Garg. A time domain eigen value method for robust indoor localization. *Wireless Telecommunications Symposium*, pages 1–8, April 2010. URL http://ieeexplore.ieee.org/xpl/articleDetails.jsp?arnumber=5479664.

[52] G.M.R.I. Godaliyadda and H. K. Garg. Robust techniques for accurate indoor localization in hazardous environments. *Wireless Sensor Network*, 2(5):390–401, May 2010. URL http://www.scirp.org/Journal/PaperInformation.aspx?paperID=1812.

[53] Xinrong Li and K. Pahlavan. Super-resolution TOA estimation with diversity for indoor geolocation. *IEEE Transactions on Wireless Communications*, 3(1):224–234, January 2004. URL http://ieeexplore.ieee.org/xpl/articleDetails.jsp?arnumber=1259415.

[54] Z. li Wu, C. hung Li, J. K.-Y. Ng, and K. R. P. H. Leung. Location estimation via support vector regression. *IEEE Trans. on Mobile Computing*, 6(3):311–321, March 2007. URL http://citeseerx.ist.psu.edu/viewdoc/summary?doi=10.1.1.155.3766.

[55] C. L. Wu, L. C. Fu, and F. L. Lian. WLAN location determination in e-home via support vector classification. *IEEE International Conference on Networking, Sensing and Control*, 2:1026–1031, 2004. URL http://ieeexplore.ieee.org/xpl/articleDetails.jsp?arnumber=1297088.

[56] R. Battiti, A. Villani, and T. Le Nhat. Neural network models for intelligent networks: deriving the location from signal patterns. *In Proceedings of AINS2002, (UCLA)*, May 2002. URL http://citeseerx.ist.psu.edu/viewdoc/summary?doi=10.1.1.12.6409.

[57] A. M. Edgar, C. Raul, and F. Jesus. Estimating user location in a WLAN using backpropagation neural networks. *In Proceedings of IBERAMIA, (UCLA)*, pages 737–746, 2004. URL http://citeseerx.ist.psu.edu/viewdoc/summary?doi=10.1.1.12.6409.

[58] Richard O. Duda, Peter E. Hart, and David G. Stork. *Pattern classification*. Wiley, New York, 2. auflage edition, 2001. ISBN 978-0-471-05669-0.

[59] S.M. Kay. *Fundamentals of Statistical Signal Processing: Estimation Theory*. Number v. 1 in Prentice Hall Signal Processing Series. Prentice Hall, 1993. ISBN 9780133457117. URL http://books.google.co.il/books?id=aFwESQAACAAJ.

[60] Christopher M. Bishop. *Pattern Recognition and Machine Learning*. Springer, Berlin, Heidelberg, 1st ed. 2006. corr. 2nd printing edition, 2006. ISBN 978-0-387-31073-2. URL http://books.google.co.il/books?id=kTNoQgAACAAJ.

[61] H. Leppkoski, S. Tikkinen, and J. Takala. Optimizing radio map for WLAN fingerprinting. *Ubiquitous Positioning Indoor Navigation and Location Based Service (UPINLBS)*, pages 1–8, October 2010. URL http://ieeexplore.ieee.org/xpl/articleDetails.jsp?arnumber=5654332.

[62] J. M. Moguerza and A. Muoz. Support vector machines with applications. *Statistical Science*, 21(3):322–336, 2006. URL http://projecteuclid.org/euclid.ss/1166642435.

[63] Y. j. Lee, O. L. Mangasarian, and W. H. Wolberg. Breast cancer survival and chemotherapy: A support vector machine analysis. Technical report, Data Mining Institute, Computer Sciences Department, University of Wisconsin, 2000. URL http://citeseerx.ist.psu.edu/viewdoc/summary?doi=10.1.1.17.4298.

[64] P. Bahl, V. N. Padmanabhan, and A. Balachandran. Enhancements to the RADAR user location and tracking system. Technical Report MSR-TR-2000-12, February 2000. URL http://research.microsoft.com/apps/pubs/default.aspx?id=69861.

[65] Lang Tong and S. Perreau. Multichannel blind identification: from subspace to maximum likelihood methods. *Proceedings of the IEEE*, 86(10):1951–1968, October 1998. URL http://ieeexplore.ieee.org/xpl/articleDetails.jsp?arnumber=720247.

[66] R. O. Schmidt. Multiple emitter location and signal parameter estimation. *IEEE Transactions on Antennas and Propagation*, 34(3):276–280, March 1986. URL http://ieeexplore.ieee.org/xpl/articleDetails.jsp?arnumber=1143830.

[67] A. G. Jaffer. Maximum likelihood direction finding of stochastic sources: a separable solution. *ICASSP*, 5:2893–2896, April 1988. URL http://ieeexplore.ieee.org/xpl/articleDetails.jsp?arnumber=197258.

[68] P. Stoica and A. Nehorai. On the concentrated stochastic likelihood function in array signal processing. *Circuits, Systems and Signal Processing*, 14(5):669–674, 1995. URL http://link.springer.com/article/10.1007%2FBF01213963.

[69] M. Wax, T. J. Shan, and T. Kailath. Spatio–temporal spectral analysis by eigenstructure methods. *IEEE Transactions on Acoustics, Speech and Signal Processing*, 32(4):817–827, August 1984. URL http://ieeexplore.ieee.org/xpl/articleDetails.jsp?arnumber=1164400.

[70] M. Wax and T. Kailath. Detection of signals by information theoretic criteria. *IEEE Transactions on Acoustics, Speech and Signal Processing*, 33(2):387–392, April 1985. URL http://ieeexplore.ieee.org/xpl/articleDetails.jsp?arnumber=1164557.

[71] M. Wax and I. Ziskind. On unique localization of multiple sources by passive sensor arrays. *IEEE Transactions on Acoustics, Speech and Signal Processing*, 37(7):996–1000, July 1989. URL http://ieeexplore.ieee.org/xpl/articleDetails.jsp?arnumber=32277.

[72] H. Krim and M. Viberg. Two decades of array signal processing research: the parametric approach. *IEEE Signal Processing Magazine*, 13(4):67–94, July 1996. URL http://ieeexplore.ieee.org/xpl/articleDetails.jsp?arnumber=526899.

[73] M. Wax and A. Leshem. Joint estimation of time delays and directions of arrival of multiple reflections of a known signal. *IEEE Transactions on Signal Processing*, 45(10):2477–2484, October 1997. URL http://ieeexplore.ieee.org/xpl/articleDetails.jsp?arnumber=640713.

[74] I. Ziskind and M. Wax. Maximum likelihood localization of multiple sources by alternating projection. *IEEE Transactions on Acoustics, Speech and Signal Processing*, 36(10):1553–1560, October 1988. URL http://ieeexplore.ieee.org/xpl/articleDetails.jsp?arnumber=7543.

[75] H. L. Van Trees. *Detection, estimation, and modulation theory – Optimum array processing*. Wiley-Interscience, New York, 2002. ISBN 978-0-471-09390-9.

[76] A. L. Swindlehurst. Time delay and spatial signature estimation using known asynchronous signals. *IEEE Transactions on Signal Processing*, 46(2):449–462, February 1998. URL http://ieeexplore.ieee.org/xpl/articleDetails.jsp?arnumber=655429.

[77] Panagiotis Tsakalides. *Array signal processing with alpha stable distributions*. PhD thesis, University of Southern California, December 1995.

[78] A. Bjorck and G. H. Golub. Numerical methods for computing angles between linear subspaces. *Mathematics of Computation*, 27(123):579–594, July 1973. URL http://www.ams.org/journals/mcom/1973-27-123/S0025-5718-1973-0348991-3/S0025-5718-1973-0348991-3.pdf.

[79] Merico Edward Argentati. *Principal angles between subspaces as related to Rayleich quotient and Rayleich Ritz inequalities with applications to eigenvalue accuracy and an eigenvalue solver*. PhD thesis, University of Colorado at Denver, 2003. URL http://130.203.133.150/showciting;jsessionid=CCD6B717924F5F28BE1ADC506984FA5D?cid=4228237.

[80] D. Tse and P. Viswanath. *Fundamentals of Wireless Communication*, pages 10–42. Cambridge University Press, Cambridge, 2005. ISBN 978-0-521-84527-4. URL http://www.eecs.berkeley.edu/~dtse/book.html.

[81] E. Perahia, A. Sheth, T. Kenney, R. Stacey, and D. Halperin. Investigation into the Doppler component of the IEEE 802.11n channel model. *IEEE GLOBECOM*, pages

1–5, December 2010. URL http://ieeexplore.ieee.org/xpl/articleDetails.jsp?arnumber=5684207.

[82] E. Perahia and R. Stacey. *Next Generation Wireless LANs - Throughput, Robustness, and Reliability in 802.11n*, pages 61,107. Cambridge University Press, Cambridge, 2008. ISBN 978-0-521-88584-3.

[83] Andrea Goldsmith. *Wireless Communications*. Cambridge University Press, Cambridge, 2005. ISBN 978-0-521-83716-3.

איכון בתוך מבנים מבוסס על חתימות רב-נתיב

יבגני קופרשטיין

איכון בתוך מבנים מבוסס על חתימות רב-נתיב

חיבור על מחקר

לשם מילוי חלקי של הדרישות לקבלת התואר

מגיסטר למדעים בהנדסת חשמל

יבגני קופרשטיין

הוגש לסנט הטכניון - מכון טכנולוגי לישראל

אייר, 5773 חיפה אפריל 2013

המחקר נעשה בהנחיית פרופ' ישראל כהן וד"ר מתי וקס בפקולטה להנדסת חשמל.

אני מודה לחברת אלווריון ולקרן הלאומי למדע (מענק מס' 1130/11) על התמיכה הכספית הנדיבה בהשתלמותי.

ברצוני להביע את תודתי והערכתי העמוקה לפרופ' ישראל כהן וד"ר מתי וקס על ההנחיה רבת ערך ועידוד מתמיד במהלך כל שלבי המחקר.

תקציר

איכון משדרים אלחוטיים הינה בעיה ידועה עם הרבה יישומים צבאיים ומסחריים. שיטות רבות פותחו לפתרון הבעיה במהלך 60 השנים האחרונות, רובן מבוססות על הנחת קו-ראיה בין משדר למקלט (LOS). השיטות הקלסיות לאיכון, כגון direction-of-arrival (DOA), time-of-arrival (TOA), differential-time-of-arrival (DTOA), כולן מבוססות על הנחה זו, הן מנצלות מספר מדידות כאלה לבצוע טריאנגולציה.

בשנים האחרונות הולכת וגוברת התעניינות באיכון בתוך מבנים, בהם תנאי קו-ראיה אינם קיימים בד"כ. במבנים טיפוסיים, התפשטות האותות מהמשדר למקלט מתרחשת בד"כ בעזרת החזרות רבות מגופים ומקירות, המכונות רב-נתיב.

לפתרון בעית האיכון בתנאים של חוסר בקו-ראיה פותחו לאחרונה שיטות איכון המבוססות על חתימות. שיטות אלה מבוססות על הנחה כי קיימת התאמה חד-ערכית בין מאפייני האותות הנקלטים ע"י תחנת בסיס למיקום המשדר, כלומר, ניתן להשתמש בחתימה המתקבלת מהאותות הנקלטים בתור מזהה ייחודי של מיקום המשדר. שיטות אלה הופכות את בעית האיכון לבעיית זיהוי, כלומר המיקום נקבע על ידי התאמת החתימה המתקבלת מהאות הנקלט לאוסף החתימות במאגר המידע.

שתי שיטות איכון שונות המבוססות על חתימות פותחו בערך באותו זמן. הראשונה, שפותחה ע"י Wax et al. [3-6], מבוססת על שימוש באותות הרב-נתיב, כפי שהם נקלטים ע"י מערך האנטנות, בתור חתימת המיקום. השניה, שפותחה ע"י Bahl and Padmanabhan [11] וע"י Laitinen, Lahteenmaki, and Nordstrom [12], מבוססת על שימוש בעוצמת האות הנקלט (Received Signal Strength - RSS), כפי שהיא מתקבלת ממספר תחנות בסיס, בתור חתימת המיקום.

חתימת-RSS סובלת מתלות בפרמטרים לא רלוונטיים רבים, כגון אורינטצית המשדר והנחתת עוצמת הסיגנל ע"י גופים שונים, אך מה שיותר קריטי, היא סובלת מהשתנות עוצמת אות גבוהה לאורך מרחק קצר מאורך הגל הנגרמת על ידי התאבכות בונה והורסת של אותות רב-נתיב. כתוצאה מכך, הדיוק של טכניקה זו הוא מוגבל ונדרשות מדידות עוצמת אות מתחנות בסיס מרובות בכדי להבטיח דיוק סביר. לעומת זאת, החתימה שמבוססת על אותות רב-נתיב שנקלטו באופן קוהרנטי ע"י מערך אנטנות, מנצלת את

הרב-נתיב לטובתה, ובכך מאפשרת דיוק גבוה בהרבה.

העבודה של Wax, Hilsenrath, and Meng ב-[3-5] התמקדה בסביבת outdoor, הייתה מוגבלת לאותות צרי סרט של תקשורת סלולרית אנאלוגית הראשונה (AMPS) והשתמשה בחתימות המבוססות על כיווני הגעה של אותות רב-נתיב. ב-[6] Wax, Hilsenrath, and Bar הרחיבו את עבודתם לאותות רחבי סרט במערכות Code Division Multiple Access (CDMA) ע"י הוספת חתימה נפרדת המבוססת על פרופיל עוצמת ההחזרות power delay profile (PDP) של אותות רב-נתיב.

המחקר הנוכחי מרחיב את העבודה של Wax et al. [3-6] במספר היבטים. ראשית, הוא מציג חתימה חדשנית ויעילה יותר המנצלת גם את כיווני ההגעה וגם את ההפרשים בזמני ההגעה של ההחזרות השונות של האותות רב-נתיב. חתימה חדשנית זו מתקבלת מתת-מרחב של מטריצת השונות זמן-מרחב, המכונה גם תת-מרחב האותות. שערוך התת-מרחב אינו דורש שערוך כיווני ההגעה וההפרשים בזמני ההגעה של אותות רב-נתיב, בעיה שהיא גם קשה וגם בעלת סיבוכיות חישובית גבוהה בסביבה עשירת רב-נתיב. יתר על כן, התת-מרחב מכיל בעיקר את ההחזרות הדומיננטיות, ובכך מתקבלת חתימה עשירה, אמינה ויציבה, שמשמשת יחד עם קריטריון יעיל להשוואת חתימות (similarity profile matching) לאיכון מדויק בעזרת תחנת בסיס יחידה. שנית, הוא מציג תנאים הכרחיים ומספיקים המבטיחים יחידות האיכון. שלישית, בניגוד ל-[6], שיטה זו ישימה לכל אות רחב סרט בעל קטע אות קבוע. באופן כזה, היא ישימה לרוב טכניקות תקשורת מודרניות, מאחר וכולן משתמשות בקטע קבוע של האות למטרות סנכרון ושערוך הערוץ. שיטה זו ישימה גם לאיכון באמצעות תגובת ההלם של ערוצי המערך (CIR) ותגובת התדר של ערוצי המערך (CFR). בנוסף, בניגוד ל-[3-6], עבודה זו מתמקדת בסביבת indoor, אך גם ישימה לסביבות outdoor. למרות ששתי הסביבות מתאפיינות ברב-נתיב עשיר, הרב-נתיב בתוך מבנים בד"כ עשיר יותר ומאופיין בפיזור גדול יותר של כיווני ההגעה וזמני ההגעה של ההחזרות.

כמו כן, עבודה זו מציגה גם שיטת איכון המבוססת על חתימות רב-נתיב בתחום התדר. רמת הדיוק של שיטה זו אמנם דומה לזו בתחום הזמן ,אך יתרונה הוא ביכולת עבודה עם פילוטים (pilots), ללא צורך באות עם קטע קבוע, שהוא נוח וטבעי יותר בחלק ממערכות התקשורת המודרניות.

בנוסף, שיטת האיכון המוצעת מכילה מספר אלגוריתמי אופטימיזציה המביאים להורדה משמעותית בסיבוכיות חישובית, ולחיסכון בגודל מאגר החתימות ובזמן החיפוש בתוכו.

ביצועי האלגוריתמים נבדקו הן עם נתונים שהתקבלו בסימולציות והן עם נתונים ממדידות שדה, ועומדים על דיוק של כ-1 מטר במבנים טיפוסיים.